Investigating mechanisms of neutralization of *staph* enterotoxin B

Clint Vorauer

A dissertation

Submitted in partial fulfillment of the

Requirements for the degree of

Doctor of Philosophy

University of Washington

2023

Reading Committee

Miklos Guttman, Chair

Abhinav Nath

William Atkins

University of Washington

Abstract

Investigating mechanisms of neutralization of *staph* enterotoxin B

Clint Vorauer

Chair of the Supervisory Committee

Miklos Guttman

Medicinal Chemistry

Staphylococcal enterotoxin B (SEB) is a small, secreted protein that causes food poisoning-like symptoms and can be lethal in microgram amounts. SEB elicits a profound immune response via the bridging of major histocompatibility complex class II (MHCII) molecules on antigen-presenting cells with T-cell receptors (TCR). Several monoclonal antibodies (mAbs) have been identified as capable of neutralizing SEB. Using structural mass spectrometry, the epitopes of several neutralizing antibodies were successfully mapped, and allosteric as well as synergistic effects that contribute to the efficacy of select mAbs were determined. Having established a robust approach for tracking mAb-SEB interactions, we examined the interactions within raw, polyclonal sera for understanding antibody responses to SEB and their resulting protective efficacy. This dissertation provides mechanistic insight into the neutralization of SEB and highlights technical advances to the Hydrogen Deuterium Exchange Mass Spectrometry (HDX-MS) method.

Table of Contents

Chapter 1: Introduction……1

Chapter 2: Rapid assessment of pepsin column activity for reliable HDX-MS studies……24

Chapter 3: Mapping epitopes and allosteric behavior of *staph* enterotoxin B……37

Chapter 4: Direct mapping of polyclonal epitopes in serum by HDX-MS……58

Chapter 5: Future directions……82

Chapter 1 – Introduction

Portions of the text of this chapter have been modified with the permissions from:

Ellie I. James,* Taylor A. Murphree,* Clint Vorauer,* John R. Engen, and Miklos Guttman. *Chemical Reviews* **2022** *122* (8), 7562-7623**. *Equal contributing authors**

1.1 Overview

Hydrogen Deuterium Exchange (HDX) coupled to Mass Spectrometry (MS) probes the accessibility of backbone amide hydrogens (Figure 1) which depend on local secondary structure, higher order structure, and conformational dynamics [1]. Proteins are exposed to deuterium oxide for fixed amounts of time and quenched by low pH to slow deuterium exchange. Acid-active proteases are then used to cleave the protein, and the resulting peptides are separated by liquid chromatography and monitored by MS (Figure 2). Structural changes that arise from binding an antibody or protein partner binding will be detected with this technique via the differential uptake in deuterium represented by the mass shift of the isotopic peptide envelope (Figure 3). Due to the relatively small size of the exchanging deuterium, the reaction is unlikely to perturb the global protein structure.

The HDX-MS experiment relies on methodological innovation from the last several decades, notably in integrating non-specific acid-active proteases to generate peptides — an element vital to the bottom-up MS approach. Peptide digestion prior to MS analysis as opposed to intact protein ionization and in-instrument fragmentation distinguishes bottom-up from top-down proteomics. Unlike specific proteases that have become routine in proteomic workflows, non-specific proteases pose challenges due to their lack of specificity and the tendency of columns with coupled protease to become less active over time. A user might struggle to recognize diminished protease activity. The work herein addresses this conundrum and proposes a test for protease efficiency agnostic of the studied protein with the aim of more streamlined HDX experimentation.

One of the reasons HDX-MS has been so successful in studying the interactions of proteins is its inherent versatility; it can be applied to nearly any protein system, many of which are too large, flexible, heterogeneous, or sample-limited to be analyzed by other existing structural tools. HDX-MS can adeptly identify the interface of two binding pairs as well as allosteric perturbations distal to the binding site. Unlike other structural MS approaches, HDX probes all amino acids, a feature that produces expansive results that often span the entirety of the protein sequence.

This dissertation details work that sheds light on the protein interface of *Staph* enterotoxin B (SEB) and neutralizing binding partners— introduced here in section 1.4. SEB is a notable adept model protein system considering the toxin is small, robust, and monomeric. Beyond mapping epitopes, associated allosteric interactions are identified and a novel approach for studying protein interactions in complex solutions is proposed.

1.2 Protease considerations for bottom-up HDX-MS

The classic and still most widely adopted approach for analyzing HDX of proteins is a bottom-up approach based on the pre-MS protocol from Rosa and Richards[2] where proteins are digested with an acid-active protease after the quench step and the mixture of peptides is analyzed by mass spectrometry [3]. Over the past two decades there have been many developments and advances in approaches for protein denaturation, digestion, and tools for resolving and detecting the maximum number of observable peptides for analyses utilizing continued improvements in LC-MS technology. In each step, there are inherent considerations that lead to a balancing act with regard to data quality, processing time, and back-exchange that needs to be tailored to a given protein analyte.

Theoretically, the conditions used to quench deuterium labeling should denature the protein to allow it to be easily digested and favor high activity for the protease utilized to effectively cleave the protein, all while keeping the sample as cold as possible and keeping sample processing times as short as possible to minimize back-exchange. Practically, there is some leeway in quench conditions and parameters for denaturation, protease activity, time, temperature, and buffer compositions that are often adjusted, in most cases established on an empirical basis, to obtain the best coverage for a given protein analyte.

Many proteins are inherently destabilized by the low pH used for the quench step and may not require additional denaturants for effective digestion under the quench condition constraints of time and temperature. However, the addition of chaotropic agents such as urea and guanidinium are often required for effective unfolding and subsequent digestion of the target protein [4-6]. Use of high concentrations of chaotropic agents does not compromise back-exchange, but it is important to consider that high levels may also inhibit the proteases used for the digestion. For example, pepsin, the most widely employed protease for HDX-MS, retains activity up to 4 M urea, but loses nearly all activity above 3 M guanidine [7]. For some recalcitrant proteins that require higher concentrations of denaturant, studies have opted for a

two-step quench approach in which the deuterium labeled protein is first added to a very high concentration of denaturant to induce unfolding, and the denaturant is subsequently diluted just prior to the digestion step.

The need to maintain low pH during digestion imposes a major limit on the number of available proteases for HDX-MS. The typical proteases used for proteomics (e.g. trypsin) cleave with very high specificity, but are not active at the low pH necessary for minimizing back-exchange [8,9]. All available proteases active at low pH and reliable for HDX-MS cleave at a wide range of amino acid sequences. This is both a strength and a weakness. The lack of specific sequences for cleavage complicates identification and effective prediction of peptides generated from the protein analyte. At the same time, the broad cleavage specificity enables the proteases to cleave the proteins in different combinations of sites to generate many overlapping peptides which provide information across the protein sequence [2,8,10,11].

Porcine pepsin is the original and by far the most common protease utilized for HDX-MS studies. It has reliably high activity under HDX quench conditions, is readily available in highly purified forms, and has relatively broad cleavage preference [3]. In general, pepsin prefers to cleave adjacent to hydrophobic residues, but is able to cleave C-terminal to all amino acids except histidine, lysine, arginine, and proline [12-14]. While pepsin generally produces a wide array of peptides covering the analyte protein sequence, there has been a continued desire for more peptides to increase coverage, redundancy, and spatial resolution [2]. To this end, several additional proteases with different cleavage preferences have been explored and some implemented into HDX-MS workflows to provide complementary coverage to pepsin. Protease type XIII from *Aspergillus saitoi* (also known as aspergillopepsin or Fungal XIII) and Protease type XVIII (Rhizopuspepsin) were found to be effective proteases for HDX-MS with different cleavage preferences compared to pepsin [8,10]. Other acid-active enzymes have been explored, including rice field eel pepsin [15], pepsin from Antarctic rock cod [16], and cathepsin-L [17]. An aspartic protease from *Nepenthes* carnivorous plants was shown to have strong protease activity under quench conditions with cleavage preference that was broader than pepsin, namely it is able to efficiently cleave after basic residues [18,19]. A homologue, Nepenthesin II ('NepII') has similar protease activity and exhibits much greater resistance to denaturants, on par with pepsin [7,14] (Figure 4). More recently, a prolyl endopeptidase (An-PEP) was found suitable for HDX-MS [20] and has some similarities to pepsin. Importantly, it cleaves after proline residues which most available acid active proteases cannot do [13], thereby adding another useful option for expanding sequence coverage for HDX-MS studies. Beyond having a range of protease options for HDX-MS, several groups have combined multiple proteases to greatly improve coverage and spatial resolution

[8]. In fact, the practice of utilizing multiple proteases simultaneously is now common practice for many bottom-up HDX-MS approaches [11,21-23].

The development of immobilized proteases in a column format [24,25] offers several advantages over the traditional in-solution protease digest. The major advantage is the high enzyme:substrate ratio that can be achieved during the relatively short contact-time. Pepsin immobilized onto bead support was found to be highly efficient and allowed for short digestion times (under 1 minute), online sample processing, and minimal interference from the peptides generated from pepsin autolysis, which was common with solution pepsin digestion. Optimized protocols have since been generated for fabrication of pepsin columns and their tolerance to various conditions (including reducing agents and denaturants) has been well-established [26]. Because of the relatively short digestion times needed with protease columns, it is possible to use elevated temperatures to enhance proteolysis without a large impact on levels of back-exchange [15]. For example, increasing the protease column temperature from 0°C to 10°C significantly improved digestion efficiency and without increasing back-exchange [27].

1.3 Mapping interactions with HDX

The interaction of proteins with other proteins and ligands is central to nearly all biological processes and the study of these processes is vital for the development of new therapeutics. HDX-MS is particularly powerful for investigating protein binding interactions and this has been one of the most prevalent applications of HDX-MS [28]. By comparing the exchange kinetics between a free (unbound) and a bound protein, it is easy to localize and track the structural changes associated with the binding event. In most cases, ligand binding leads to stabilization of the local structure at the interface, leading to slowed deuterium exchange [28,29], and provides an efficient way to map interaction surfaces [30-32].

To best resolve differences upon binding, it is important to make the comparison between a fully free population and an as-fully-bound-as-possible population. With weak binding interactions it is often difficult to achieve saturation as it may require very high concentrations of ligand [33,34]. Often even a several-fold molar excess of ligand is not sufficient for achieving >99% of the protein bound in solution. Furthermore, a complex should be formed prior to deuterium exchange to ensure the fully bound state is being probed. For ligands with fast dissociation kinetics (> 1e5 s^{-1}), it is important to consider that the protein will spend time in the unbound state during deuterium exchange [35,36], which in some cases leads to the appearance of two species in the deuteration profiles [37-39]. Though data like this can be

confounding, such experiments actually offer a way to gain more insight into an interaction. For example, Zhang and Vachet were able to use this effect to measure dissociation kinetics for the beta-lactoglobulin dimer [40].

Another consideration with free vs. bound comparative HDX-MS is that small ligands can act to globally stabilize a protein. The measured changes in the deuterium exchange profiles will reflect both global domain stabilization and local contacts with the ligand, which can sometimes be resolved by varying the concentrations of the ligand [41]. Though generally ligand binding increases protection of amides, thereby slowing deuterium exchange ('type 1' binding), it is also possible for ligand binding to actually lead to increased deuterium exchange at the binding site ('type 2' binding) [42,43]. It is also possible for an interaction to not perturb the backbone amide hydrogen environment thereby producing no observable HDX changes at all [44].

With antibodies, comparative HDX-MS is now well defined. Most antibodies generally have strong affinities (K_D ~ low nM) with sufficiently slow dissociation kinetics and recognize a very specific surface patch on proteins. As such, HDX-MS has been particularly useful for mapping the protein surfaces on antigens that are recognized by monoclonal antibodies (mAbs) (often termed 'epitope mapping') (Figure 5). Epitopes can be linear, where the binding site is a single stretch of amino acids on the antigen protein, or conformational, which are made up of discrete segments of the protein sequence that are close together in three-dimensional structure. HDX-MS has proven particularly useful for mapping conformational epitopes for which there are fewer techniques to characterize. In fact, epitope mapping is now one of the primary uses of HDX-MS in the biopharmaceutical industry [45].

While HDX-MS is effective in characterizing protein interfaces and ligand binding events in many instances, there are protein-ligand interactions that require other considerations and caution must be exercised as data interpretation depends on the protein system. Allostery, global protein stabilization, and lack of influence on backbone amide hydrogens as a result of various binding modes (hydrophobic, electrostatic, etc.) can present challenges in some systems. Even with antibodies, allosteric effects can occur at distal sites on the protein(s) that are not always structurally foreseeable [46,47]. Depending on the system being examined, the intrinsic ability to see all changes across a protein upon binding can be either tremendously insightful or confounding.

For systems where the interaction interface has been established and especially when high resolution structures of complexes are available, detection of allosteric effects presents a powerful way

to detect indirect effects of binding [48-50]. A very clear demonstration of allosteric changes were observed in Nipah Virus G ectodomain upon binding its receptor, epherinB2 [51]. Comparative HDX-MS revealed the surface of the ectodomain directly interacting with epherinB2 becoming more protected, while several sites on the opposite side of the protein show increased exchange (Figure 6). Interestingly, the allosteric effects are relayed all the way to the stalk helices, implicating this binding event in the mechanism of activation leading to host/virus membrane fusion.

Pinpointing allosteric effects has also been tremendously insightful in recent years for understanding how antibodies are able to neutralize their targets. For example, Dagbay et al. [52] found that binding of mAb SRK-015 elicits extensive changes on its target protein myostatin (Figure 7). In addition to increased protection at the epitope at the end of the arms, there was a large degree of protection at the center of the protein, particularly around the furin cleavage site. This long-range allosteric effect provides a rationale for how SRK-015 inhibits the activation of myostatin, inhibiting access to the furin cleavage site. Similar insights into how antibodies are able to protect from various pathogens have been elucidated by HDX-MS including diptheria toxin [53], Japanese encephalovirus envelope protein [54], *Neisseria Meningitis* adhesin A [55,56], S*taphylococcus aureus* manganese transporter protein [32], HIV envelope glycoprotein [43,57], influenza hemagglutinin [58,59], Malaria P vivax Duffy binding protein, [60,61] and Dengue Virus [62]. A recent nanoparticle vaccine against SARS-CoV-2 utilized HDX-MS to elucidate binding epitopes of known neutralizing mAbs [63]. The ability to detail the mechanisms of neutralization, in part from HDX-MS input, has paved the way for advanced therapeutic and vaccination approaches for a multitude of diseases.

When HDX-MS is used to characterize a protein-protein interface with no prior structural information, allosteric effects can become a complicating factor since the allosteric changes can be misinterpreted as part of a binding interface [64,65]. A common strategy is to use HDX-MS to identify regions of change in a protein, then use targeted site-directed mutagenesis to probe the involvement of the regions shown by HDX-MS. If mutation prevents binding, as compared to decoupling allosteric effects, the non-binding mutants can be identified in binding assays (usually not HDX-MS). HDX-MS is also often combined with other approaches such as chemical crosslinking to help better define interaction surfaces [66]. It has been observed that shorter deuterium labeling times (< 5 min) are more likely to reveal changes associated solvent accessibility and protein interaction surfaces, whereas longer time points can reveal allosteric changes at structured regions and other global structural effects [50,67-70]. A “kinetic” millisecond HDX workflow was recently proposed as an alternative approach to differentiate direct binding from allosteric changes [71]. Instead of pre-incubating the protein with the antibody prior to exchange, the

deuterium labeling step is combined with the antibody binding step. Using a time-resolved ESI system on a chip, rapid in-line exchange and quenching on short timescales (as low as 200 msec) were achieved [72]. Only the changes at the direct binding interface were observed by the kinetic HDX-MS approach as compared to a pre-incubated ('equilibrium') complex. The study suggests that HDX-MS experiments at very short timescales during the binding event may help specifically identify surfaces directly involved in the binding interface.

HDX-MS also serves as a useful tool for assessing interactions with polyclonal antibodies. Mapping polyclonal antibody response provides critical insight into the immune response, but they are much more challenging to characterize than mAbs as the mixtures of antibodies are present at different concentrations, bind at different rates, and may be cross-reactive [73]. To address these challenges, Zhang et al. digested and purified Fab fragments from a polyclonal mixture before analyzing the sample using HDX [74]. The experiments revealed and localized four epitopes relevant to the measured immune response to nut allergen Ana o 2. In other work, HDX-MS was used to track epitope specificity and diversity in polyclonal serum following immunizations [75]. To get around the issue of matrix effects associated with the complexity of serum, an affinity purification step was incorporated into the workflow to fractionate only the antigen-reactive antibody population. A similar study compared the binding of various mAbs to human cystatin C with that obtained from polyclonal serum and used a similar enrichment procedure to fractionate only the antigen-reactive antibody population [76]. These few examples already show the potential of HDX-MS to aid in mapping epitopes of complex polyclonal responses.

Beyond epitope mapping, HDX-MS continues to be utilized for studying protein-protein interactions in complex protein systems and revealing mechanisms of activation in a range of systems including: Clotting factors [69,77-79], metabolic enzymes [48,80-89], heat shock proteins [65,90,91] and other chaperones [92-99], signaling complexes [100-111], and complexes exclusively residing in membranes [112]. HDX-MS has also been extensively used to study interactions between proteins with nucleic acids, including activation of transcription factors [113-122]. Other notable applications are the characterization of ligands with weak affinity such as metals [49,122-127] or carbohydrates [33,128]. For proteins with multiple distinct ligand binding sites, it has been shown that by performing a concentration series it is possible to characterize individual interactions [129,130]. The strength of HDX-MS to provide detailed insight into such a wide range of interactions continues to drive its use to study increasingly complex biological systems.

1.4 Staph enterotoxin B (SEB) epitopes, dynamics, and allostery

Staphylococcal enterotoxins (SEs) cause food poisoning-like symptoms and are lethal in microgram amounts. Multiple species of SEs, often denoted through the nomenclature "*Staph* Enterotoxin [insert letter A-U]," are part of a family of fever-inducing Superantigens (SAs). *Staphylococcus aureus (S. aureus)* is a Gram-positive opportunistic bacterium that has been found to colonize the nasal mucosa of up to 40% of humans [131]. SEs are persistent in 80% of S. aureus genes, and a study found the median number of SE genes in a given species to be five, four an alarming fact given that horizontal transfer between strains is common [132].

SEs hijack what is typically a deliberate response by the adaptive immune system. Under normal circumstances, harmful pathogens that evade the innate immune system are ingested and digested by professional Antigen Presenting Cells (APC), and a fragment of the pathogen is displayed on an extracellular receptor, the Major Histocompatibility Complex class II (MHC II). The unique molecular surface created by the pathogen fragment and MHC II binding cleft is recognized by specific T-Cell Receptors (TCRs) expressed on CD4+ T-Cells—an exceedingly calculated event. Within any given individual exists a diverse repertoire of the molecular surfaces on TCRs that have come from VDJ recombination. MHC II molecules also generate a vast number of unique surfaces as a result of being polygenic, polymorphic, and co-dominantly expressed as well as being able to grasp a diverse collection of fragmented peptides. When these molecules bind, it sets off a release of cytokines that triggers T-Cell proliferation in order to terminate the unwanted invader.

SEs elicit profound immune responses via the bridging of an MHC II with a TCR (Figure 8) [133]. Given SEs are typically consumed orally from contaminated food, it comes as no surprise that injury is gastrointestinal (GI) [134]. SEs have been found to cross the gastrointestinal mucous membrane as quickly as fifteen minutes in rat models [135]. GI injury occurs through acute inflammation at the site of MHC II molecules expressed on subepithelial myofibroblasts [136]. SEs bind regions of the MHC II that are common across large populations of the receptors, regions irrelevant to normal immune activation. While a typical adaptive immune response would rely on specific molecular recognition on binding surfaces, SEs bind to MHC II and TCR regions that are conserved across large populations of the receptors. The bridging of these immune molecules triggers a cytokine storm capable of hyperactivating up to 30% of the whole T-Cell population [137]. The tri-molecular interaction mediated by SEB binding causes the release of proinflammatory cytokines, including IFN-gamma, TNF-α, IL-1β, IL-6, and IL-8, species capable of causing superantigen-mediated acute inflammation and shock [138-140]. The extensive inflammation at the intestinal

epithelial lead to increased permeability through decreased expression of tight junction proteins. As a result, antigens increasingly flow through the disrupted mucosal layer, further perpetuating SEs effects. Additionally, the increased T-Cell proliferation eventually leads to widespread apoptosis and anergy, the inability elicit a normal immune response against an antigen [141].

Due to its high potency and potential use as a biological warfare agent when aerosolized, *Staphylococcal* enterotoxin B (SEB) has become a research focus [142-144]. SEB has been crystalized alone [144,145], in complex with the MHC II [146], and with the TCR [147]. Relative to other SEs, SEB mainly stimulates cytokine release, a fact supported by crystal structures revealing the proximity the MHC II and TCR have with each other when both are in complex with SEB (Figure 9) [148]. The physical properties of SEB confer its toxicity. SEB contains 239 amino acids while weighing 28kDa. It is resistant to alcohol and stable at high heat. While the robustness innate to SEB makes it incredibly toxic, the same properties make it uniquely well suited for study and for use as a model system for assay development.

1.5 Figures

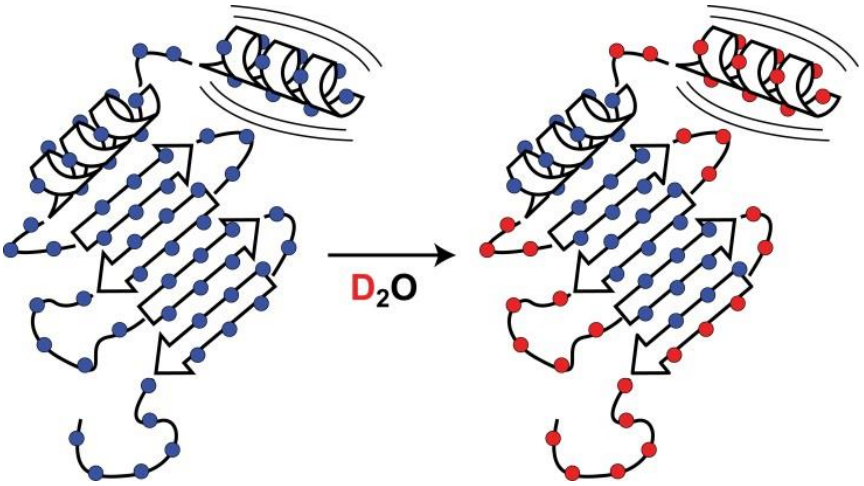

Figure 1. Backbone amide hydrogens (blue) exchange with deuterium (red) at differing rates depending on "ordering" of residue. Order structures like helices or sheets exchange slower or no at all, while disordered loops exchange quickly. The probing of solvent accessibility is sensitive to minute changes. (Image courtesy of Mike Guttman).

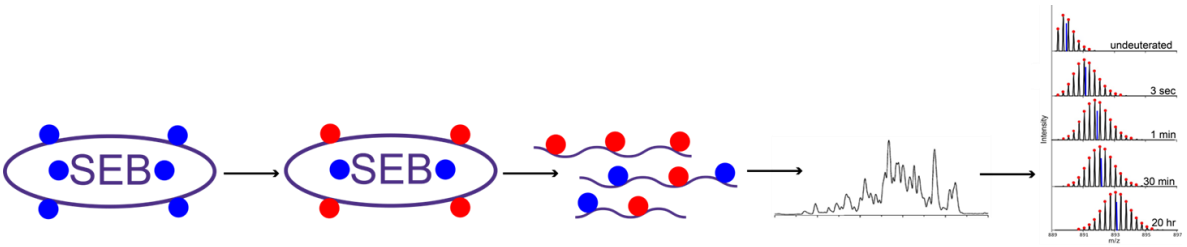

Figure 2. HDX example workflow with *Staph* enterotoxin B (SEB) protein.

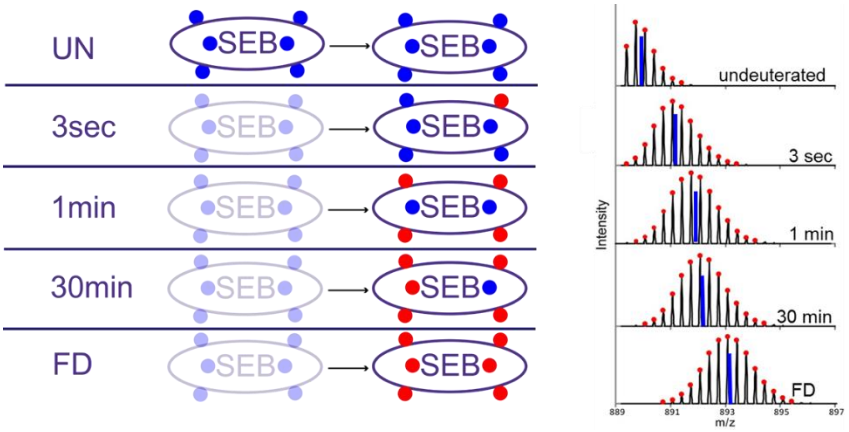

Figure 3. Differential uptake of backbone amide hydrogens over time reveals structural features. Uptake plot at right show deuterium envelope with blue line indicating centroid value often used to measure "uptake" as a single value.

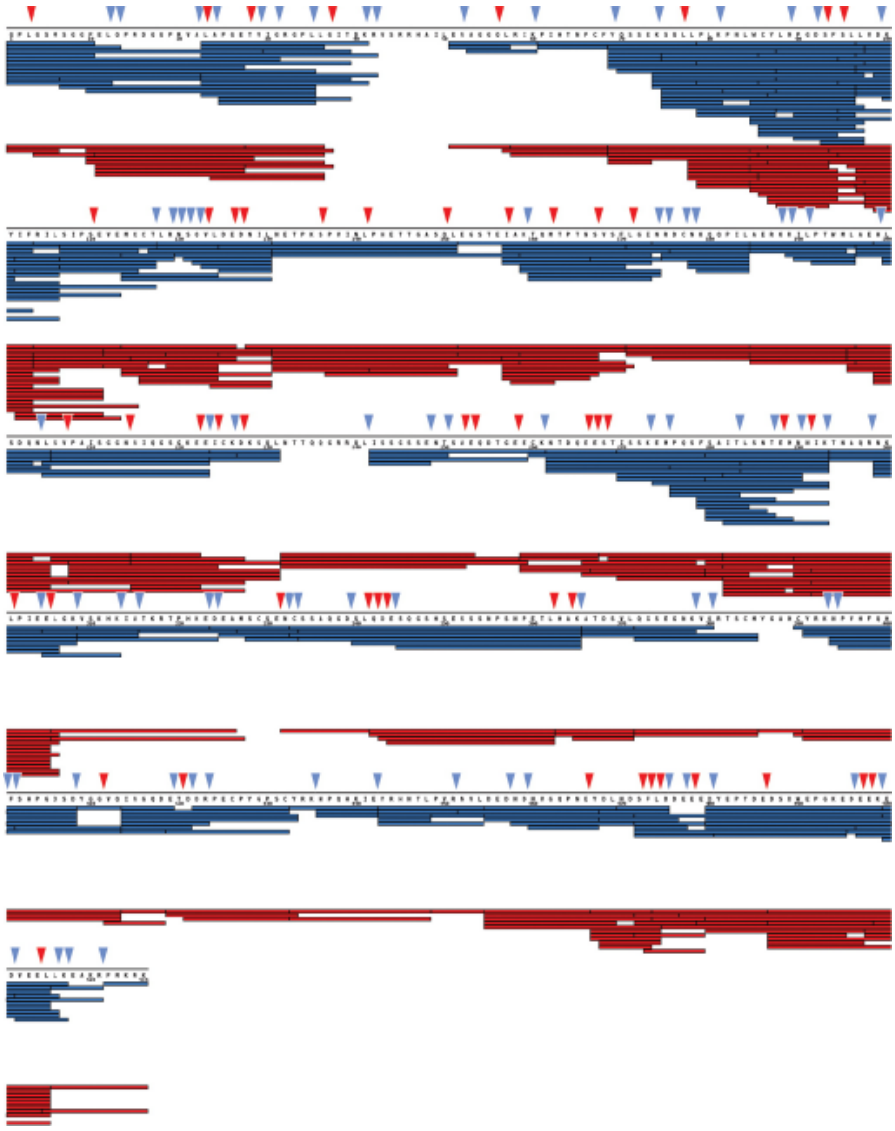

Figure 4. Comparison of peptides for Aprataxin and PNKP-Like Factor (APLF). Each bar under the primary sequence shows a peptide from either pepsin (red) or NepII (blue) digest. Sites indicated with triangles show sites that are uniquely cleaved by pepsin (red) or NepII (blue). Reproduced with permission from Yang et al. [137]. (Copyright 2015 American Chemical Society).

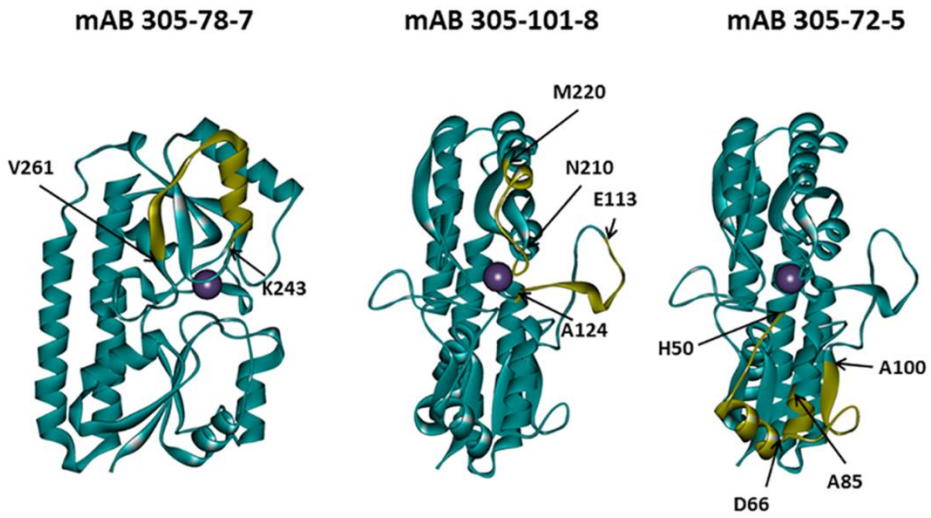

Figure 5. Epitope mapping of three monoclonal antibodies to *Staphylococcus aureus* manganese transporter protein (MntC). 3 different views of MntC. Regions in yellow exhibited slowed exchange when bound to the antibody. (Figure adapted with permissions from Gribenko et al.).

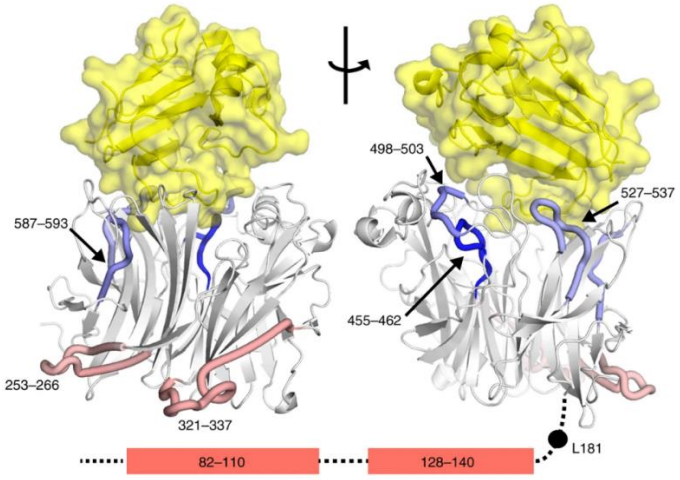

Figure 6. Allosteric changes observed in the Nipah Virus G ectodomain upon binding ephrinB2. Regions of the G ectodomain that do not change (white), become more protected (blue), or less protected (red) are indicated on the structure. The N-terminal stalk helices that also become less protected are shown in the bottom with their predicted positions. The position of EprhinB2 is shown in yellow. (Figure adapted from Wong et al.).

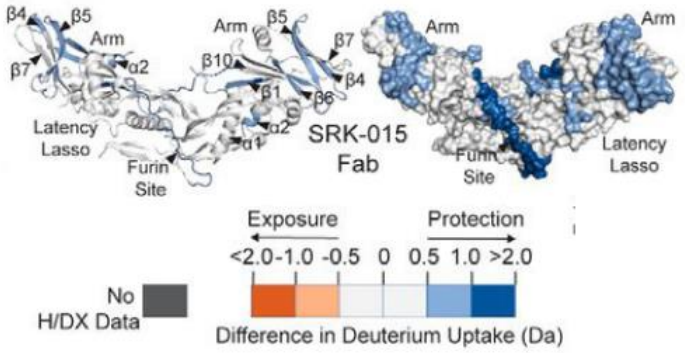

Figure 7. Mechanism of action of Mab SRK-015 on the inhibition of myostatin. Antibody binding to the distal arm of myostatin elicits allosteric effects throughout the protein including protection around the furin cleavage site to limit its accessibility for proteolytic cleavage. (Figure adapted from Dagbay et al.).

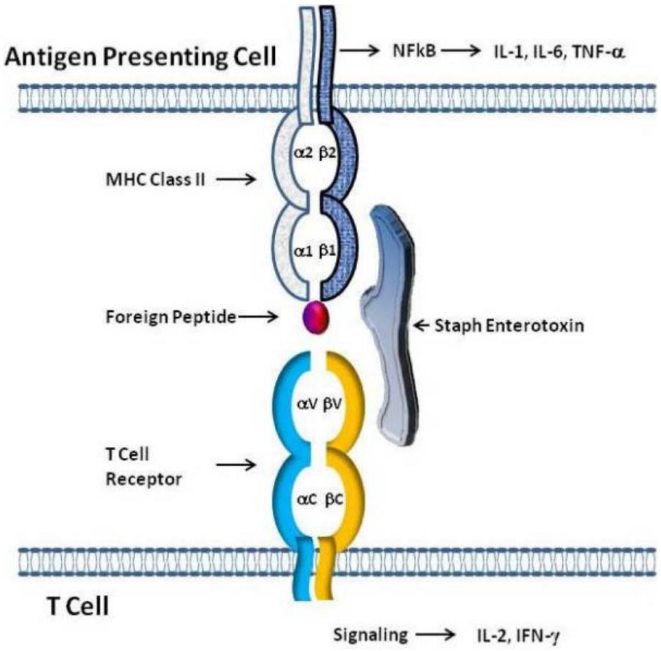

Figure 8. Model of SE interaction with T cell Receptors and class II MHC Molecules. The simultaneous binding of SEs outside of the antigen binding pocket of class II MHC on antigen presenting cells (APC) and to T cell receptors expressing certain Vβ elements allows SEs to act as superantigens. The tripartite interaction of class II MHC:SEs:TcR results in the stimulation of both APC and T cells leading to the production of cytokines by both cell types. (Figure adapted from Pinchuk et al.).

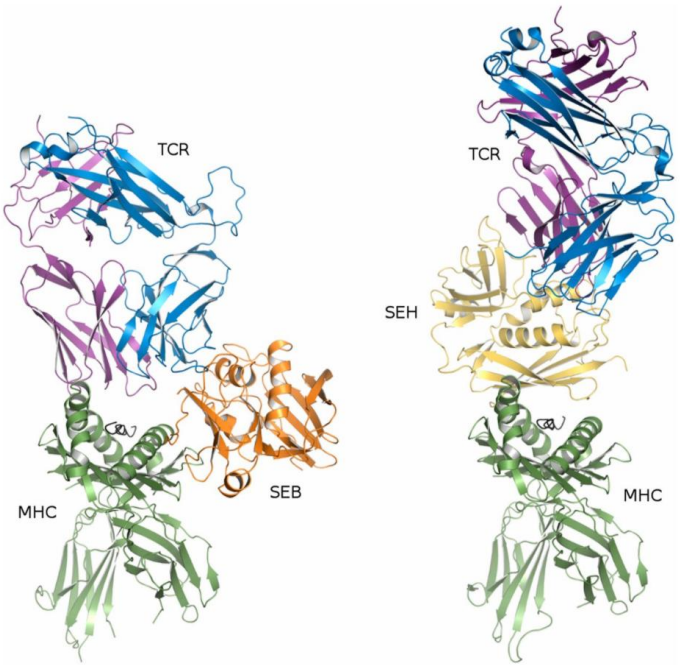

Figure 9. Comparison of the ternary TCR–SAg–MHC complexes with SEB and SEH. All proteins are shown in ribbon representation. SEB (left panel) is shown in orange and SEH (right panel) in yellow, the TCR α-chain in purple, the TCR β-chain in blue, and MHC class II in green. (Figure adapted from Rödström et al.).

1.6 References

1 Englander, S. W. Hydrogen exchange and mass spectrometry: A historical perspective. *J Am Soc Mass Spectrom* **17**, 1481-1489 (2006). https://doi.org:10.1016/j.jasms.2006.06.006

2 Rosa, J. J. & Richards, F. M. An experimental procedure for increasing the structural resolution of chemical hydrogen-exchange measurements on proteins: application to ribonuclease S peptide. *J Mol Biol* **133**, 399-416 (1979). https://doi.org:10.1016/0022-2836(79)90400-5

3 Zhang, Z. & Smith, D. L. Determination of amide hydrogen exchange by mass spectrometry: a new tool for protein structure elucidation. *Protein Science* **2**, 522-531 (1993). https://doi.org:10.1002/pro.5560020404

4 Brezski, R. J. & Jordan, R. E. Cleavage of IgGs by proteases associated with invasive diseases: an evasion tactic against host immunity? *mAbs* **2**, 212-220 (2010). https://doi.org:10.4161/mabs.2.3.11780

5 Hamuro, Y. & Coales, S. J. Optimization of Feasibility Stage for Hydrogen/Deuterium Exchange Mass Spectrometry. *J Am Soc Mass Spectrom* **29**, 623-629 (2018). https://doi.org:10.1007/s13361-017-1860-3

6 Möller, I. R. *et al.* Improving the Sequence Coverage of Integral Membrane Proteins during Hydrogen/Deuterium Exchange Mass Spectrometry Experiments. *Analytical Chemistry* **91**, 10970-10978 (2019). https://doi.org:10.1021/acs.analchem.9b00973

7 Yang, M. *et al.* Recombinant Nepenthesin II for Hydrogen/Deuterium Exchange Mass Spectrometry. *Analytical Chemistry* **87**, 6681-6687 (2015). https://doi.org:10.1021/acs.analchem.5b00831

8 Cravello, L., Lascoux, D. & Forest, E. Use of different proteases working in acidic conditions to improve sequence coverage and resolution in hydrogen/deuterium exchange of large proteins. *Rapid Commun Mass Spectrom* **17**, 2387-2393 (2003). https://doi.org:10.1002/rcm.1207

9 Giansanti, P., Tsiatsiani, L., Low, T. Y. & Heck, A. J. R. Six alternative proteases for mass spectrometry–based proteomics beyond trypsin. *Nature Protocols* **11**, 993-1006 (2016). https://doi.org:10.1038/nprot.2016.057

10 Zhang, H. M. *et al.* Enhanced digestion efficiency, peptide ionization efficiency, and sequence resolution for protein hydrogen/deuterium exchange monitored by Fourier transform ion cyclotron resonance mass spectrometry. *Anal Chem* **80**, 9034-9041 (2008). https://doi.org:10.1021/ac801417d

11 Mayne, L. *et al.* Many overlapping peptides for protein hydrogen exchange experiments by the fragment separation-mass spectrometry method. *Journal of the American Society for Mass Spectrometry* **22**, 1898-1905 (2011). https://doi.org:10.1007/s13361-011-0235-4

12 Powers, J. C., Harley, A. D. & Myers, D. V. Subsite specificity of porcine pepsin. *Adv Exp Med Biol* **95**, 141-157 (1977). https://doi.org:10.1007/978-1-4757-0719-9_9

13 Hamuro, Y., Coales, S. J., Molnar, K. S., Tuske, S. J. & Morrow, J. A. Specificity of immobilized porcine pepsin in H/D exchange compatible conditions. *Rapid Commun Mass Spectrom* **22**, 1041-1046 (2008). https://doi.org:10.1002/rcm.3467

14 Zheng, J. *et al.* Comparative Analysis of Cleavage Specificities of Immobilized Porcine Pepsin and Nepenthesin II under Hydrogen/Deuterium Exchange Conditions. *Analytical Chemistry* **92**, 11018-11028 (2020). https://doi.org:10.1021/acs.analchem.9b05694

15 Ahn, J., Cao, M.-J., Yu, Y. Q. & Engen, J. R. Accessing the reproducibility and specificity of pepsin and other aspartic proteases. *Biochim Biophys Acta* **1834**, 1222-1229 (2013). https://doi.org:10.1016/j.bbapap.2012.10.003

16 Brier, S. *et al.* Purification and characterization of pepsins A1 and A2 from the Antarctic rock cod Trematomus bernacchii. *Febs j* **274**, 6152-6166 (2007). https://doi.org:10.1111/j.1742-4658.2007.06136.x

17 Papanastasiou, M. *et al.* Chasing Tails: Cathepsin-L Improves Structural Analysis of Histones by HX-MS. *Mol Cell Proteomics* **18**, 2089-2098 (2019). https://doi.org:10.1074/mcp.RA119.001325

18 Rey, M. *et al.* Nepenthesin from monkey cups for hydrogen/deuterium exchange mass spectrometry. *Molecular & cellular proteomics : MCP* **12**, 464-472 (2013). https://doi.org:10.1074/mcp.M112.025221

19 Kadek, A. *et al.* Aspartic protease nepenthesin-1 as a tool for digestion in hydrogen/deuterium exchange mass spectrometry. *Anal Chem* **86**, 4287-4294 (2014). https://doi.org:10.1021/ac404076j

20 Tsiatsiani, L., Akeroyd, M., Olsthoorn, M. & Heck, A. J. R. Aspergillus niger Prolyl Endoprotease for Hydrogen-Deuterium Exchange Mass Spectrometry and Protein Structural Studies. *Anal Chem* **89**, 7966-7973 (2017). https://doi.org:10.1021/acs.analchem.7b01161

21 Hamuro, Y. & Zhang, T. High-Resolution HDX-MS of Cytochrome c Using Pepsin/Fungal Protease Type XIII Mixed Bed Column. *J Am Soc Mass Spectrom* **30**, 227-234 (2019). https://doi.org:10.1007/s13361-018-2087-7

22 Nirudodhi, S. N., Sperry, J. B., Rouse, J. C. & Carroll, J. A. Application of Dual Protease Column for HDX-MS Analysis of Monoclonal Antibodies. *J Pharm Sci* **106**, 530-536 (2017). https://doi.org:10.1016/j.xphs.2016.10.023

23 Mullahoo, J. *et al.* Dual protease type XIII/pepsin digestion offers superior resolution and overlap for the analysis of histone tails by HX-MS. *Methods* **184**, 135-140 (2020). https://doi.org:10.1016/j.ymeth.2020.01.016

24 Ehring, H. Hydrogen exchange/electrospray ionization mass spectrometry studies of structural features of proteins and protein/protein interactions. *Anal Biochem* **267**, 252-259 (1999). https://doi.org:10.1006/abio.1998.3000

25 Wang, L., Pan, H. & Smith, D. L. Hydrogen exchange-mass spectrometry: optimization of digestion conditions. *Mol Cell Proteomics* **1**, 132-138 (2002). https://doi.org:10.1074/mcp.m100009-mcp200

26 Busby, S. A., Chalmers, M. J. & Griffin, P. R. Improving digestion efficiency under H/D exchange conditions with activated pepsinogen coupled columns. *International Journal of Mass Spectrometry* **259**, 130-139 (2007). https://doi.org:https://doi.org/10.1016/j.ijms.2006.08.006

27 Ahn, J., Jung, M. C., Wyndham, K., Yu, Y. Q. & Engen, J. R. Pepsin immobilized on high-strength hybrid particles for continuous flow online digestion at 10,000 psi. *Analytical chemistry* **84**, 7256-7262 (2012). https://doi.org:10.1021/ac301749h

28 Sun, H. *et al.* Research advances in hydrogen-deuterium exchange mass spectrometry for protein epitope mapping. *Anal Bioanal Chem* **413**, 2345-2359 (2021). https://doi.org:10.1007/s00216-020-03091-9

29 Hager-Braun, C. & Tomer, K. B. Determination of protein-derived epitopes by mass spectrometry. *Expert Rev Proteomics* **2**, 745-756 (2005). https://doi.org:10.1586/14789450.2.5.745

30 Vance, D. J. *et al.* High-Resolution Epitope Positioning of a Large Collection of Neutralizing and Nonneutralizing Single-Domain Antibodies on the Enzymatic and Binding Subunits of Ricin Toxin. *Clin Vaccine Immunol* **24**, e00236-00217 (2017). https://doi.org:10.1128/CVI.00236-17

31 Zhang, Q. *et al.* Epitope Mapping by HDX-MS Elucidates the Surface Coverage of Antigens Associated with High Blocking Efficiency of Antibodies to Birch Pollen Allergen. *Anal Chem* **90**, 11315-11323 (2018). https://doi.org:10.1021/acs.analchem.8b01864

32 Gribenko, A. V. *et al.* High Resolution Mapping of Bactericidal Monoclonal Antibody Binding Epitopes on Staphylococcus aureus Antigen MntC. *PLOS Pathogens* **12**, e1005908 (2016). https://doi.org:10.1371/journal.ppat.1005908

33 Zhang, J. *et al.* Localizing Carbohydrate Binding Sites in Proteins Using Hydrogen/Deuterium Exchange Mass Spectrometry. *Journal of The American Society for Mass Spectrometry* **27**, 83-90 (2016). https://doi.org:10.1007/s13361-015-1263-2

34 Kochert, B. A., Iacob, R. E., Wales, T. E., Makriyannis, A. & Engen, J. R. Hydrogen-Deuterium Exchange Mass Spectrometry to Study Protein Complexes. *Methods Mol Biol* **1764**, 153-171 (2018). https://doi.org:10.1007/978-1-4939-7759-8_10

35 Mandell, J. G., Baerga-Ortiz, A., Akashi, S., Takio, K. & Komives, E. A. Solvent accessibility of the thrombin-thrombomodulin interface. *J Mol Biol* **306**, 575-589 (2001). https://doi.org:10.1006/jmbi.2000.4416

36 Percy, A. J., Rey, M., Burns, K. M. & Schriemer, D. C. Probing protein interactions with hydrogen/deuterium exchange and mass spectrometry-a review. *Anal Chim Acta* **721**, 7-21 (2012). https://doi.org:10.1016/j.aca.2012.01.037

37 Jørgensen, T. J. D., Gårdsvoll, H., Danø, K., Roepstorff, P. & Ploug, M. Dynamics of Urokinase Receptor Interaction with Peptide Antagonists Studied by Amide Hydrogen Exchange and Mass Spectrometry. *Biochemistry* **43**, 15044-15057 (2004). https://doi.org:10.1021/bi048706j

38 Guttman, M., Kahn, M., Garcia, N. K., Hu, S. L. & Lee, K. K. Solution structure, conformational dynamics, and CD4-induced activation in full-length, glycosylated, monomeric HIV gp120. *J Virol* **86**, 8750-8764 (2012). https://doi.org:10.1128/jvi.07224-11

39 Leurs, U. *et al.* Dissecting the binding mode of low affinity phage display peptide ligands to protein targets by hydrogen/deuterium exchange coupled to mass spectrometry. *Analytical chemistry* **86**, 11734-11741 (2014). https://doi.org:10.1021/ac503137u

40 Zhang, Z. & Vachet, R. W. Kinetics of Protein Complex Dissociation Studied by Hydrogen/Deuterium Exchange and Mass Spectrometry. *Analytical chemistry* **87**, 11777-11783 (2015). https://doi.org:10.1021/acs.analchem.5b03123

41 Wildes, D. & Marqusee, S. Hydrogen exchange and ligand binding: ligand-dependent and ligand-independent protection in the Src SH3 domain. *Protein science : a publication of the Protein Society* **14**, 81-88 (2005). https://doi.org:10.1110/ps.04990205

42 Sowole, M. A. & Konermann, L. Effects of Protein–Ligand Interactions on Hydrogen/Deuterium Exchange Kinetics: Canonical and Noncanonical Scenarios. *Analytical Chemistry* **86**, 6715-6722 (2014). https://doi.org:10.1021/ac501849n

43 Guttman, M. *et al.* Antibody potency relates to the ability to recognize the closed, pre-fusion form of HIV Env. *Nat Commun* **6**, 6144 (2015). https://doi.org:10.1038/ncomms7144

44 Engen, J. R. Analysis of protein complexes with hydrogen exchange and mass spectrometry. *Analyst* **128**, 623-628 (2003). https://doi.org:10.1039/b212800b

45 Deng, B., Lento, C. & Wilson, D. J. Hydrogen deuterium exchange mass spectrometry in biopharmaceutical discovery and development - A review. *Anal Chim Acta* **940**, 8-20 (2016). https://doi.org:10.1016/j.aca.2016.08.006

46 Ahn, J. & Engen, J. R. The use of hydrogen/deuterium exchange mass spectrometry in epitope mapping. *Chimica Oggi* **31**, 25-28 (2013).

47 Konermann, L. Heavy lessons in protein allostery. *Nat Struct Mol Biol* **23**, 511-512 (2016). https://doi.org:10.1038/nsmb.3234

48 Sowole, M. A., Simpson, S., Skovpen, Y. V., Palmer, D. R. J. & Konermann, L. Evidence of Allosteric Enzyme Regulation via Changes in Conformational Dynamics: A Hydrogen/Deuterium Exchange Investigation of Dihydrodipicolinate Synthase. *Biochemistry* **55**, 5413-5422 (2016). https://doi.org:10.1021/acs.biochem.6b00764

49 Zhang, J., Li, J., Craig, T. A., Kumar, R. & Gross, M. L. Hydrogen–Deuterium Exchange Mass Spectrometry Reveals Calcium Binding Properties and Allosteric Regulation of Downstream Regulatory Element Antagonist Modulator (DREAM). *Biochemistry* **56**, 3523-3530 (2017). https://doi.org:10.1021/acs.biochem.7b00100

50 Ramirez-Sarmiento, C. A. & Komives, E. A. Hydrogen-deuterium exchange mass spectrometry reveals folding and allostery in protein-protein interactions. *Methods* **144**, 43-52 (2018). https://doi.org:10.1016/j.ymeth.2018.04.001

51 Wong, J. J. W. *et al.* Monomeric ephrinB2 binding induces allosteric changes in Nipah virus G that precede its full activation. *Nat Commun* **8**, 781 (2017). https://doi.org:10.1038/s41467-017-00863-3

52 Dagbay, K. B. *et al.* Structural basis of specific inhibition of extracellular activation of pro- or latent myostatin by the monoclonal antibody SRK-015. *Journal of Biological Chemistry* **295**, 5404-5418 (2020). https://doi.org:https://doi.org/10.1074/jbc.RA119.012293

53 Zhu, S. *et al.* Hydrogen–Deuterium Exchange Epitope Mapping Reveals Distinct Neutralizing Mechanisms for Two Monoclonal Antibodies against Diphtheria Toxin. *Biochemistry* **58**, 646-656 (2019). https://doi.org:10.1021/acs.biochem.8b01123

54 Fernandez, E. *et al.* Mouse and Human Monoclonal Antibodies Protect against Infection by Multiple Genotypes of Japanese Encephalitis Virus. *mBio* **9**, e00008-00018 (2018). https://doi.org:10.1128/mBio.00008-18

55 Malito, E. *et al.* Structure of the meningococcal vaccine antigen NadA and epitope mapping of a bactericidal antibody. *Proc Natl Acad Sci U S A* **111**, 17128-17133 (2014). https://doi.org:10.1073/pnas.1419686111

56 Grauslund, L. R., Calvaresi, V., Pansegrau, W., Norais, N. & Rand, K. D. Epitope and Paratope Mapping by HDX-MS Combined with SPR Elucidates the Difference in Bactericidal Activity of Two Anti-NadA Monoclonal Antibodies. *J Am Soc Mass Spectrom* **32**, 1575–1582 (2021). https://doi.org:10.1021/jasms.0c00431

57 Kim, M. *et al.* Antibody mechanics on a membrane-bound HIV segment essential for GP41-targeted viral neutralization. *Nat Struct Mol Biol* **18**, 1235-1243 (2011). https://doi.org:10.1038/nsmb.2154

58 Thornburg, N. J. *et al.* H7N9 influenza virus neutralizing antibodies that possess few somatic mutations. *J Clin Invest* **126**, 1482-1494 (2016). https://doi.org:10.1172/JCI85317

59 Puchades, C. *et al.* Epitope mapping of diverse influenza Hemagglutinin drug candidates using HDX-MS. *Scientific Reports* **9**, 4735 (2019). https://doi.org:10.1038/s41598-019-41179-0

60 Chen, E. *et al.* Broadly neutralizing epitopes in the Plasmodium vivax vaccine candidate Duffy Binding Protein. *Proc Natl Acad Sci U S A* **113**, 6277-6282 (2016). https://doi.org:10.1073/pnas.1600488113

61 Urusova, D. *et al.* Structural basis for neutralization of Plasmodium vivax by naturally acquired human antibodies that target DBP. *Nat Microbiol* **4**, 1486-1496 (2019). https://doi.org:10.1038/s41564-019-0461-2

62 Lim, X. X. *et al.* Epitope and Paratope Mapping Reveals Temperature-Dependent Alterations in the Dengue-Antibody Interface. *Structure* **25**, 1391-1402.e1393 (2017). https://doi.org:10.1016/j.str.2017.07.007

63 Walls, A. C. *et al.* Elicitation of Potent Neutralizing Antibody Responses by Designed Protein Nanoparticle Vaccines for SARS-CoV-2. *Cell* **183**, 1367-1382.e1317 (2020). https://doi.org:10.1016/j.cell.2020.10.043

64 Pandit, D. *et al.* Mapping of discontinuous conformational epitopes by amide hydrogen/deuterium exchange mass spectrometry and computational docking. *J Mol Recognit* **25**, 114-124 (2012). https://doi.org:10.1002/jmr.1169

65 Chandramohan, A. *et al.* Predicting Allosteric Effects from Orthosteric Binding in Hsp90-Ligand Interactions: Implications for Fragment-Based Drug Design. *PLoS Comput Biol* **12**, e1004840 (2016). https://doi.org:10.1371/journal.pcbi.1004840

66 Zhang, M. M. *et al.* Epitope and Paratope Mapping of PD-1/Nivolumab by Mass Spectrometry-Based Hydrogen-Deuterium Exchange, Cross-linking, and Molecular Docking. *Anal Chem* **92**, 9086-9094 (2020). https://doi.org:10.1021/acs.analchem.0c01291

67 Mandell, J. G., Falick, A. M. & Komives, E. A. Identification of protein-protein interfaces by decreased amide proton solvent accessibility. *Proc Natl Acad Sci U S A* **95**, 14705-14710 (1998). https://doi.org:10.1073/pnas.95.25.14705

68 Dharmasiri, K. & Smith, D. L. Mass spectrometric determination of isotopic exchange rates of amide hydrogens located on the surfaces of proteins. *Anal Chem* **68**, 2340-2344 (1996). https://doi.org:10.1021/ac9601526

69 Peacock, R. B., Davis, J. R., Markwick, P. R. L. & Komives, E. A. Dynamic Consequences of Mutation of Tryptophan 215 in Thrombin. *Biochemistry* **57**, 2694-2703 (2018). https://doi.org:10.1021/acs.biochem.8b00262

70 Truhlar, S. M. E., Croy, C. H., Torpey, J. W., Koeppe, J. R. & Komives, E. A. Solvent Accessibility of Protein Surfaces by Amide H/2H Exchange MALDI-TOF Mass Spectrometry. *Journal of the American Society for Mass Spectrometry* **17**, 1490-1497 (2006). https://doi.org:10.1016/j.jasms.2006.07.023

71 Deng, B. *et al.* Suppressing allostery in epitope mapping experiments using millisecond hydrogen / deuterium exchange mass spectrometry. *mAbs* **9**, 1327-1336 (2017). https://doi.org:10.1080/19420862.2017.1379641

72 Resetca, D. & Wilson, D. J. Characterizing rapid, activity-linked conformational transitions in proteins via sub-second hydrogen deuterium exchange mass spectrometry. *The FEBS Journal* **280**, 5616-5625 (2013). https://doi.org:https://doi.org/10.1111/febs.12332

73 Donnarumma, D., Faleri, A., Costantino, P., Rappuoli, R. & Norais, N. The role of structural proteomics in vaccine development: recent advances and future prospects. *Expert Rev Proteomics* **13**, 55-68 (2016). https://doi.org:10.1586/14789450.2016.1121113

74 Zhang, Q. *et al.* Rapid screening for potential epitopes reactive with a polycolonal antibody by solution-phase H/D exchange monitored by FT-ICR mass spectrometry. *J Am Soc Mass Spectrom* **24**, 1016-1025 (2013). https://doi.org:10.1007/s13361-013-0644-7

75 Yang, D. *et al.* Efficient Qualitative and Quantitative Determination of Antigen-induced Immune Responses. *J Biol Chem* **291**, 16361-16374 (2016). https://doi.org:10.1074/jbc.M116.736660

76 Pradzinska, M. *et al.* Application of amide hydrogen/deuterium exchange mass spectrometry for epitope mapping in human cystatin C. *Amino Acids* **48**, 2809-2820 (2016). https://doi.org:10.1007/s00726-016-2316-y

77 Bar Barroeta, A. *et al.* Hydrogen-deuterium exchange mass spectrometry highlights conformational changes induced by factor XI activation and binding of factor IX to factor XIa. *Journal of Thrombosis and Haemostasis* **17**, 2047-2055 (2019). https://doi.org:https://doi.org/10.1111/jth.14632

78 Koeppe, J. R., Seitova, A., Mather, T. & Komives, E. A. Thrombomodulin tightens the thrombin active site loops to promote protein C activation. *Biochemistry* **44**, 14784-14791 (2005). https://doi.org:10.1021/bi0510577

79 Handley, L. D., Treuheit, N. A., Venkatesh, V. J. & Komives, E. A. Thrombomodulin Binding Selects the Catalytically Active Form of Thrombin. *Biochemistry* **54**, 6650-6658 (2015). https://doi.org:10.1021/acs.biochem.5b00825

80 Karamitros, C. S. *et al.* Conformational Dynamics Contribute to Substrate Selectivity and Catalysis in Human Kynureninase. *ACS Chem Biol* **15**, 3159-3166 (2020). https://doi.org:10.1021/acschembio.0c00676

81 Thompson, E. J., Paul, A., Iavarone, A. T. & Klinman, J. P. Identification of Thermal Conduits That Link the Protein-Water Interface to the Active Site Loop and Catalytic Base in Enolase. *J Am Chem Soc* **143**, 785-797 (2021). https://doi.org:10.1021/jacs.0c09423

82 Gao, S. *et al.* Hydrogen-Deuterium Exchange within Adenosine Deaminase, a TIM Barrel Hydrolase, Identifies Networks for Thermal Activation of Catalysis. *J Am Chem Soc* **142**, 19936-19949 (2020). https://doi.org:10.1021/jacs.0c07866

83 Hu, S. *et al.* Biophysical Characterization of a Disabled Double Mutant of Soybean Lipoxygenase: The "Undoing" of Precise Substrate Positioning Relative to Metal Cofactor and an Identified Dynamical Network. *J Am Chem Soc* **141**, 1555-1567 (2019). https://doi.org:10.1021/jacs.8b10992

84 Zhang, J., Balsbaugh, J. L., Gao, S., Ahn, N. G. & Klinman, J. P. Hydrogen deuterium exchange defines catalytically linked regions of protein flexibility in the catechol O-methyltransferase reaction. *Proc Natl Acad Sci U S A* **117**, 10797-10805 (2020). https://doi.org:10.1073/pnas.1917219117

85 Offenbacher, A. R., Iavarone, A. T. & Klinman, J. P. Hydrogen-deuterium exchange reveals long-range dynamical allostery in soybean lipoxygenase. *J Biol Chem* **293**, 1138-1148 (2018). https://doi.org:10.1074/jbc.M117.817197
86 Tyukhtenko, S. *et al.* Conformational gating, dynamics and allostery in human monoacylglycerol lipase. *Scientific Reports* **10**, 18531 (2020). https://doi.org:10.1038/s41598-020-75497-5
87 Corless, E. I. *et al.* The flexible N-terminus of BchL autoinhibits activity through interaction with its [4Fe-4S] cluster and released upon ATP binding. *J Biol Chem* **296**, 100107 (2021). https://doi.org:10.1074/jbc.RA120.016278
88 Tsirigotaki, A., Elzen, R. V., Veken, P. V. D., Lambeir, A.-M. & Economou, A. Dynamics and ligand-induced conformational changes in human prolyl oligopeptidase analyzed by hydrogen/deuterium exchange mass spectrometry. *Scientific Reports* **7**, 2456 (2017). https://doi.org:10.1038/s41598-017-02550-1
89 Fast, C. S., Vahidi, S. & Konermann, L. Changes in Enzyme Structural Dynamics Studied by Hydrogen Exchange-Mass Spectrometry: Ligand Binding Effects or Catalytically Relevant Motions? *Anal Chem* **89**, 13326-13333 (2017). https://doi.org:10.1021/acs.analchem.7b03506
90 Fassler, R., Edinger, N., Rimon, O. & Reichmann, D. Defining Hsp33's Redox-regulated Chaperone Activity and Mapping Conformational Changes on Hsp33 Using Hydrogen-deuterium Exchange Mass Spectrometry. *J. Vis. Exp*, 57806-57806 (2018). https://doi.org:10.3791/57806
91 Clouser, A. F. *et al.* Interplay of disordered and ordered regions of a human small heat shock protein yields an ensemble of 'quasi-ordered' states. *eLife* **8**, e50259 (2019). https://doi.org:10.7554/eLife.50259
92 Georgescauld, F., Wales, T. E. & Engen, J. R. Hydrogen deuterium exchange mass spectrometry applied to chaperones and chaperone-assisted protein folding. *Expert Rev Proteomics* **16**, 613-625 (2019). https://doi.org:10.1080/14789450.2019.1633920
93 Singh, A. K., Balchin, D., Imamoglu, R., Hayer-Hartl, M. & Hartl, F. U. Efficient Catalysis of Protein Folding by GroEL/ES of the Obligate Chaperonin Substrate MetF. *J Mol Biol* **432**, 2304-2318 (2020). https://doi.org:10.1016/j.jmb.2020.02.031
94 Imamoglu, R., Balchin, D., Hayer-Hartl, M. & Hartl, F. U. Bacterial Hsp70 resolves misfolded states and accelerates productive folding of a multi-domain protein. *Nat Commun* **11**, 365 (2020). https://doi.org:10.1038/s41467-019-14245-4
95 Vandova, V. *et al.* HSPA1A conformational mutants reveal a conserved structural unit in Hsp70 proteins. *Biochim Biophys Acta Gen Subj* **1864**, 129458 (2020). https://doi.org:10.1016/j.bbagen.2019.129458
96 Trcka, F. *et al.* Human Stress-inducible Hsp70 Has a High Propensity to Form ATP-dependent Antiparallel Dimers That Are Differentially Regulated by Cochaperone Binding. *Mol Cell Proteomics* **18**, 320-337 (2019). https://doi.org:10.1074/mcp.RA118.001044
97 Siegel, A. *et al.* A Disorder-to-Order Transition Activates an ATP-Independent Membrane Protein Chaperone. *J Mol Biol* **432**, 166708 (2020). https://doi.org:10.1016/j.jmb.2020.11.007
98 Calabrese, A. N. *et al.* Inter-domain dynamics in the chaperone SurA and multi-site binding to its outer membrane protein clients. *Nat Commun* **11** (2020). https://doi.org:10.1038/s41467-020-15702-1
99 Coufalova, D. *et al.* An inter-subunit protein-peptide interface that stabilizes the specific activity and oligomerization of the AAA+ chaperone Reptin. *J Proteomics* **199**, 89-101 (2019). https://doi.org:10.1016/j.jprot.2019.02.012
100 Ghode, A. *et al.* Synergistic Allostery in Multiligand-Protein Interactions. *Biophys J* **119**, 1833-1848 (2020). https://doi.org:10.1016/j.bpj.2020.09.019
101 Park, J. Y. *et al.* Structural Mechanism of the Arrestin-3/JNK3 Interaction. *Structure* **27**, 1162-1170.e1163 (2019). https://doi.org:10.1016/j.str.2019.04.002

102 McPhail, J. A. *et al.* Characterization of the c10orf76-PI4KB complex and its necessity for Golgi PI4P levels and enterovirus replication. *EMBO Rep* **21**, e48441 (2020). https://doi.org:10.15252/embr.201948441

103 Heitz, S. D. *et al.* A single discrete Rab5-binding site in phosphoinositide 3-kinase β is required for tumor cell invasion. *J Biol Chem* **294**, 4621-4633 (2019). https://doi.org:10.1074/jbc.RA118.006032

104 Loving, H. S. & Underbakke, E. S. Conformational Dynamics of FERM-Mediated Autoinhibition in Pyk2 Tyrosine Kinase. *Biochemistry* **58**, 3767-3776 (2019). https://doi.org:10.1021/acs.biochem.9b00541

105 Chen, M. *et al.* Structure and regulation of human epithelial cell transforming 2 protein. *Proc Natl Acad Sci U S A* **117**, 1027-1035 (2020). https://doi.org:10.1073/pnas.1913054117

106 Anandapadamanaban, M. *et al.* Architecture of human Rag GTPase heterodimers and their complex with mTORC1. *Science* **366**, 203-210 (2019). https://doi.org:10.1126/science.aax3939

107 MacPherson, D. J., Mills, C. L., Ondrechen, M. J. & Hardy, J. A. Tri-arginine exosite patch of caspase-6 recruits substrates for hydrolysis. *J Biol Chem* **294**, 71-88 (2019). https://doi.org:10.1074/jbc.RA118.005914

108 Lumpkin, R. J., Ahmad, A. S., Blake, R., Condon, C. J. & Komives, E. A. The Mechanism of NEDD8 Activation of CUL5 Ubiquitin E3 Ligases. *Mol Cell Proteomics* **20**, 100019 (2021). https://doi.org:10.1074/mcp.RA120.002414

109 Lumpkin, R. J., Baker, R. W., Leschziner, A. E. & Komives, E. A. Structure and dynamics of the ASB9 CUL-RING E3 Ligase. *Nat Commun* **11**, 2866 (2020). https://doi.org:10.1038/s41467-020-16499-9

110 Faull, S. V. *et al.* Structural basis of Cullin 2 RING E3 ligase regulation by the COP9 signalosome. *Nat Commun* **10**, 3814 (2019). https://doi.org:10.1038/s41467-019-11772-y

111 Cook, M. *et al.* The ubiquitin ligase SspH1 from Salmonella uses a modular and dynamic E3 domain to catalyze substrate ubiquitylation. *J Biol Chem* **294**, 783-793 (2019). https://doi.org:10.1074/jbc.RA118.004247

112 Harrison, R. A. & Engen, J. R. Conformational insight into multi-protein signaling assemblies by hydrogen-deuterium exchange mass spectrometry. *Curr Opin Struct Biol* **41**, 187-193 (2016). https://doi.org:10.1016/j.sbi.2016.08.003

113 Ahmad, F. *et al.* Hydrogen–deuterium exchange reveals a dynamic DNA-binding map of replication protein A. *Nucleic Acids Research* **49**, 1455-1469 (2021). https://doi.org:10.1093/nar/gkaa1288

114 Zheng, J. *et al.* HDX reveals the conformational dynamics of DNA sequence specific VDR co-activator interactions. *Nat Commun* **8**, 923 (2017). https://doi.org:10.1038/s41467-017-00978-7

115 Corrales-Guerrero, L. *et al.* Molecular architecture of the DNA-binding sites of the P-loop ATPases MipZ and ParA from Caulobacter crescentus. *Nucleic Acids Res* **48**, 4769-4779 (2020). https://doi.org:10.1093/nar/gkaa192

116 Xu, J. *et al.* Crl activates transcription by stabilizing active conformation of the master stress transcription initiation factor. *Elife* **8** (2019). https://doi.org:10.7554/eLife.50928

117 Hastie, K. M. *et al.* Crystal structure of the Lassa virus nucleoprotein-RNA complex reveals a gating mechanism for RNA binding. *Proc Natl Acad Sci U S A* **108**, 19365-19370 (2011). https://doi.org:10.1073/pnas.1108515108

118 Medina, E. *et al.* Intrinsically Disordered Regions of the DNA-Binding Domain of Human FoxP1 Facilitate Domain Swapping. *J Mol Biol* **432**, 5411-5429 (2020). https://doi.org:10.1016/j.jmb.2020.07.017

119 Ramsey, K. M., Narang, D. & Komives, E. A. Prediction of the presence of a seventh ankyrin repeat in IκBε from homology modeling combined with hydrogen-deuterium exchange mass spectrometry (HDX-MS). *Protein Sci* **27**, 1624-1635 (2018). https://doi.org:10.1002/pro.3459

120 Narang, D., Chen, W., Ricci, C. G. & Komives, E. A. RelA-Containing NFκB Dimers Have Strikingly Different DNA-Binding Cavities in the Absence of DNA. *J Mol Biol* **430**, 1510-1520 (2018). https://doi.org:10.1016/j.jmb.2018.03.020
121 Trelle, M. B. *et al.* Binding of NFκB Appears to Twist the Ankyrin Repeat Domain of IκBα. *Biophys J* **110**, 887-895 (2016). https://doi.org:10.1016/j.bpj.2016.01.001
122 Huang, H. T. *et al.* Co(II) and Ni(II) binding of the Escherichia coli transcriptional repressor RcnR orders its N terminus, alters helix dynamics, and reduces DNA affinity. *J Biol Chem* **293**, 324-332 (2018). https://doi.org:10.1074/jbc.RA117.000398
123 Burke, J. E. *et al.* Interaction of Group IA Phospholipase A2 with Metal Ions and Phospholipid Vesicles Probed with Deuterium Exchange Mass Spectrometry. *Biochemistry* **47**, 6451-6459 (2008). https://doi.org:10.1021/bi8000962
124 Gudlur, A. *et al.* Calcium sensing by the STIM1 ER-luminal domain. *Nat Commun* **9**, 4536 (2018). https://doi.org:10.1038/s41467-018-06816-8
125 Mazur, S. J. *et al.* Conformational Changes in Active and Inactive States of Human PP2Cα Characterized by Hydrogen/Deuterium Exchange–Mass Spectrometry. *Biochemistry* **56**, 2676-2689 (2017). https://doi.org:10.1021/acs.biochem.6b01220
126 Houde, D. & Berkowitz, S. A. Conformational comparability of factor IX–Fc fusion protein, factor IX, and purified Fc fragment in the absence and presence of calcium. *Journal of Pharmaceutical Sciences* **101**, 1688-1700 (2012). https://doi.org:https://doi.org/10.1002/jps.23064
127 Skorupska, A., Bystranowska, D., Dąbrowska, K. & Ożyhar, A. Calcium ions modulate the structure of the intrinsically disordered Nucleobindin-2 protein. *Int J Biol Macromol* **154**, 1091-1104 (2020). https://doi.org:doi: 10.1016/j.ijbiomac.2020.03.110
128 Seyfried, N. T. *et al.* Fourier transform mass spectrometry to monitor hyaluronan-protein interactions: use of hydrogen/deuterium amide exchange. *Rapid Commun Mass Spectrom* **21**, 121-131 (2007). https://doi.org:10.1002/rcm.2817
129 Zhu, M. M., Rempel, D. L., Zhao, J., Giblin, D. E. & Gross, M. L. Probing Ca2+-induced conformational changes in porcine calmodulin by H/D exchange and ESI-MS: effect of cations and ionic strength. *Biochemistry* **42**, 15388-15397 (2003). https://doi.org:10.1021/bi035188o
130 Sperry, J. B., Huang, R. Y. C., Zhu, M. M., Rempel, D. L. & Gross, M. L. Hydrophobic Peptides Affect Binding of Calmodulin and Ca as Explored by H/D Amide Exchange and Mass Spectrometry. *International journal of mass spectrometry* **302**, 85-92 (2011). https://doi.org:10.1016/j.ijms.2010.08.013
131 Wertheim, H. F. L. *et al.* The role of nasal carriage in Staphylococcus aureus infections. *Lancet Infect Dis* **5**, 751-762 (2005). https://doi.org:Doi 10.1016/S1473-3099(05)70295-4
132 Lindsay, J. A., Ruzin, A., Ross, H. F., Kurepina, N. & Novick, R. P. The gene for toxic shock toxin is carried by a family of mobile pathogenicity islands in Staphylococcus aureus. *Mol Microbiol* **29**, 527-543 (1998). https://doi.org:DOI 10.1046/j.1365-2958.1998.00947.x
133 Krakauer, T. & Stiles, B. G. The staphylococcal enterotoxin (SE) family: SEB and siblings. *Virulence* **4**, 759-773 (2013). https://doi.org:10.4161/viru.23905
134 Banwell, J. G. & Sherr, H. Effect of bacterial enterotoxins on the gastrointestinal tract. *Gastroenterology* **65**, 467-497 (1973).
135 Beery, J. T., Taylor, S. L., Schlunz, L. R., Freed, R. C. & Bergdoll, M. S. Effects of staphylococcal enterotoxin A on the rat gastrointestinal tract. *Infect Immun* **44**, 234-240 (1984). https://doi.org:10.1128/iai.44.2.234-240.1984
136 Pinchuk, I. V., Beswick, E. J. & Reyes, V. E. Staphylococcal enterotoxins. *Toxins (Basel)* **2**, 2177-2197 (2010). https://doi.org:10.3390/toxins2082177
137 Schlievert, P. M. Role of superantigens in human disease. *J Infect Dis* **167**, 997-1002 (1993). https://doi.org:10.1093/infdis/167.5.997

138 Carlsson, R. & Sjogren, H. O. Kinetics of IL-2 and interferon-gamma production, expression of IL-2 receptors, and cell proliferation in human mononuclear cells exposed to staphylococcal enterotoxin A. *Cell Immunol* **96**, 175-183 (1985). https://doi.org:10.1016/0008-8749(85)90349-1

139 al-Daccak, R., Mehindate, K., Poubelle, P. E. & Mourad, W. Signalling via MHC class II molecules selectively induces IL-1 beta over IL-1 receptor antagonist gene expression. *Biochem Biophys Res Commun* **201**, 855-860 (1994). https://doi.org:10.1006/bbrc.1994.1779

140 Assenmacher, M. *et al.* Sequential production of IL-2, IFN-gamma and IL-10 by individual staphylococcal enterotoxin B-activated T helper lymphocytes. *Eur J Immunol* **28**, 1534-1543 (1998). https://doi.org:10.1002/(SICI)1521-4141(199805)28:05<1534::AID-IMMU1534>3.0.CO;2-R

141 Bell, S. J., Vroegop, S. M. & Buxser, S. E. Early activation and cell trafficking induced by staphylococcal enterotoxin B: effects of high- versus low-dose challenge on induction of anergy. *Cell Immunol* **154**, 440-452 (1994). https://doi.org:10.1006/cimm.1994.1090

142 Reichert, J. M. & Dewitz, M. C. Anti-infective monoclonal antibodies: perils and promise of development. *Nat Rev Drug Discov* **5**, 191-195 (2006). https://doi.org:10.1038/nrd1987

143 Spero, D., Levitz, L. & De Groot, A. S. Report from the field: Overview of the Sixth Annual Vaccine Renaissance Conference. *Hum Vaccin Immunother* **9**, 1555-1557 (2013). https://doi.org:10.4161/hv.24833

144 Swaminathan, S., Furey, W., Pletcher, J. & Sax, M. Crystal structure of staphylococcal enterotoxin B, a superantigen. *Nature* **359**, 801-806 (1992). https://doi.org:10.1038/359801a0

145 Papageorgiou, A. C., Tranter, H. S. & Acharya, K. R. Crystal structure of microbial superantigen staphylococcal enterotoxin B at 1.5 A resolution: implications for superantigen recognition by MHC class II molecules and T-cell receptors. *J Mol Biol* **277**, 61-79 (1998). https://doi.org:10.1006/jmbi.1997.1577

146 Jardetzky, T. S. *et al.* Three-dimensional structure of a human class II histocompatibility molecule complexed with superantigen. *Nature* **368**, 711-718 (1994). https://doi.org:10.1038/368711a0

147 Li, H. *et al.* Three-dimensional structure of the complex between a T cell receptor beta chain and the superantigen staphylococcal enterotoxin B. *Immunity* **9**, 807-816 (1998). https://doi.org:10.1016/s1074-7613(00)80646-9

148 Rodstrom, K. E., Elbing, K. & Lindkvist-Petersson, K. Structure of the superantigen staphylococcal enterotoxin B in complex with TCR and peptide-MHC demonstrates absence of TCR-peptide contacts. *J Immunol* **193**, 1998-2004 (2014). https://doi.org:10.4049/jimmunol.1401268

Chapter 2: Rapid assessment of pepsin column activity for reliable HDX-MS studies.

Portions of the text of this chapter have been modified with permissions from:

Clint Vorauer, Michael S. Wrigley, Juan P. Rincon Pabon, Michael J. Watson, Charlie C. Mundorff, David D. Weis, and Miklos Guttman. *Journal of the American Society for Mass Spectrometry* **2021** *32* (9), 2386-2390

1.1 Introduction

Hydrogen/deuterium exchange mass spectrometry (HDX-MS) has become a widely adopted structural tool for protein characterization and is now used routinely within the biopharmaceutical industry to characterize protein therapeutics [1]. The most common use of HDX-MS is a bottom-up approach where deuterium-labeled proteins are rapidly digested with a protease and LC-MS is used to measure deuterium uptake of all observable peptides across the protein sequence. After the labeling step, samples must be kept at 'quench' conditions by lowering the pH and temperature to minimize loss of the deuterium label ('back-exchange'). Pepsin has emerged as the most widely used protease for HDX-MS as it retains moderate activity under typical quench conditions (pH 2.5 and 0°C) and can achieve short digestion times [2]. While pepsin has little substrate specificity, it can reliably produce the same fragmentation under identical conditions and can generate many overlapping peptides to provide detailed information on deuterium exchange across the protein [3,4]. Immobilized pepsin has been commonly used to improve digestion efficiency, throughput, and decrease the background from pepsin autolytic products that are prevalent with solution pepsin digests [5,6].

Optimizing digestion conditions is fundamental to effective HDX-MS analysis of a given protein [7]. The analyte protein should be digested to produce a broad range of peptides observable by LC-MS. Under-digestion leads to low peptide signal or large peptides that do not provide high spatial resolution, while over-digestion can result in mainly very small peptides that are not effectively detected by LC-MS resulting in a loss in sequence coverage [8]. For rigorous HDX-MS studies it is critical that the digestion process also be highly repeatable. At the same time sample carry-over, which is highly detrimental to HDX-MS studies is often attributed to the protease column and necessitates stringent wash steps between injections [7,9] . Though pepsin is a resilient enzyme, such harsh washes can lead to a loss of activity of the column over time. Having the ability to 'benchmark' optimal pepsin activity and quickly check the activity of pepsin columns would be highly advantageous. Pepsin is a widely utilized enzyme for a variety of analytical, industrial, and biomedical applications and several colorimetric and spectroscopic assays are established

for quantifying pepsin activity [10-12]. However, to our knowledge, there is no well-established mass spectrometry-based assay to quantitatively measure pepsin activity for an immobilized pepsin column.

Several labs examine digestion profiles of proteins based on their own experience for assessment of digestion efficiency [6,13], or, for example, looking at the number of peptides identified from a phosphorylase B standard. While assessing the number of peptides generated from phosphorylase B is a useful check of pepsin activity, the number of detected peptides may be offset by changes in MS settings or the search algorithms used for peptide identification. Furthermore, the number of peptides alone may not necessarily correlate with digestion efficiency or the total level of pepsin activity. Here we present a simple, rapid, and reliable readout for the activity of a given pepsin column based upon the digestion of a cocktail of three commonly used peptide standards that plugs directly into the HDX-MS analytical platform.

1.2 Materials and methods

1.2.1 Reagents

Peptides [Glu1]-Fibrinopeptide B (GluFib), substance P (SubP), and fibrinopeptide A (FibA) were purchased from either Sigma Aldrich or Anaspec. Purified cytochrome c from equine heart and myoglobin from horse skeletal muscle were purchased from Sigma Aldrich. Highly purified porcine pepsin was from either Sigma Aldrich or Worthington Biochemicals.

1.2.2 Pepsin Columns

Pepsin columns used for the study were either commercial (Enzymate, Waters), or custom pepsin columns prepared using two approaches. Porcine pepsin was immobilized onto either POROS 20 AL resin (ThermoFisher Scientific) resin as described previously [5], or NuGel Poly-Aldehyde support (BioTech Support Group) following a modified version of the procedures described previously [5,6]. Immobilized pepsin resin was custom packed into 2.1 x 50 mm stainless steel columns or a 2.1 x 5 mm stainless steel trapping column. Pepsin columns were washed with 0.1% formic acid (FA) for at least 30 minutes and run with at least one blank injection prior to using them for HDX-MS studies. Columns were stored in 0.1% formic acid at 4°C when not in use.

1.2.3 Sample Preparation

Peptide samples were prepared in 0.1% FA. Each injected sample contained 20 picomoles GluFib, 20 picomoles FibA, and 30 picomoles SubP. For protein tests, equine cytochrome c and myoglobin were suspended in PBS (20 mM sodium phosphate, 150 mM NaCl) to concentration of 0.01 mg/mL (each) and adjusted to pH 7.39. Protein samples were added to an equal volume (100 µL) of quench buffer (8 M urea, 0.2% formic acid) for a final pH of 2.5, frozen in a dry ice ethanol bath, and kept at -80°C until LC-MS analysis.

1.2.4 LC-MS and data analysis

MS/MS data was obtained using a Thermo LTQ-Orbitrap as described previously [14]. Peptide assignments were made using data dependent acquisition MS/MS analyzed with Byonic (Protein Metrics) with a score cutoff of 100. Digestion efficiency tests were collected on a second custom HDX-MS system coupled to a Waters Synapt G2-Si as described previously [15]. The flow rate over the pepsin column was 400 µL/min, which corresponds a digest time of approximately 13 seconds, assuming a 50% bed volume in a 2.1 x 50 mm column. Peptides chromatographic peak areas from LC-MS runs were integrated and processed in Skyline [16]. The sum of monoisotopic peak area, [M+1], and [M+2] peaks for a peptide was used to calculate peak areas.

An additional subset of LC-MS runs were collected in a second laboratory using a custom HDX-MS setup coupled to an Agilent 6530 Q-TOF as described previously [17,18]. The flow rate through the protease column was 200 µL/min, corresponding to a digestion time of approximately 26 seconds. Peak areas were integrated with MassHunter Qualitative Analysis software. Peak area quantification included the summation of the monoisotopic peak areas across all observed charge states.

1.3 Results and discussion

From screening a range of different peptides commonly used as mass spectrometry standards, we identified three that were effectively digested by pepsin: [Glu1]-fibrinopeptide B (GluFib), substance P (SubP), and fibrinopeptide A (FibA). LC-MS/MS analysis of the resulting cleaved products revealed the predominant site of cleavage C-terminal to a phenylalanine residue, consistent with the cleavage preference of pepsin [3] (Supporting table). To test whether the degree of peptide cleavage would correlate with pepsin activity we looked at the extracted ion intensities of the cleaved and uncleaved peptides at digestion temperatures of 0°C and 20°C, which is known to highly alter pepsin activity [6]. At higher temperature, the amount of cleaved product increases, as seen by the large increase in the cleaved

product peak area (Figure 1). Both GluFib and FibA are only partially cleaved at 0°C, but nearly completely digested at 20°C. Substance P appears to be less susceptible to digestion with nearly half remaining uncleaved at 20°C (Figure 1C). In the case of SubP, the precursor ion was observed as both an unmodified species and with methionine oxidation (Figure 1C, shown in gray).

To assess whether the cleavage efficiency of the peptide cocktail tracks with cleavage efficiency of a typical protein we examined the chromatograms generated from an injection of a protein sample containing myoglobin and cytochrome c. Total ion chromatograms at 0 and 20°C reveals notably more undigested protein at the lower temperature and more pronounced peptide peaks across the spectrum at the higher temperature (Figure 1D).

To get a quantitative metric of pepsin efficiency we calculated the areas of the cleaved vs. uncleaved signals from the peptide cocktail. The area of the cleaved peptide extracted ion chromatographic peak was divided by the sum of the cleaved and uncleaved peptide peak areas, which encapsulates both depletion of intact protein and increase in fragment peptide (Figure 2A). Additionally, looking at the relative ratio of cleaved:(cleaved + uncleaved) chromatographic peak areas helps to account for small variations in run-to-run sample intensity. The resulting ratio is highly reproducible and provides a numeric assessment of pepsin activity across each of the peptides in the cocktail. We note that several of the peptides produced multiple observable fragments in the LC-MS/MS data, but we only utilized the most abundant cleaved product for this analysis. While it was not necessary with the conditions used in this study, we note that the smaller pepsin-derived fragments of the three peptides may be useful for assaying more extreme conditions where higher pepsin activity could lead to further digestion of the cleaved products.

To assess the broad applicability of this peptide cocktail to assay pepsin activity, we applied the same analysis in a second laboratory using a very different HDX-MS system. We note that nearly all elements including LC system, mass spectrometer, custom packed pepsin column, and analysis workflow differed between the two labs. This second analysis showed a similar response in pepsin activity for all three peptides, though notably the experiments revealed that pepsin digestion on this platform was significantly more efficient (Figure 2B). This enhanced digestion efficiency can be attributed to both different pepsin column preparations and differences in loading conditions resulting in different approximate digestion times (26 vs. 13 seconds).

Lastly, we sought to test whether the peptide cocktail could be used as a quick way to determine if a pepsin column has lost activity. Peptides were run over either a 2.1 x 50 mm custom packed pepsin column or a packed 2.1 x 5 mm trapping column that is ten times shorter to mimic decreased pepsin activity. As expected, the short column showed a much lower response in the cleavage of the peptide cocktail. The GluFib and FibA peptides showed only a slight fraction cleavage (0.004 and 0.015, respectively) (Figure 3A, B), while the SubP had an almost undetectable level of cleavage (Figure 3C). The comparisons reveal that an injection of this set of peptides can immediately determine the health of a given pepsin column. Based on the digestion profiles of cytochrome c and myoglobin, we recommend aiming for a fraction cleaved of at least 0.8 for GluFib and FibA and 0.3 for SubP.

We envision these three pepsin substrate peptides could be included in a system suitability mix to check the initial performance of the HDX-MS platform as commonly used for routinely assessing the condition of LC-MS systems [19]. An advantage of including multiple pepsin substrates rather than just a single is that it can sample a broader range of pepsin activities. For example, at very high pepsin activities, FibA and GluFib are entirely digested, but SubP still provides a valuable measure to detect any minor changes in pepsin activity. Additionally, having multiple peptides will be a benefit as one or more of them may be able to assay the activity of alternative proteases that are effective for HDX-MS, many of which are now commercially available in an immobilized column format [13,20]. Having a readout of proteolysis can facilitate more reproducible studies by benchmarking the level of pepsin activity for a given study. Recent inter-laboratory comparisons have revealed that one of the major differences in HDX-MS analyses across different labs was the set of proteolytic peptides generated [21]. Having a quick reporter of protease activity that is consistent across different LC-MS platforms can greatly aid in standardizing digestion conditions for better inter-laboratory consistency.

1.4 Figures

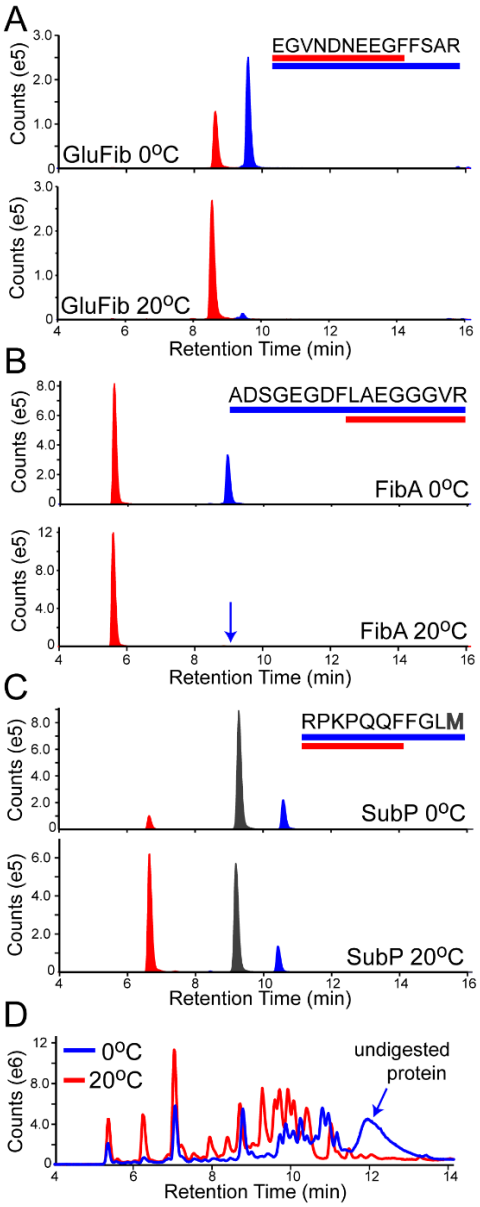

Figure 1. Extracted ion chromatograms of GluFib (A), FibA (B), and SubP (C) to test pepsin activity at either 0°C or 20°C using a new Enzymate (Waters) pepsin column. The traces for the uncleaved precursor (blue), and cleaved fragments (red) are shown for each condition with the sequences shown in the inset. For SubP the precursor was observed both as unmodified and with methionine oxidation (gray). D) Total ion chromatogram of cytochrome c and myoglobin digested over a pepsin column at either 0°C (blue) or 20°C (red). The later eluting species around 12 min are primarily undigested proteins.

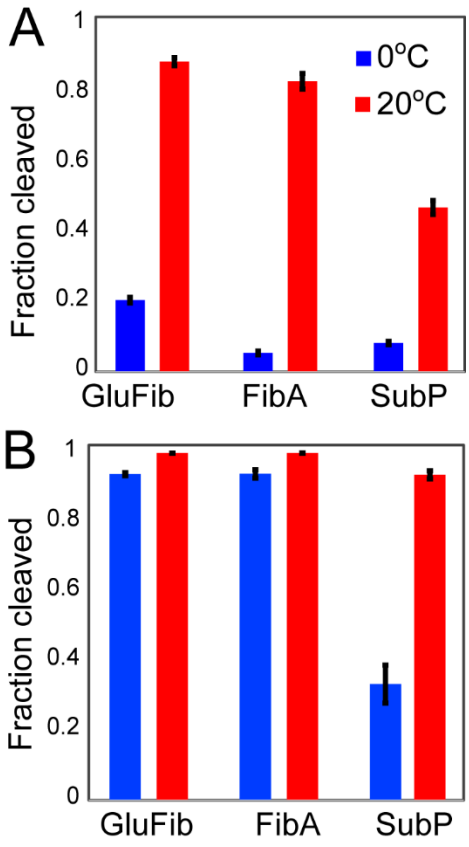

Figure 2. Fraction digested for GluFib, FibA, and SubP to test pepsin activity at either 0°C (blue) or 20°C (red) in two different laboratories with different custom packed columns and different instrumentation (A vs. B). Error bars show standard deviations obtained from at least triplicate measurements.

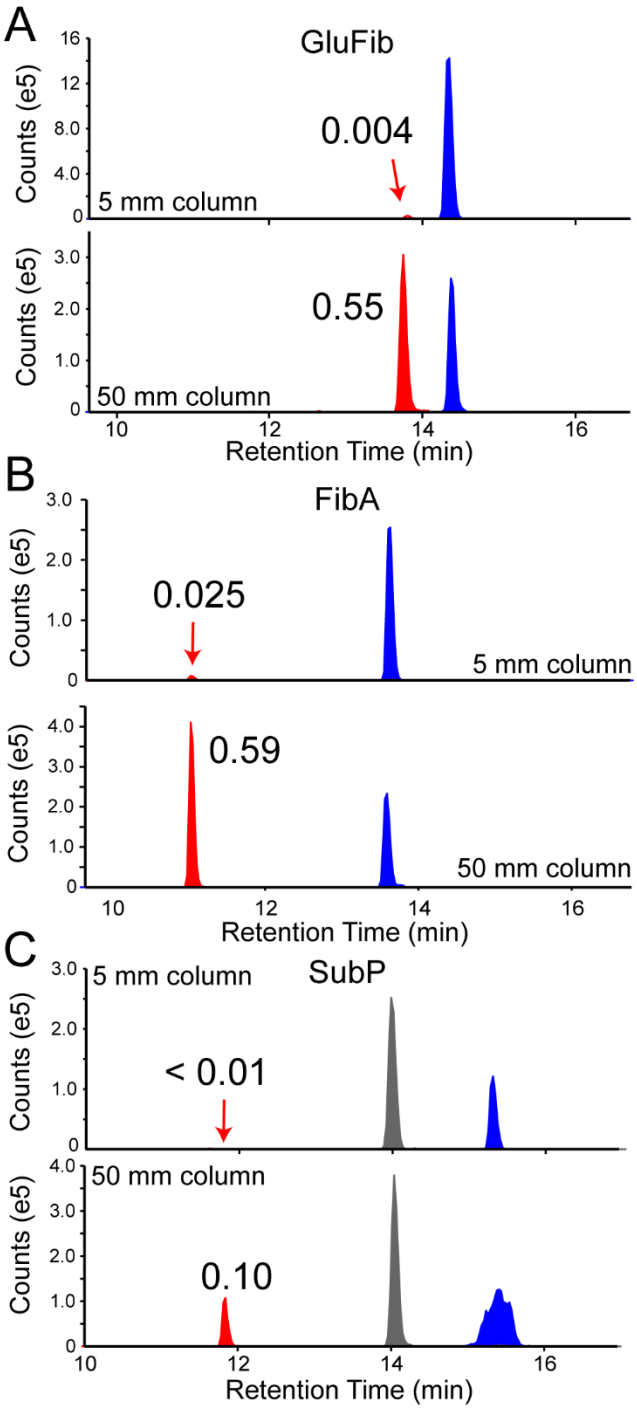

Figure 3. Extracted ion chromatograms of GluFib (A), FibA (B), and SubP (C) digested over either a 2.1 x 5 mm or 2.1 x 50 mm custom packed pepsin column at 10°C. Precursor and cleaved traces are shows with coloring used in figure 1. The fraction cleaved as assessed by the area of the cleaved product relative to the cleaved + uncleaved product(s) is shown in the inset.

1.5 Supplemental Figures

Peptide	Modification Type(s)	Observed m/z	z	Mass error (ppm)	Starting position	Score	|Log Prob|	# of unique peptides
-.RPPGFSPFR.-		354.195	3	1.7	1	161.5	1.47	1
-.RPPGFSPFR.-		530.789	2	1.4	1	266.4	1.82	1
-.RPPGFSPFR.-		530.788	2	-0.6	1	276.7	2.42	1
-.RPPGFSPFR.-		530.789	2	2.5	1	288.1	2.44	1
-.RPPGFSPFR.-		354.194	3	0.1	1	167.7	0.06	1
-.RPPGFSPFR.-		530.787	2	-2.2	1	258.4	0.08	1
-.RPPGFSPFR.-		530.787	2	-2.1	1	289.0	0.29	1
-.RPPGFSPFR.-		530.787	2	-1.5	1	316.0	0.17	1
-.ADSGEGDFL.A		910.378	1	-0.9	1	284.7	2.14	6
-.ADSGEGDFLAE.G		1110.457	1	-1.2	1	172.8	0.84	6
-.ADSGEGDFLAEG.G		1167.479	1	-1.1	1	167.0	0.84	6
-.ADSGEGDFLAEGGGVR.-		512.904	3	2.9	1	373.0	3.13	6
-.ADSGEGDFLAEGGGVR.-		768.850	2	0.0	1	377.1	5.35	6
-.ADSGEGDFLAEGGGVR.-		768.850	2	-0.5	1	517.8	6.21	6
-.ADSGEGDFLAEGGGVR.-		768.850	2	0.5	1	523.7	6.26	6
D.SGEGDFLAEGGGVR.-		675.820	2	2.5	3	443.8	5.29	6
D.FLAEGGGVR.-		453.246	2	0.9	8	226.4	1.33	6
-.ADSGEGDF.L		797.293	1	-2.5	1	313.3	0.77	4
-.ADSGEGDF.L		797.294	1	-1.5	1	321.0	1.16	4
-.ADSGEGDFL.A		910.377	1	-2.4	1	301.2	1.01	4
D.FLAEGGGVR.-		453.245	2	-1.4	8	254.3	0.08	4
F.LAEGGGVR.-		379.712	2	0.7	9	265.8	0.10	4
F.LAEGGGVR.-		758.414	1	-1.9	9	277.1	0.01	4
F.LAEGGGVR.-		379.711	2	-0.1	9	293.2	0.53	4
-.EGVNDNEEGFFSAR.-		785.842	2	-0.2	1	384.4	5.50	4
-.EGVNDNEEGFFSAR.-		785.842	2	-0.1	1	407.4	6.27	4
-.EGVNDNEEGFFSAR.-		785.842	2	-0.6	1	468.8	6.14	4
-.E[-18.011]GVNDNEEGFFSAR.-	pyroE[-18]	776.837	2	-0.1	1	343.3	4.50	4
-.E[-18.011]GVNDNEEGFFSAR.-	pyroE[-18]	776.837	2	0.1	1	347.2	4.11	4
E.GVNDNEEGFFSAR.-		721.320	2	-0.6	2	318.9	3.24	4
D.NEEGFFSAR.-		528.741	2	0.5	6	247.9	1.76	4
-.EGVNDNEEGF.F		1109.436	1	-2.0	1	266.7	2.03	4
-.EGVNDNEEGF.F		1109.435	1	-3.1	1	287.2	2.22	4
-.EGVNDNEEGF.F		555.222	2	-2.0	1	333.3	3.48	4
-.EGVNDNEEGF.F		555.222	2	-1.4	1	333.3	3.10	4
-.EGVNDNEEGFF.S		628.755	2	-2.4	1	245.2	2.20	4
-.EGVNDNEEGFF.S		628.756	2	-2.2	1	250.3	2.83	4
-.EGVNDNEEGFF.S		628.756	2	-1.7	1	250.5	2.35	4
-.EGVNDNEEGFF.S		628.756	2	-1.9	1	306.2	3.08	4
-.EGVNDNEEGFF.S		628.756	2	-1.2	1	309.8	3.08	4
-.EGVNDNEEGFFSAR.-		785.840	2	-2.7	1	420.4	3.23	4
F.FSAR.-		480.256	1	-0.3	11	213.1	0.00	4
-.RPKPQQFFGLM.[-0.984].-	amidation;[-1]	674.371	2	-0.7	1	200.1	1.57	2
-.RPKPQQFFGLM.[-0.984].-	amidation;[-1]	674.371	2	-0.7	1	211.6	1.64	2
-.RPKPQQFFGLM[+15.995].[-0.984].-	amidation;[-1], oxidation M[+16]	682.369	2	-0.3	1	310.7	2.76	2
-.RPKPQQFFGLM[+15.995].[-0.984].-	amidation;[-1], oxidation M[+16]	682.369	2	-0.3	1	330.8	3.29	2
-.RPKPQQF.F		450.756	2	-1.1	1	259.0	0.37	1
Table S1. Assigned peptic peptides from the peptide cocktail								

Supplemental 1. Reporter peptides identified in HDX experiment.

Peptide	Modification Type(s)	Observed m/z	z	Mass error (ppm)	Starting position	Score	|Log Prob|	Protein Name	Retention Time
F.AGIKKKTEREDL.I		463.268	3	0.3	84	171.2	4.65	>Cytochrome C	11.6272
F.AGIKKKTEREDL.I		694.397	2	-2.3	84	211.6	4.11	>Cytochrome C	11.7178
F.AGIKKKTEREDLIA.Y		524.642	3	-0.2	84	17.9	3.06	>Cytochrome C	12.4548
F.AGIKKKTEREDLIA.Y		786.458	2	-1.2	84	294.0	6.11	>Cytochrome C	12.4635
F.AGIKKKTEREDLIAY.L		578.997	3	0.1	84	63.5	3.14	>Cytochrome C	13.358
T.DANKNKGITWKEETL.M		582.972	3	0.1	51	189.0	5.21	>Cytochrome C	13.6967
T.DANKNKGITWKEETL.M		873.954	2	-0.7	51	260.9	5.85	>Cytochrome C	13.6916
T.DANKNKGITWKEETLME.Y		669.667	3	0.3	51	50.4	3.06	>Cytochrome C	14.1053
T.DANKNKGITWKEETLME.Y		1003.996	2	-0.4	51	353.0	7.30	>Cytochrome C	14.1194
M.EYLENPKKYIPGTKM.I		604.319	3	0.5	67	134.2	3.90	>Cytochrome C	13.3151
M.EYLENPKKYIPGTKM.I		905.974	2	-0.6	67	436.1	8.07	>Cytochrome C	13.3964
M.EYLENPKKYIPGTKMIF.A		691.036	3	0.1	67	263.0	6.02	>Cytochrome C	15.2754
M.EYLENPKKYIPGTKMIF.A		1036.049	2	-1.1	67	370.9	7.94	>Cytochrome C	15.2848
F.GRKTGQAPGFTYTDANKNKGITWKEETL.M		778.652	4	0.3	38	354.6	7.30	>Cytochrome C	13.9038
F.GRKTGQAPGFTYTDANKNKGITWKEETL.M		1037.866	3	-1.1	38	541.1	8.20	>Cytochrome C	13.7347
F.GRKTGQAPGFTYTDANKNKGITWKEETLM.E		811.412	4	-0.7	38	307.5	6.19	>Cytochrome C	14.2085
F.GRKTGQAPGFTYTDANKNKGITWKEETLM.E		1081.546	3	-1.1	38	479.2	7.53	>Cytochrome C	14.1729
F.GRKTGQAPGFTYTDANKNKGITWKEETLME.Y		843.672	4	-1.0	38	344.7	6.65	>Cytochrome C	14.0337
F.GRKTGQAPGFTYTDANKNKGITWKEETLME.Y		1124.559	3	-1.9	38	466.1	6.91	>Cytochrome C	14.0218
L.IAY.L		366.203	1	1.5	96	109.2	1.76	>Cytochrome C	13.1511
L.IAYL.K		479.287	1	0.8	96	135.5	2.68	>Cytochrome C	15.9872
L.IAYLKKATNE.-		1150.645	1	-1.1	96	356.1	5.28	>Cytochrome C	11.9842
L.IAYLKKATNE.-		575.825	2	-2.9	96	367.0	5.36	>Cytochrome C	11.9415
M.IFAGIKKKTEREDL.I		549.986	3	0.5	82	150.0	4.22	>Cytochrome C	13.0956
M.IFAGIKKKTEREDL.I		824.474	2	-1.3	82	412.5	7.42	>Cytochrome C	13.0275
M.IFAGIKKKTEREDLIA.Y		611.360	3	0.4	82	199.9	4.78	>Cytochrome C	13.3917
M.IFAGIKKKTEREDLIA.Y		916.535	2	-1.1	82	340.4	6.65	>Cytochrome C	13.4107
G.IKKKTEREDL.I		630.370	2	0.7	86	237.5	4.43	>Cytochrome C	11.545
Y.IPGTKM.I		646.359	1	-0.1	76	68.9	1.73	>Cytochrome C	14.6337
Y.LENPKKYIPGTKM.I		506.950	3	-0.3	69	231.7	5.48	>Cytochrome C	12.6948
Y.LENPKKYIPGTKM.I		759.920	2	-1.2	69	414.6	7.42	>Cytochrome C	12.666
Y.LENPKKYIPGTKMIF.A		593.667	3	0.2	69	181.0	5.05	>Cytochrome C	14.8478
Y.LENPKKYIPGTKMIF.A		889.997	2	-0.4	69	296.7	6.40	>Cytochrome C	14.8805
L.MEY.L		442.165	1	1.5	66	132.5	1.76	>Cytochrome C	13.4799
L.MEYLENPKKYIPGTKM.I		647.999	3	0.4	66	328.2	6.08	>Cytochrome C	13.7446
L.MEYLENPKKYIPGTKM.I		971.493	2	-0.9	66	440.8	8.09	>Cytochrome C	13.7041
L.MEYLENPKKYIPGTKMIF.A		551.289	4	-0.4	66	134.9	4.34	>Cytochrome C	15.6037
L.MEYLENPKKYIPGTKMIF.A		734.715	3	-1.5	66	311.9	6.11	>Cytochrome C	15.7574
L.MEYLENPKKYIPGTKMIF.A		1101.567	2	-2.9	66	382.5	7.31	>Cytochrome C	15.7172
L.MEYLENPKKYIPGTKMIFAGIKKKTEREDL.I		893.481	4	-1.1	66	503.4	8.01	>Cytochrome C	15.0416
L.MEYLENPKKYIPGTKMIFAGIKKKTEREDL.I		1190.972	3	-1.5	66	609.1	9.51	>Cytochrome C	15.0835
L.MEYLENPKKYIPGTKMIFAGIKKKTEREDLIA.Y		939.512	4	-0.6	66	421.9	8.07	>Cytochrome C	15.2138
F.TYTDANKNKGITWKEETL.M		704.692	3	0.1	48	238.2	5.39	>Cytochrome C	13.864
F.TYTDANKNKGITWKEETL.M		1056.533	2	-0.9	48	361.8	7.24	>Cytochrome C	13.77
F.TYTDANKNKGITWKEETLM.E		748.372	3	-0.1	48	182.6	5.21	>Cytochrome C	14.4627
F.TYTDANKNKGITWKEETLME.Y		791.386	3	0.3	48	232.7	5.39	>Cytochrome C	14.2412
F.TYTDANKNKGITWKEETLME.Y		1186.575	2	-0.9	48	314.1	6.27	>Cytochrome C	14.1783
E.YLENPKKYIP.G		632.851	2	0.5	68	49.1	2.04	>Cytochrome C	16.0233
E.YLENPKKYIPGTKM.I		561.304	3	-0.3	68	227.8	5.39	>Cytochrome C	13.159
E.YLENPKKYIPGTKM.I		841.452	2	-1.3	68	393.0	7.37	>Cytochrome C	13.1546
E.YLENPKKYIPGTKMIF.A		486.269	4	0.9	68	127.6	3.90	>Cytochrome C	15.1566
E.YLENPKKYIPGTKMIF.A		648.022	3	0.1	68	187.4	5.21	>Cytochrome C	15.2707
E.YLENPKKYIPGTKMIF.A		971.528	2	-1.3	68	340.6	7.21	>Cytochrome C	15.0575
E.YLENPKKYIPGTKMIFAGIKKKTEREDL.I		828.461	4	-0.6	68	474.3	8.17	>Cytochrome C	14.7188
E.YLENPKKYIPGTKMIFAGIKKKTEREDL.I		828.461	4	-0.7	68	525.6	8.28	>Cytochrome C	14.6288
E.YLENPKKYIPGTKMIFAGIKKKTEREDLIA.Y		874.491	4	-0.5	68	404.3	8.07	>Cytochrome C	14.8215
E.YLENPKKYIPGTKMIFAGIKKKTEREDLIA.Y		874.491	4	-0.5	68	444.1	8.17	>Cytochrome C	14.9037
E.YLENPKKYIPGTKMIFAGIKKKTEREDLIA.Y		1165.652	3	-1.2	68	528.0	8.20	>Cytochrome C	14.9158
A.YLKKATNE.-		966.523	1	-2.4	98	271.2	3.99	>Cytochrome C	11.1659
A.YLKKATNE.-		483.766	2	-0.5	98	340.8	5.37	>Cytochrome C	11.3701
T.YTDANKNKGITWKEETL.M		671.009	3	0.2	49	238.2	5.39	>Cytochrome C	13.7396
T.YTDANKNKGITWKEETL.M		1006.010	2	-0.5	49	359.5	7.00	>Cytochrome C	13.7651

Supplemental 2. Cytochrome C peptides identified in HDX experiment.

Peptide	Modification Type(s)	Observed m/z	z	Mass error (ppm)	Starting position	Score	|Log Prob|	Protein Name	Retention Time
E.ADIAGHGQEVL.I		555.283	2	0.4	20	277.4	4.97	>Myoglobin	13.2917
D.AIIHVLHSKHPGDFGADAQGAMT.K		791.730	3	-0.5	111	271.7	6.02	>Myoglobin	13.4204
D.AIIHVLHSKHPGDFGADAQGAMTKA.L		858.107	3	-0.9	111	501.2	8.01	>Myoglobin	13.1801
D.AIIHVLHSKHPGDFGADAQGAMTKA.L		1286.657	2	-1.0	111	600.2	9.51	>Myoglobin	13.3257
D.AIIHVLHSKHPGDFGADAQGAMTKALEL.F		1464.262	2	-1.3	111	391.9	7.24	>Myoglobin	15.5774
D.AIIHVLHSKHPGDFGADAQGAMTKALEL.F		976.509	3	-2.2	111	477.9	7.47	>Myoglobin	15.7227
A.DIAGHGQEVL.I		519.765	2	0.7	21	295.8	5.05	>Myoglobin	13.3828
A.DIAGHGQEVL.I		1038.521	1	-0.6	21	344.1	5.47	>Myoglobin	13.4508
E.DLKKHGTVVL.T		555.337	2	-0.7	61	336.5	6.44	>Myoglobin	12.8308
A.EMKASEDLKKHGTVVL.T		892.981	2	-1.5	55	393.1	7.94	>Myoglobin	12.935
E.FISD.A		481.230	1	0.7	107	202.1	3.52	>Myoglobin	12.4886
L.FRNDIA.A		368.194	2	2.5	139	176.6	3.43	>Myoglobin	12.5087
L.FRNDIAAKYKELGF.Q		836.446	2	-0.4	139	362.7	6.75	>Myoglobin	15.4385
L.FRNDIAAKYKELGF.Q		836.446	2	0.0	139	366.9	7.45	>Myoglobin	15.5648
L.FRNDIAAKYKELGFQG.M		619.660	3	-0.5	139	199.7	5.21	>Myoglobin	14.7443
L.FRNDIAAKYKELGFQG.M		928.985	2	-1.4	139	436.7	7.99	>Myoglobin	14.749
L.FTGHPETLEKFDKFKHLKTEAEM.K		691.601	4	0.3	34	245.6	5.89	>Myoglobin	13.8694
L.FTGHPETLEKFDKFKHLKTEAEM.K		921.798	3	-0.3	34	480.7	8.09	>Myoglobin	13.8416
W.GKVEADIAGHGQEVL.I		761.896	2	-0.4	16	403.8	7.29	>Myoglobin	13.4258
M.GLSDGEW.Q		763.325	1	-0.8	2	236.6	4.42	>Myoglobin	15.9303
M.GLSDGEWQ.Q		891.384	1	-0.6	2	248.5	5.24	>Myoglobin	14.6975
M.GLSDGEWQQVL.N		616.302	2	0.9	2	449.2	6.92	>Myoglobin	16.6654
M.GLSDGEWQQVLNV.W		722.857	2	-0.1	2	466.2	7.67	>Myoglobin	17.1626
D.IAGHGQEVL.I		462.251	2	1.0	22	281.3	3.66	>Myoglobin	13.1955
D.IAGHGQEVL.I		923.495	1	0.1	22	319.6	5.05	>Myoglobin	13.0647
A.IIHVLHSKHPGDFGADAQGAMTKALEL.F		952.832	3	-0.2	112	474.9	8.17	>Myoglobin	15.5048
L.IRLFTGHPETL.E		642.359	2	-0.3	31	316.6	5.91	>Myoglobin	15.0517
L.IRLFTGHPETLE.K		706.880	2	0.2	31	308.6	6.09	>Myoglobin	14.5257
L.IRLFTGHPETLEKFDKFKHLKTEAE.M		1005.541	3	-0.9	31	313.2	6.89	>Myoglobin	14.2139
L.IRLFTGHPETLEKFDKFKHLKTEAEM.K		787.168	4	-0.2	31	348.0	7.30	>Myoglobin	14.7837
L.IRLFTGHPETLEKFDKFKHLKTEAEM.K		1049.221	3	-1.1	31	363.1	6.67	>Myoglobin	14.7535
F.ISDAIIHVLHSKHPGDF.G		629.336	3	0.2	108	323.1	7.05	>Myoglobin	14.8154
F.ISDAIIHVLHSKHPGDFGADAQGAMT.K		896.778	3	-0.7	108	319.5	6.40	>Myoglobin	14.4768
F.ISDAIIHVLHSKHPGDFGADAQGAMTKA.L		722.619	4	0.3	108	293.6	5.97	>Myoglobin	14.2037
F.ISDAIIHVLHSKHPGDFGADAQGAMTKA.L		963.156	3	0.6	108	549.8	7.84	>Myoglobin	14.4237
F.ISDAIIHVLHSKHPGDFGADAQGAMTKALE.L		1043.863	3	-1.5	108	620.8	9.51	>Myoglobin	15.0784
F.ISDAIIHVLHSKHPGDFGADAQGAMTKALEL.F		811.421	4	-0.7	108	108.9	4.21	>Myoglobin	15.9137
F.ISDAIIHVLHSKHPGDFGADAQGAMTKALEL.F		1081.558	3	-0.9	108	519.1	8.01	>Myoglobin	16.0964
M.KASEDLKKHGTVVL.T		508.963	3	0.2	57	133.3	4.34	>Myoglobin	12.4592
M.KASEDLKKHGTVVL.T		762.940	2	-1.2	57	418.7	7.99	>Myoglobin	12.4505
A.KYKELGFQG.M		535.288	2	0.6	146	300.2	5.08	>Myoglobin	13.2612
E.LFRNDIAAKYKELGFQG.M		657.355	3	0.0	138	151.8	5.05	>Myoglobin	15.1807
E.LFRNDIAAKYKELGFQG.M		985.528	2	-0.7	138	428.3	8.07	>Myoglobin	15.186
L.NVWGKVEADIAGHGQEVL.I		641.331	3	1.3	13	172.0	4.22	>Myoglobin	16.9017
L.NVWGKVEADIAGHGQEVL.I		961.491	2	-0.7	13	429.6	7.99	>Myoglobin	17.0859
W.QQVL.N		487.288	1	0.6	9	137.2	3.14	>Myoglobin	13.1198
W.QQVL.N		487.287	1	-0.2	9	188.1	4.13	>Myoglobin	13.2134
W.QQVLNVWGKVEADIAGHGQEVL.I		797.419	3	-1.3	9	190.2	4.74	>Myoglobin	17.2622
W.QQVLNVWGKVEADIAGHGQEVL.I		1195.626	2	-0.6	9	554.8	8.28	>Myoglobin	17.1337
A.SEDLKKHGTVVL.T		663.374	2	-0.7	59	471.5	8.17	>Myoglobin	12.7921
L.TALGGILKKKGHHEAEL.K		601.348	3	0.8	71	196.5	4.87	>Myoglobin	13.4392
L.TALGGILKKKGHHEAELKPLAQSHATKHKIPIKYLEF.I		689.565	6	0.3	71	206.6	4.87	>Myoglobin	14.3675
L.TALGGILKKKGHHEAELKPLAQSHATKHKIPIKYLEF.I		827.277	5	0.0	71	307.8	5.30	>Myoglobin	14.4522
L.TALGGILKKKGHHEAELKPLAQSHATKHKIPIKYLEF.I		827.277	5	0.2	71	361.2	6.43	>Myoglobin	14.3371
L.TALGGILKKKGHHEAELKPLAQSHATKHKIPIKYLEF.I		1033.843	4	-1.1	71	618.9	8.57	>Myoglobin	14.4476
V.WGKVEADIAGHGQEVL.I		854.935	2	-1.0	15	411.6	7.99	>Myoglobin	14.7793
E.WQQVL.N		673.366	1	-1.3	8	197.4	3.87	>Myoglobin	15.7126
L.KPLAQSHATKHKIPIKYLEF.I		783.786	3	-0.2	88	271.6	6.23	>Myoglobin	14.5197
Table S3. Identified peptic peptides from myoglobin									

Supplemental 3. Myoglobin peptides identified in HDX experiment.

1.6 References

1 Engen, J. R., Botzanowski, T., Peterle, D., Georgescauld, F. & Wales, T. E. Developments in Hydrogen/Deuterium Exchange Mass Spectrometry. *Anal Chem* **93**, 567-582 (2021). https://doi.org:10.1021/acs.analchem.0c04281

2 Zhang, Z. & Smith, D. L. Determination of amide hydrogen exchange by mass spectrometry: a new tool for protein structure elucidation. *Protein Sci* **2**, 522-531 (1993). https://doi.org:10.1002/pro.5560020404

3 Hamuro, Y., Coales, S. J., Molnar, K. S., Tuske, S. J. & Morrow, J. A. Specificity of immobilized porcine pepsin in H/D exchange compatible conditions. *Rapid Commun Mass Spectrom* **22**, 1041-1046 (2008). https://doi.org:10.1002/rcm.3467

4 Mayne, L. *et al.* Many overlapping peptides for protein hydrogen exchange experiments by the fragment separation-mass spectrometry method. *Journal of the American Society for Mass Spectrometry* **22**, 1898-1905 (2011). https://doi.org:10.1007/s13361-011-0235-4

5 Wang, L., Pan, H. & Smith, D. L. Hydrogen exchange-mass spectrometry: optimization of digestion conditions. *Mol Cell Proteomics* **1**, 132-138 (2002). https://doi.org:10.1074/mcp.m100009-mcp200

6 Busby, S. A., Chalmers, M. J. & Griffin, P. R. Improving digestion efficiency under H/D exchange conditions with activated pepsinogen coupled columns. *International Journal of Mass Spectrometry* **259**, 130-139 (2007). https://doi.org:https://doi.org/10.1016/j.ijms.2006.08.006

7 Hamuro, Y. & Coales, S. J. Optimization of Feasibility Stage for Hydrogen/Deuterium Exchange Mass Spectrometry. *J Am Soc Mass Spectrom* **29**, 623-629 (2018). https://doi.org:10.1007/s13361-017-1860-3

8 Moller, I. R. *et al.* Improving the Sequence Coverage of Integral Membrane Proteins during Hydrogen/Deuterium Exchange Mass Spectrometry Experiments. *Anal Chem* **91**, 10970-10978 (2019). https://doi.org:10.1021/acs.analchem.9b00973

9 Majumdar, R. *et al.* Minimizing Carry-Over in an Online Pepsin Digestion System used for the H/D Exchange Mass Spectrometric Analysis of an IgG1 Monoclonal Antibody. *Journal of The American Society for Mass Spectrometry* **23**, 2140-2148 (2012). https://doi.org:10.1007/s13361-012-0485-9

10 Anson, M. L. The Estimation of Pepsin, Trypsin, Papain, and Cathepsin with Hemoglobin. *J Gen Physiol* **22**, 79-89 (1938). https://doi.org:10.1085/jgp.22.1.79

11 Robinson, L. A. & White, T. T. A spectrophotometric method for the analysis of pepsin. *Gastroenterology* **58**, 798-800 (1970).

12 Furihata, C., Senma, T., Saito, D., Matsushima, T. & Sugimura, T. A new fluorescent microassay method for pepsin using succinyl-albumin. *Anal Biochem* **84**, 479-485 (1978). https://doi.org:10.1016/0003-2697(78)90066-0

13 Ahn, J., Cao, M.-J., Yu, Y. Q. & Engen, J. R. Accessing the reproducibility and specificity of pepsin and other aspartic proteases. *Biochim Biophys Acta* **1834**, 1222-1229 (2013). https://doi.org:10.1016/j.bbapap.2012.10.003

14 Murphree, T. A., Vorauer, C., Brzoska, M. & Guttman, M. Imidazolium Compounds as Internal Exchange Reporters for Hydrogen/Deuterium Exchange by Mass Spectrometry. *Anal Chem* (2020). https://doi.org:10.1021/acs.analchem.0c01328

15 Watson, M. J. *et al.* Simple Platform for Automating Decoupled LC–MS Analysis of Hydrogen/Deuterium Exchange Samples. *Journal of the American Society for Mass Spectrometry* **32**, 597-600 (2021). https://doi.org:10.1021/jasms.0c00341

16 MacLean, B. *et al.* Skyline: an open source document editor for creating and analyzing targeted proteomics experiments. *Bioinformatics* **26**, 966-968 (2010). https://doi.org:10.1093/bioinformatics/btq054

17 Keppel, T. R., Jacques, M. E., Young, R. W., Ratzlaff, K. L. & Weis, D. D. An efficient and inexpensive refrigerated LC system for H/D exchange mass spectrometry. *J Am Soc Mass Spectrom* **22**, 1472-1476 (2011). https://doi.org:10.1007/s13361-011-0152-6

18 Pabon, J. P. R., Kochert, B. A., Liu, Y.-H., Richardson, D. & Weis, D. D. Protein A does not induce allosteric structural changes in an IgG1 antibody during binding. *Journal of Pharmaceutical Sciences* (2021). https://doi.org:10.1016/j.xphs.2021.02.027

19 Krokhin, O. V. & Spicer, V. Peptide retention standards and hydrophobicity indexes in reversed-phase high-performance liquid chromatography of peptides. *Anal Chem* **81**, 9522-9530 (2009). https://doi.org:10.1021/ac9016693

20 Yang, M. *et al.* Recombinant Nepenthesin II for Hydrogen/Deuterium Exchange Mass Spectrometry. *Analytical Chemistry* **87**, 6681-6687 (2015). https://doi.org:10.1021/acs.analchem.5b00831

21 Hudgens, J. W. *et al.* Interlaboratory Comparison of Hydrogen-Deuterium Exchange Mass Spectrometry Measurements of the Fab Fragment of NISTmAb. *Anal Chem* **91**, 7336-7345 (2019). https://doi.org:10.1021/acs.analchem.9b01100

Chapter 3: Mapping epitopes and allosteric behavior of *Staph* enterotoxin B

3.1 Introduction

Staphylococcal enterotoxins (SEs) cause food poisoning-like symptoms and are lethal at microgram amounts. SEs hijack what is typically a deliberate response by the adaptive immune system. Under normal circumstances, harmful pathogens that evade the innate immune system are ingested and digested by professional Antigen Presenting Cells (APC), and a fragment of the pathogen is displayed on an extracellular receptor, the Major Histocompatibility Complex class II (MHC II) [1]. The unique molecular surface created by the pathogen fragment and MHC II binding cleft is recognized by particular T-Cell Receptors (TCRs) expressed on CD4+ T-Cells—an exceedingly conserved event. MHC II molecules also generate a vast number of unique surfaces as a result of being polygenic, polymorphic, and co-dominantly expressed, as well as being able to grasp a diverse collection of fragmented peptides. When these molecules bind, it sets off a release of cytokines specific to the pathogen that triggers a T-cell-mediated immune response.

SEs elicit a profound immune response by bridging an MHC II with a TCR [2]. SEs bind regions of the MHC II that are common across large populations of the receptors, regions irrelevant to normal immune activation. While a typical adaptive immune response would rely on specific molecular recognition on binding surfaces, SEs bind to regions of both the MHC II and TCR that are conserved across large populations of the receptors. The bridging of these immune molecules triggers a cytokine storm capable of hyperactivating up to 30% of all the full T-Cell populations [3]. The tri-molecular interaction mediated by SEs binding causes the release of proinflammatory cytokines, including IFN-gamma, TNF-α, IL-1β, IL-6, and IL-8, species capable of causing superantigen-mediated acute inflammation, shock, and ultimately widespread anergy [4-6].

Passive administration of the antibody Bezlotoxumab has been approved by the FDA to treat *Clostridium difficile* toxin A [7], sparking further interest in treatment options for SEs. Though the final FDA-approved product includes only one protein, an anti-C. difficile toxin A (CDA1) antibody, clinical studies included antibodies targeting multiple toxin subtypes [8,9]. This aim highlights a desire in SE research to target multiple toxin species for increased therapeutic yield [10]. Though the lofty goal of multi-toxin treatment for SEs remains, *Staph* enterotoxin B stands out as the most studied and drug-targeted SEB. Monoclonal antibodies (mAbs) [11-16], single-domain antibodies (sdAbs) [17], and nanobodies [18] have been explored for the detection or treatment of SEB. *Staphylococcal* enterotoxin B (SEB) is of particular

therapeutic interest due to its especially toxic character that is hypothesized to be caused by its ability to bring the MHC II into closer proximity to the TCR compared with other SEs [19].

Neutralizing antibodies against SEB bind to the toxin molecule, preventing binding to its targets, thus protecting the organism. Promising therapeutic mAbs, 3E2 and 20B1, isolated from mice, show sub-nanomolar SEB affinity and protection in murine models [12,13]. Through mutagenesis-driven epitope mapping— characterization of the molecular interface of an antibody with an antigen— of mAbs known to neutralize SEB in-vivo, it has been seen that protective therapies like 3E2 and 20B1 often bind in nonlinear, conformational MHC II (class M) or TCR (class T) amino acid binding regions. Additional crystallographic studies of SEB in complex with 3E2 reveal SEB-Y46 and SEB-K71—both part of the 3E2 and MHC II binding surfaces— to be critical to binding of the antibody, a finding corroborated by mutagenesis studies. Similarly, 20B1 was seen to bind to an epitope that largely overlaps with the TCR binding region, as seen by crystallographic comparisons [20]. The mechanism of neutralization for 3E2 and 20B1 is clear for these two antibodies; by preventing the binding of the MHC II or TCR, the effects of SEB are nullified.

Though neutralization by steric blocking can be inferred for 20B1 and 3E2, the mechanism of neutralization for anti-SEB mAbs is not always clear. Findings by Varshney et al. suggest that protein dynamics may play a role in the neutralization of SEB [20]. The generation of neutralizing antibodies yielded species that bound to a variety of epitopes on the toxin. Antibodies isolated from sera progressed as candidates based on the ability to bind to SEB, followed by the ability to neutralize SEB *in vivo* [12]. Some antibodies, like 4C7, bound to SEB but lacked the ability to protect mice exposed to toxin, exemplifying that not all anti-SEB antibodies neutralize SEB. 14G8 and 6D3, antibodies that, when administered together, showed robust ability to neutralize SEB at high and low doses of antibody. Favorable neutralizing results warranted crystallization of 14G8 and 6D3, and the findings were puzzling as it was found that both species epitopes distal to the TCR and MHC. An allosteric mechanism was proposed after NMR spectral analysis revealed changes to SEB distal to the binding site as a result of 14G8 binding as well as distal changes as a result of 6D3 binding in a separate experiment. There are differences to the dynamics of SEB that result from the binding at select epitopes and multiple epitopes at once, but current studies have only scratched the surface of determining the extent of those changes. It is vital to understand the possibility that antibodies inducing synergistic or long-range allosteric effects can render SEB unable to elicit its toxic effect.

3.2 Methods

3.2.1 Reagents

Staph Enterotoxin B (SEB) was purchased from Toxin Technologies Inc. (Sarasota, FL). 20B1, 14G8, and 6D3 anti-SEB mAbs were generated by the Fries Lab [12]. D_2O was purchased from Cambridge Isotopes. Alexafluor 488 was purchased from Thermo Fisher Scientific Inc.

3.2.2 Sample Preparation

3.2.2.1 Biolayer interferometry (BLI)

The binding kinetics for 20B1, 14G8, and 6D3 with SEB were determined using biolayer interferometry Octet Red96 (FortèBio). Mouse-Fc capture tips were presoaked in binding buffer (phosphate-buffered saline (PBS pH 7.4) supplemented with 0.1% BSA, 0.005% Tween 20) for 10 min. The hydrated tips were then loaded with each antibody (separate experiments) prepared at 12 µg/mL in binding buffer for 120 s. After reaching a stable baseline, the biosensor tips were moved into wells containing a 2-fold dilution series of SEB for 30 s. Responses were calculated and double-referenced against the buffer signal and non-specific binding of analyte to biosensor in the absence of mAb. Kinetic data were analyzed by using FortéBio Data Analysis 11.0 software. K_D, on, and off rates were determined using normalized signals.

3.2.2.2 Hydrogen Deuterium Exchange (HDX) Sample Preparation

1.0 µg (33.2 pmol) per timepoint of SEB was allowed to incubate at a 1:1 or 1:1:1 (SEB:mAb:mAb) molar ratio of antibody for 1h at room temperature before incubation in deuterium. SEB-mAb samples were diluted 10-fold into deuterated buffer (20 mM PBS, 85% D2O, pH*7.49) for 5 s, 60 s or 600 s, 10800 s, and 43200 s at room temperature while gently rocking. Protein stock included internal exchange reporters described previously [21], and back-exchange was monitored via the inclusion of bradykinin at a concentration of 1.8 pM in D_2O stocks [22]. The reaction was stopped via diluting 1:1 in ice-cold quench buffer (200 mM tris(2-chloroethyl) phosphate (TCEP), 8 M urea, 0.2% formic acid) to a final pH of 2.5 and flash frozen in liquid nitrogen followed by storage in −80°C prior to analysis. Samples were run in triplicate with minimal deviation from results observed.

3.2.2.3 In-line digestion and LC-MS of HDX samples

Online digestion was performed with a pepsin column prepared using the protocol described by Wang et al. and analyzed by LC-MS utilizing a Thermo Orbittrap Elite mass spectrometer as described

previously utilizing a 15 min gradient and a home-made HDX cold box that maintains the pepsin digestion at 5°C and the LC plumbing at 0°C [23,24]. Pepsin digestion efficiency was confirmed using the protocol described by Vorauer et al. [25]. Peptides were identified using Byonic (Version 3.8, Protein Metrics Inc.) with deamidation at N and Q, oxidation at C, M, W, and Y, and N-terminal cyclization at E and Q variable modifications selected. Deuterium uptake analysis was performed with HD-Examiner (Version 2.5, Sierra Analytics). The percentage exchange was normalized to undeuterated and fully deuterated reference samples.

3.2.2.4 X-Ray Footprinting (XRF) sample preparation

X-ray irradiation experiments were performed at Beamline 4-2 of the Stanford Synchrotron Radiation Lightsource (SSRL). The X-ray beam (11 keV with a ring current of 495–500 mA) was attenuated to give dose responses in the appropriate range for oxidative labeling as assessed on-site using samples containing 80 µM Alexa Fluor-488 dye in an identical phosphate buffer and BSA at 1 mg/ml, to mimic sample conditions [26]. Alexa Fluor 488 quenching was measured by absorbance at a wavelength of 495 nm. An optimal irradiation dose range was determined to be exposures that quenched some but not all the Alexa Fluor 488. Samples of unliganded SEB in PBS were all prepared at a total protein concentration of 1 mg/ml to avoid differences in scavenging due to protein concentration effects [27]. Leucine enkephalin (330 ng) was included in all samples as an internal peptide dosimeter to ensure consistency of labeling between sample sets. Samples (20 µl) were loaded with an autosampler using a Microlab 560 syringe pump (Hamilton) and irradiated as they passed through a quartz capillary. The flow rates during irradiation were adjusted to achieve exposure times ranging from 7.8 to 125 msec. Immediately after exposure, the samples were dispensed and mixed into a tube containing 2.5 µl of 200 mM methionine to prevent secondary oxidation and stored at −20°C. Samples with no irradiation were collected under identical conditions to serve as the nonirradiated standards [28]. All experiments were performed in triplicate.

3.2.2.5 Digestion and LC-MS of XRF samples

Irradiated samples were added to 30 mg urea (0.5 mmol) and 2 µL 1M Tris (pH 8.0) and 2 µL 1M dithiothreitol (DTT) denatured at 50°C for 30 min. Cysteines were then alkylated by incubation in the dark for 1 hr with 20 mM iodoacetamide, followed by an addition of 10 mM DTT to quench the reaction. After dilution with 20 mM Tris (pH 8.0) to achieve a final Gnd-HCl concentration of 0.5 M. GluC was then added at a ratio of 6:1 (substrate to enzyme) and left at 37°C for 18 hr. Samples were analyzed by LC-MS on a TripleTOF 5600+ (SCIEX) mass spectrometer coupled to a Aquity UPLC system (Waters). Peptides were

identified using SWATH MS/MS. Peptides were loaded onto a CSH 1 × 100 mm 1.7 µm C18 column (Waters) and resolved with a gradient of 0% to 32% B over 15 min (A: 3% acetonitrile, 0.1% formic acid; B: 100% acetonitrile, 0.1% formic acid). Peptides were identified using Byonic (Version 3.8, Protein Metrics Inc.), and chromatographic peaks were analyzed in Skyline [29].

3.3 Results

We sought to examine the changes to dynamics of SEB upon binding a panel of mAbs that have been found to neutralize. Strong binding and the binding kinetics for the mAbs were first confirmed by BLI. Next, characterization by HDX and XRF was undertaken to reveal structural implications of antibody binding.

The binding kinetics for SEB against a panel of neutralizing mAbs revealed differences in the on and off rates that may contribute to the neutralizing mechanism of 20B1, 6D3, and 14G8. Anti-mouse Fc capture tips were used to immobilize different antibodies in induvial experiments before SEB was flown over to characterize kinetics. All the different mAbs were found to bind with K_Ds in the picomolar range (Figure 1). The K_D of 20B1 was determined to be 8.8e-11(M) with an on rate of 2.5e7(M^{-1} s^{-1}) and off rate of 2.2e-3(s^{-1}). Similarly, 6D3 had a K_D observed to be 9.1e-11(M) with an on rate of 1.6e7(M^{-1} s^{-1}) and an off rate of 1.5e-3(s^{-1}). 14G8 was seen to have a slightly weaker binding, with a K_D value of 1.7e-10(M), as well as a lower on rate of 2.6e6(M^{-1} s^{-1}), but a smaller off rate of 4e-4(s^{-1}), suggesting slower dissociation of the SEB-14G8 complex relative to the other antibodies.

We next probed the full scale of structural and dynamic changes in SEB upon binding each of the mAbs. Results of the HDX experiment yielded peptide cover extending the entirety of the SEB sequence. Differential uptake was observed relative to an unbound SEB condition (Figure 2A-D). A confirmational epitope for 20B1 was observed across several peptide fragments, peptides 1-22 and 161-185, notably strong, with a statistically significant drop in deuterium uptake. Additionally, decreased deuterium uptake for the 48-64 peptide was observed with notable changes at the early time scale. Peptide 115-133 also revealed a small but statistically significant increase in the uptake of deuterium. The three peptides cover the three major conformational regions of SEB that interact with 20B1, and the binding epitope of 20B1 was mapped to the structure of SEB and was seen to be consistent with published crystal structures [20]. The heat map in Figure 2B and C reveals the minimal allosteric interactions observed distal to the 20B1 binding site observed in the differential solution HDX experiment.

The epitopes of the antibodies 14G8, 6D3, and the 14G8/6D3 bound in tandem were also mapped using HDX. Statistically significant reduction of deuterium uptake was observed upon binding different mAbs that were consistent with previously published crystal structures (Figure 2E-L). Notably, the binding of 6D3 and 14G8 produced significant, distinct changes to observed deuterium uptake. Upon binding 14G8, peptide 134-146 saw a significant decrease in the amount of deuterium exchanged. Another region in the 14G8 SEB binding epitope region, peptide 228-238, saw a statistically significant decrease in deuterium as well. Throughout the structure, many peptides distal to the epitope exhibited allostery, observed as an increase in the amount of deuterium exchanged a majority of the structure. Upon binding 6D3, peptide 126-133 saw a dramatic reduction in deuterium uptake, and peptide 147-159 also saw a significant decrease as well. Peptide 216-227 saw a decrease in deuterium uptake that was muted but also significant. From the peptide 161-185 it was observed that deuterium uptake increased, indicating allostery on the alpha helix and loop. As a result of both 14G8 and 6D3 binding, a notable decrease in deuterium uptake was observed on peptides 115-133 and 134-146. A decrease in deuterium exchange was also observed on peptides 216-227 and 228-238. The most profound region that saw an increase in the uptake of deuterium is part of an alpha helix and part of a disordered loop on peptide 161-185 on the crystal structure of SEB.

Complementary epitope mapping was achieved by covalent modification via X-ray footprinting (XRF) to probe side chain accessibility, a biophysical quality similar to backbone solvent accessibility (Figure 3). Unlike HDX, XRF modifies only select amino acids and change is represented as modified peptide relative to unmodified peptide. Covalent labeling was confirmed via a reporter peptide, leucine enkephalin. Leucine enkephalin is a short, unstructured peptide that contains a reactive phenylalanine that can report modification by oxidative labelling. As observed by an increase in the percent modified peptide, leucine enkephalin was oxidized in a dose-dependent manner (Supplemental Figure 2), indicating dose-dependent sample irradiation was achieved.

A reduction of the percent modified peptide was achieved in SEB peptides 1-22 and 160-183 as a result of 20B1 binding (Figure 4)— the same regions of the conformational epitope identified by HDX and crystal structures. Upon binding 14G8, no significant decreases in the percent modified peptide were observed. The epitope of 6D3 was elucidated by XRF at peptide 121-138, which saw a statistically significant reduction in the uptake of deuterium in the same region identified by HDX and crystal structures. An increase in the amount of deuterium exchanged was also observed on peptide 1-22 upon

6D3 binding. Upon binding both 14G8 and 6D3, a decrease in deuterium uptake was observed on peptides 121-138 and 139-159.

3.4 Discussion

Previous studies have implicated allosteric effects as playing a role in neutralization of SEB, and here we used new methods to probe the structural and dynamic changes in detail across the full sequence of SEB. To date, three mechanisms of action have been proposed for the neutralization of SEB by antibodies: the steric blocking of binding interfaces of immune molecules (antibodies 20B1 and 3E2), increased FcR-mediated crosslinking and clearance, and inhibition via allosteric disruption of binding interfaces [12,13,20]. Work here sought to provide detailed insights into the relevant epitopes and disrupted binding interfaces of SEB after mAb binding as well as more thorough kinetic characterization that offers additional perspective into the mechanism of distal multi-mAb SEB neutralization. HDX, XRF, and new BLI findings offer additional insight into the mechanism of neutralization of anti-SEB mAbs as well as synergistic effects caused by multiple antibodies binding.

An allosteric mechanism of neutralization by 14G8 and 6D3 is biologically relevant, as other modes of neutralization have been ruled out. In previous work by Dutta et al., it was hypothesized that two bound antibodies to SEB could result in an immune complex that cross-links Fc receptors (FcRs) to promote cellular uptake [20]. The uptake of 6D3 or 14G8 alone or together by macrophages was compared with WT and FcR-deficient mice (FcRγ−/−/RIIB−/−). Similar experiments were also performed to measure internalization by neutrophils. Both experiments yielded similar results: cellular uptake was not found to be promoted by the inclusion of the two antibodies 6D3 and 14G8, thus indicating allosteric interaction mediated through distal epitope binding.

Previously published BLI experiments that measure the binding of SEB with the TCR and MHC in the presence of 20B1, 14G8, and 6D3 inform the perspective of the findings of the biophysical assays performed here. Competition assays by Dutta et al. revealed the binding of 20B1, 6D3, and 14G8 individually reduced or prevented entirely the binding of the TCR or the MHC [20]. HDX and XRF results offer unique insights into epitopes and allosteric effects of anti-SEB neutralizing mAbs. HDX experiments were able to probe the allostery of the entire, non-truncated mAb species as well as 14G8 and 6D3 together. A positive allosteric interaction was identified on residue N178 as a result of 6D3, 14G8, and 14G8 together with 6D3 binding (Figure 3). Additionally, peptide 160-183 revealed a significant increase in the

percentage modified, indicating increased side-chain accessibility. Residue N178 is a disordered loop that is in close proximity to the TCR when bound. Importantly, the binding affinity of SEB with the TCR is 8.9 μM as measured by Dutta et al., though larger affinity values have also been reported [19]. With a binding affinity already so weak, mild structural alterations could drastically reduce affinity. It is proposed that changes to this loop significantly alter the ability of SEB to bind the TCR and contribute to the *in vivo* efficacy observed from co-administration of the antibodies.

Another possible reason for the increased *in vivo* efficacy observed with 14G8 and 6D3 tandem administration is antibody-mediated synergy, as observed by a change in deuterium uptake profile over time. Panels I and L in Figure 2, the major regions of the 6D3 conformational epitope, show reduced uptake of deuterium for 14G8 and 6D3 relative to the 6D3 alone. It is observed that later time points for the 6D3 only condition uptake more deuterium and, in the instance of peptide 115-133, converge with the unbound condition. This change in uptake profile is likely due to a difference in off rate of 6D3 between the singly-bound 6D3 condition and the dual-bound condition. The presence of both antibodies stabilizes 6D3, making it harder for the antibody to dissociate. A similar phenomenon is also observed upon 14G8 binding relative to both antibody species being bound (Figure 2E): later time points reveal relatively reduced uptake of deuterium. Uniquely, the uptake of deuterium for the 14G8-only condition at earlier time points is reduced relative to the tandem bound condition. This suggests either a reduced on rate of the 14G8 antibody when 6D3 is bound or a mild structural alteration to the 14G8 epitope region as a result of 6D3 binding causing more rapid deuterium exchange at the earlier time scale. Regardless of the cause of the difference in the early time scale, later time points for both antibodies indicate that off rate is longer for the condition bound in tandem, suggesting increased synergistic stabilization.

The kinetic interactions of SEB with mAbs 20B1, 14G8, and 6D3 were robustly characterized by BLI to reveal distinct differences in on and off rate that might lead to complementary neutralizing activity when multiple mAbs are used. To date, experiments that quantified interactions of SEB and neutralizing mAbs were limited to affinity values. While useful, affinity values tell an incomplete story of binding events as similar affinity values can have wildly different on and off rates. Notably, our results revealed 14G8, an antibody with no *in vivo* protective efficacy, had a slightly higher overall K_D relative to the other protective (20B1) or semi-protective (6D3) mAbs, but a smaller on rate and slower off rate relative to the other mAbs. While seemingly less favorable, the 20-fold greater than 20B1 increased off-rate could reasonably contribute to *in-vivo* efficacy of 14G8 as the antibody binds more tightly to SEB. It can be reasoned that

combining the kinetic profile of 14G8 with a mAb with a different kinetic profile might improve protection against toxin exposure.

Precision epitope mapping of conformational epitopes is a vital element in understanding the modes of SEB neutralization by mAbs. Shown here, HDX can adeptly interrogate the effects of one or multiple antibodies to reveal a more complete picture of structure and dynamics to inform the mechanism of antibody-mediated neutralization. Allosteric inhibition is a noted mechanism neutralization, though effects of multiple mAbs binding necessitate additional hypotheses about antibody synergy. 14G8 and 6D3 binding appears to increase antibody off rate. Synergy from unique kinetic profiles for 14G8 and 6D3 could also inform the ability of both antibodies to neutralize in tandem. Though not explored in these studies, the steric effects of two antibodies binding may contribute to the ability of these mAbs to neutralize. An IgG is roughly five times the size of SEB. These studies do not rule out the possibility that the high-affinity association alone of two large immune species leads to neutralization. That said, structural and kinetic findings here suggest a unique, synergistic binding phenomenon that warrants further investigation of SEB as well as consideration when characterizing other proteins.

3.5 Acknowledgments

The authors wish to thank Dale Whittington and J. Scott Edgar for their assistance with data collection and David Weis for insightful discussions. We also thank Thomas Weiss and Tsutomu Matsui for their assistance with XRF data collection. This work was supported by SSRL (DOE) grant that funds BL4-2 at SSRL.

3.6 Figures

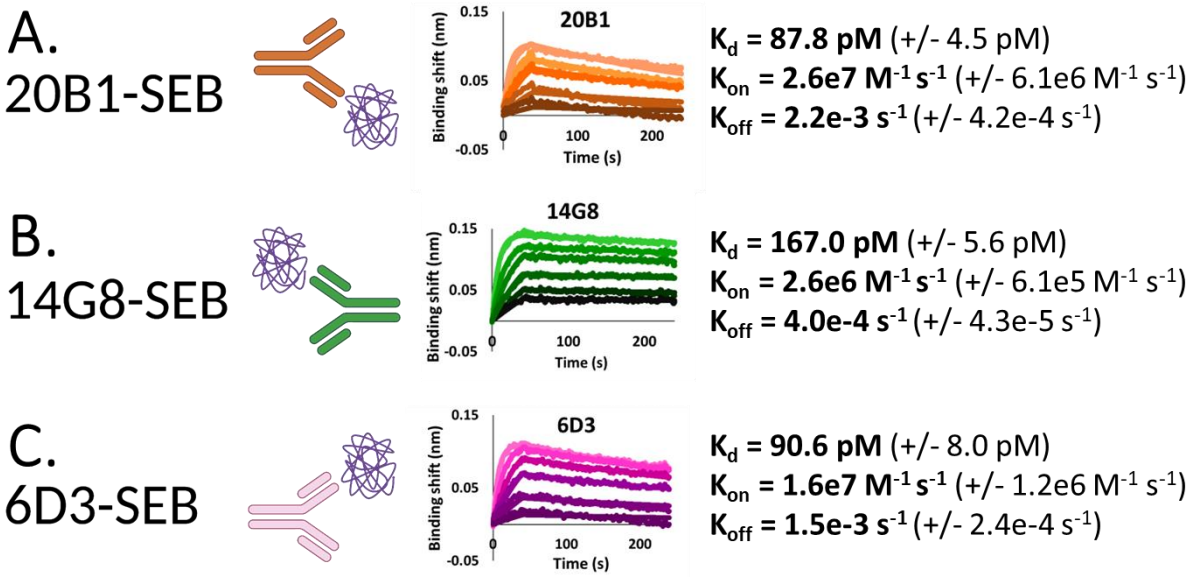

Figure 1. Kinetic measurement and fits of anti-SEB mAbs associating SEB using BLI. Samples run in triplicate. **A.** 20B1 on and off rates. **B.** 14G8 on and off rates. **C.** 6D3 on and off rates.

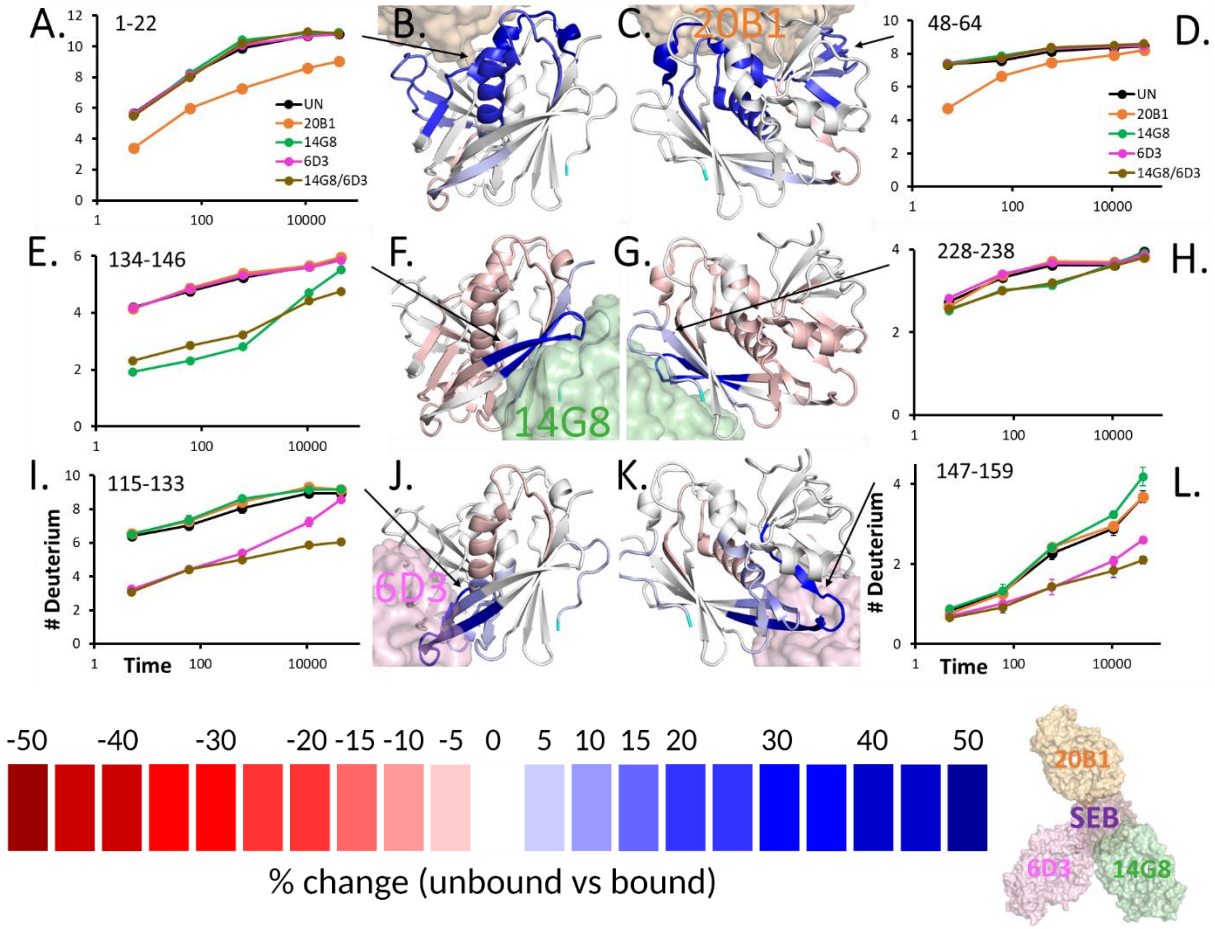

Figure 2. Differences in deuterium uptake between neutralizing antibodies reveal binding epitopes on SEB. HDX data is imposed on crystal structures of SEB, with globular antibodies represented at identified epitopes. Bluer regions represent a reduced uptake of deuterium relative to unbound condition, redder regions represent an increased uptake of deuterium relative to unbound condition. Views are rotated 180˚ to show two perspectives. Relative locations of different antibodies are shown below, right of the heat map guide. **A.** Uptake plot, peptide 1-22. **B./C.** Differential uptake of deuterium for mAb 20B1. **D.** Uptake plot, peptide 48-64. **E.** Uptake plot, peptide 134-146. **F./G.** Differential uptake of deuterium for mAb 14G8. **H.** Uptake plot, peptide 228-238. **I.** Uptake plot, peptide 115-133. **J./K.** Differential uptake of deuterium for mAb 6D3. **L.** Uptake plot, peptide 147-159.

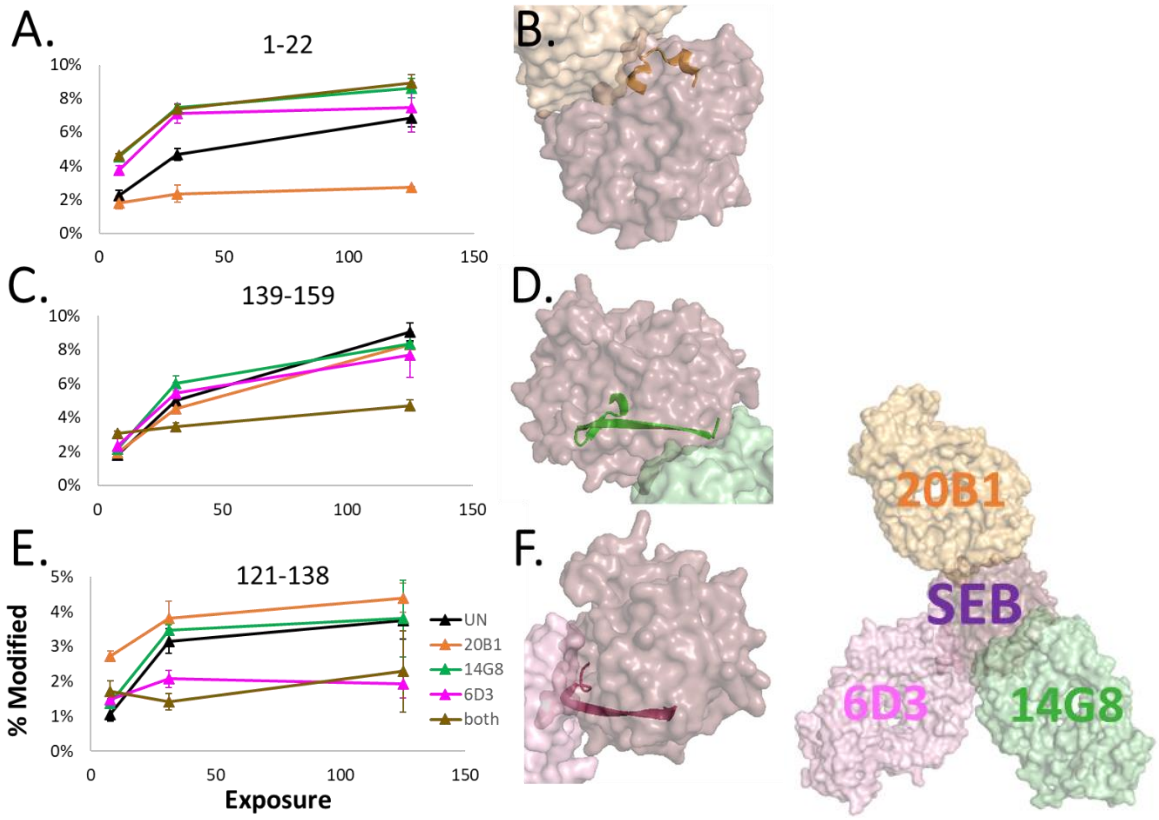

Figure 3. Differences in the percent modified of specific peptides by X-ray footprinting reveals changes to protein structure upon antibody binding. Relative locations of antibodies shown at right. **A.** % modified plot, peptide 1-22. **B.** Location of peptide 1-22. **C.** % modified plot, peptide 139-159. **D.** Location of peptide 139-159. **E.** % modified plot, peptide 121-138. **B.** Location of peptide 121-138.

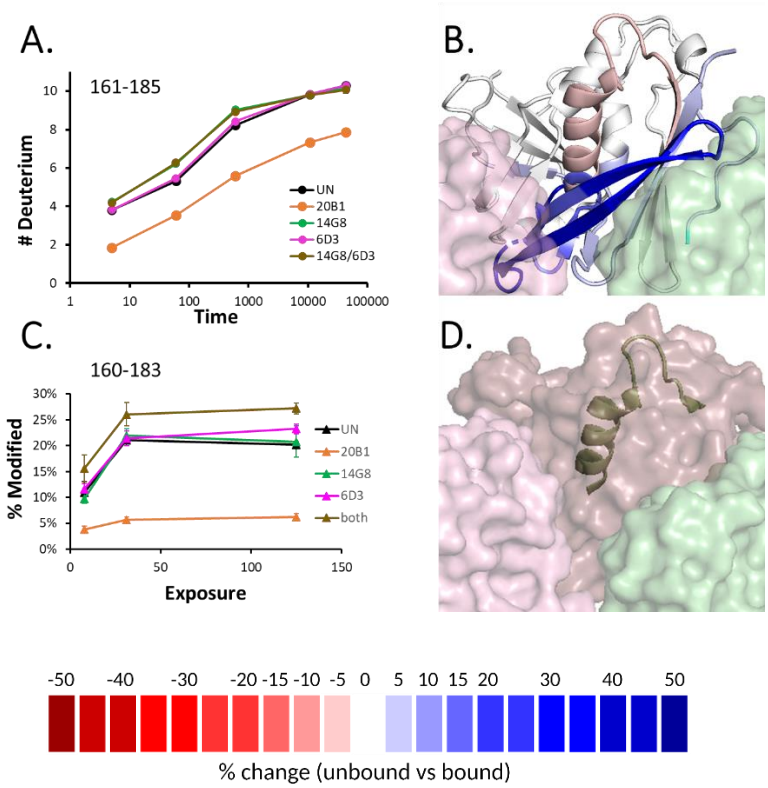

Figure 4. HDX and XRF reveal allosteric interactions. **A.** Uptake plot, peptide 161-185. **B.** Differential uptake of deuterium upon binding 14G8 and 6D3. **C.** % modified plot, peptide 160-183. **D.** Location of peptide 160-183 on the structure of SEB.

3.7 Supplemental Figures

Supplemental Figure 1. SEB peptides identified for analysis. **A.** HDX peptides from peptic digest. **B.** XRF peptides from digest with GluC.

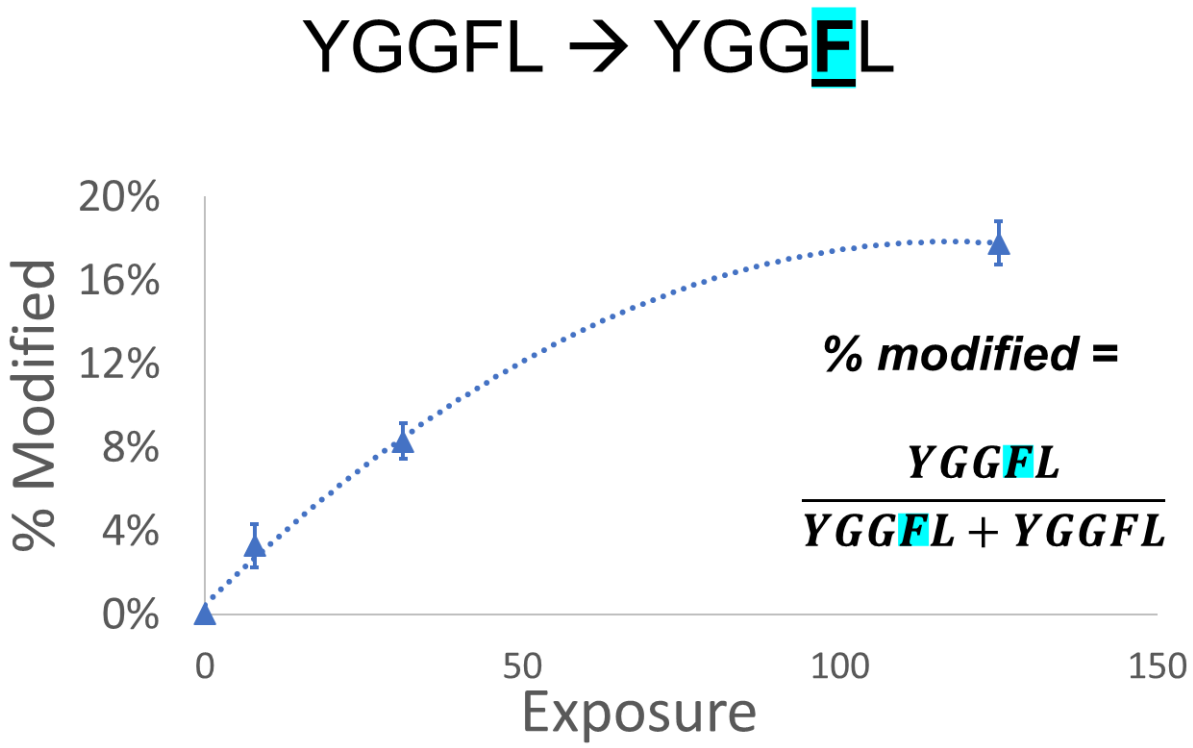

Supplemental Figure 2. Monitoring of leucine enkephalin reveals dose response relative to irradiation exposure in XRF.

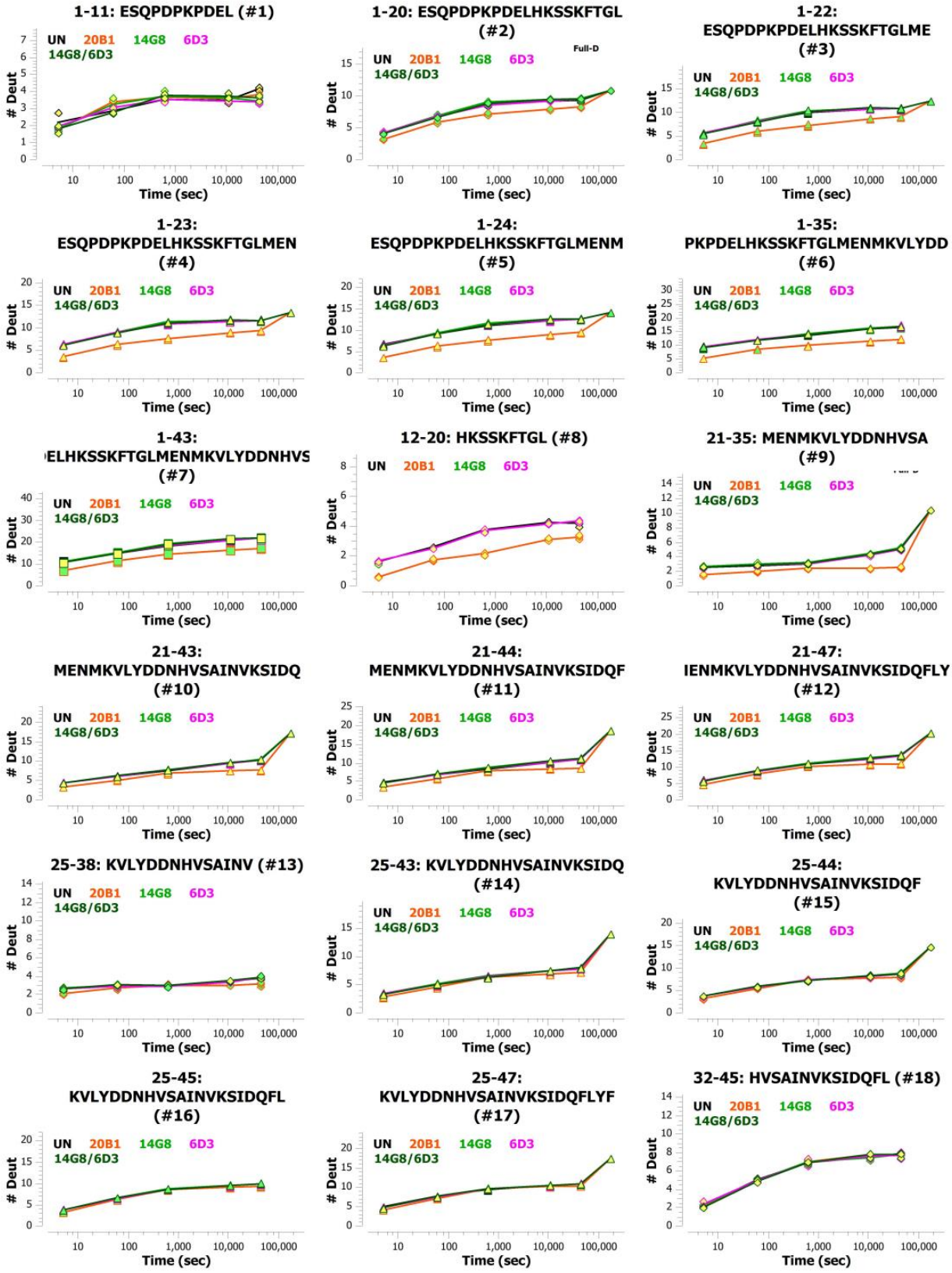
1-11: ESQPDPKPDEL (#1)
1-20: ESQPDPKPDELHKSSKFTGL (#2)
1-22: ESQPDPKPDELHKSSKFTGLME (#3)
1-23: ESQPDPKPDELHKSSKFTGLMEN (#4)
1-24: ESQPDPKPDELHKSSKFTGLMENM (#5)
1-35: PKPDELHKSSKFTGLMENMKVLYDD (#6)
1-43: ELHKSSKFTGLMENMKVLYDDNHVS (#7)
12-20: HKSSKFTGL (#8)
21-35: MENMKVLYDDNHVSA (#9)
21-43: MENMKVLYDDNHVSAINVKSIDQ (#10)
21-44: MENMKVLYDDNHVSAINVKSIDQF (#11)
21-47: IENMKVLYDDNHVSAINVKSIDQFLY (#12)
25-38: KVLYDDNHVSAINV (#13)
25-43: KVLYDDNHVSAINVKSIDQ (#14)
25-44: KVLYDDNHVSAINVKSIDQF (#15)
25-45: KVLYDDNHVSAINVKSIDQFL (#16)
25-47: KVLYDDNHVSAINVKSIDQFLYF (#17)
32-45: HVSAINVKSIDQFL (#18)
UN 20B1 14G8 6D3
14G8/6D3
Deut
Time (sec)
Full-D

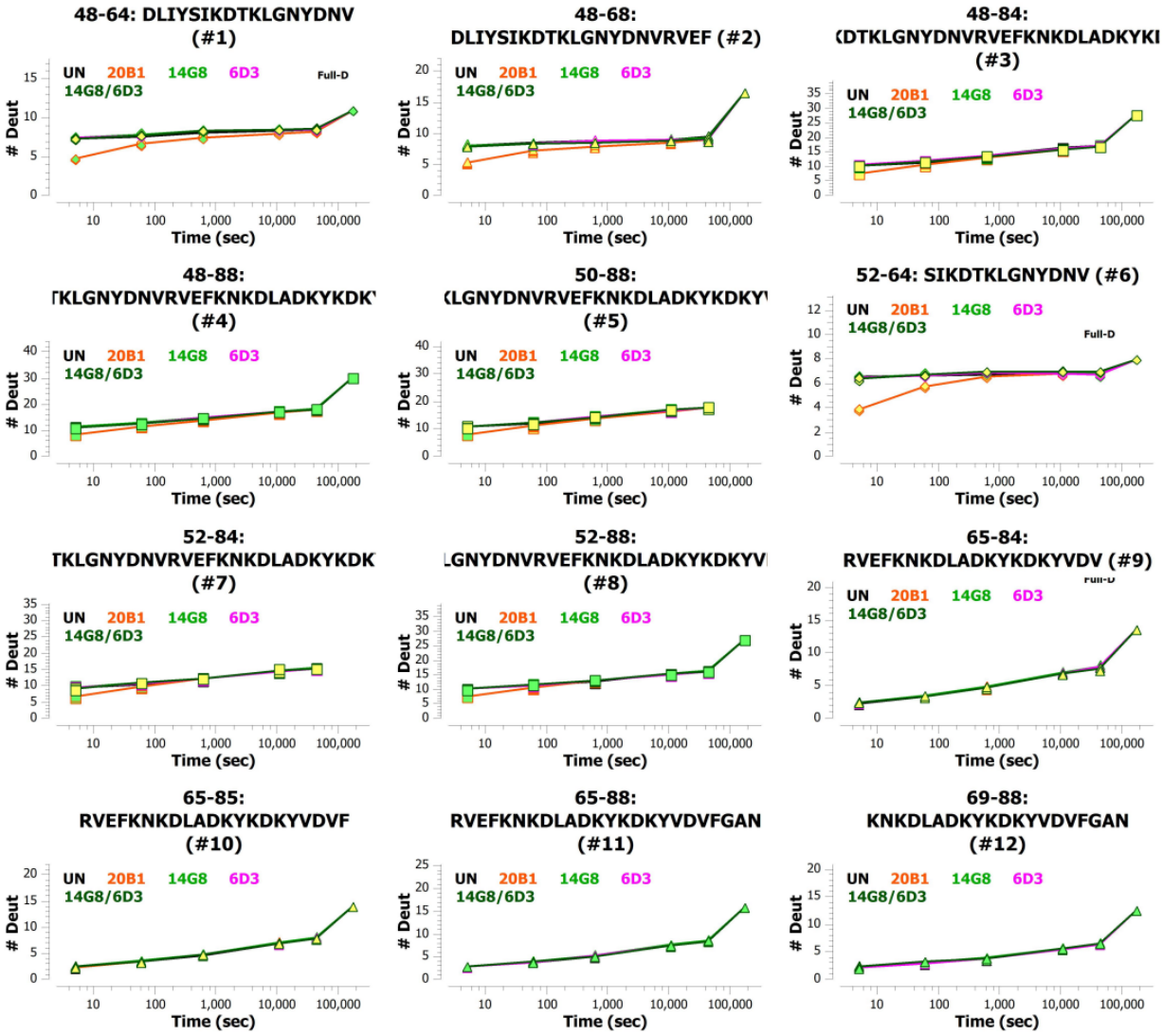
48-64: DLIYSIKDTKLGNYDNV
(#1)
48-68:
DLIYSIKDTKLGNYDNVRVEF (#2)
48-84:
(DTKLGNYDNVRVEFKNKDLADKYKI
(#3)
48-88:
(#4)
50-88:
(#5)
52-64: SIKDTKLGNYDNV (#6)
52-84:
(#7)
52-88:
(#8)
65-84:
RVEFKNKDLADKYKDKYVDV (#9)
65-85:
RVEFKNKDLADKYKDKYVDVF
(#10)
65-88:
RVEFKNKDLADKYKDKYVDVFGAN
(#11)
69-88:
KNKDLADKYKDKYVDVFGAN
(#12)
UN
20B1
14G8
6D3
14G8/6D3
Full-D
Deut
Time (sec)

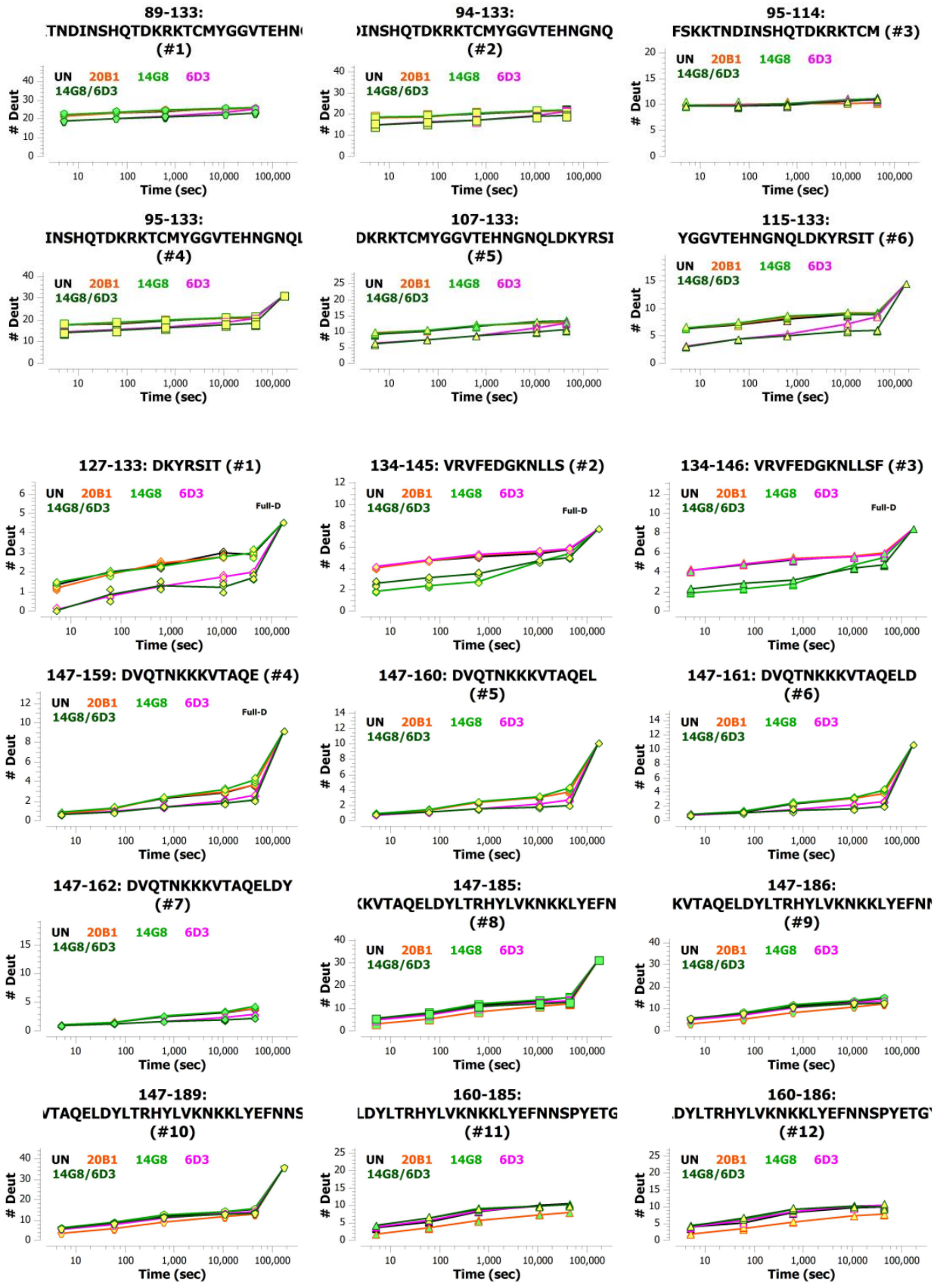
89-133: TNDINSHQTDKRKTCMYGGVTEHN (#1)
94-133: INSHQTDKRKTCMYGGVTEHNGNQ (#2)
95-114: FSKKTNDINSHQTDKRKTCM (#3)
95-133: INSHQTDKRKTCMYGGVTEHNGNQI (#4)
107-133: DKRKTCMYGGVTEHNGNQLDKYRSI (#5)
115-133: YGGVTEHNGNQLDKYRSIT (#6)
127-133: DKYRSIT (#1)
134-145: VRVFEDGKNLLS (#2)
134-146: VRVFEDGKNLLSF (#3)
147-159: DVQTNKKKVTAQE (#4)
147-160: DVQTNKKKVTAQEL (#5)
147-161: DVQTNKKKVTAQELD (#6)
147-162: DVQTNKKKVTAQELDY (#7)
147-185: KVTAQELDYLTRHYLVKNKKLYEFN (#8)
147-186: KVTAQELDYLTRHYLVKNKKLYEFNI (#9)
147-189: VTAQELDYLTRHYLVKNKKLYEFNNS (#10)
160-185: LDYLTRHYLVKNKKLYEFNNSPYETG (#11)
160-186: DYLTRHYLVKNKKLYEFNNSPYETGY (#12)
UN 20B1 14G8 6D3
14G8/6D3
Full-D
Deut
Time (sec)

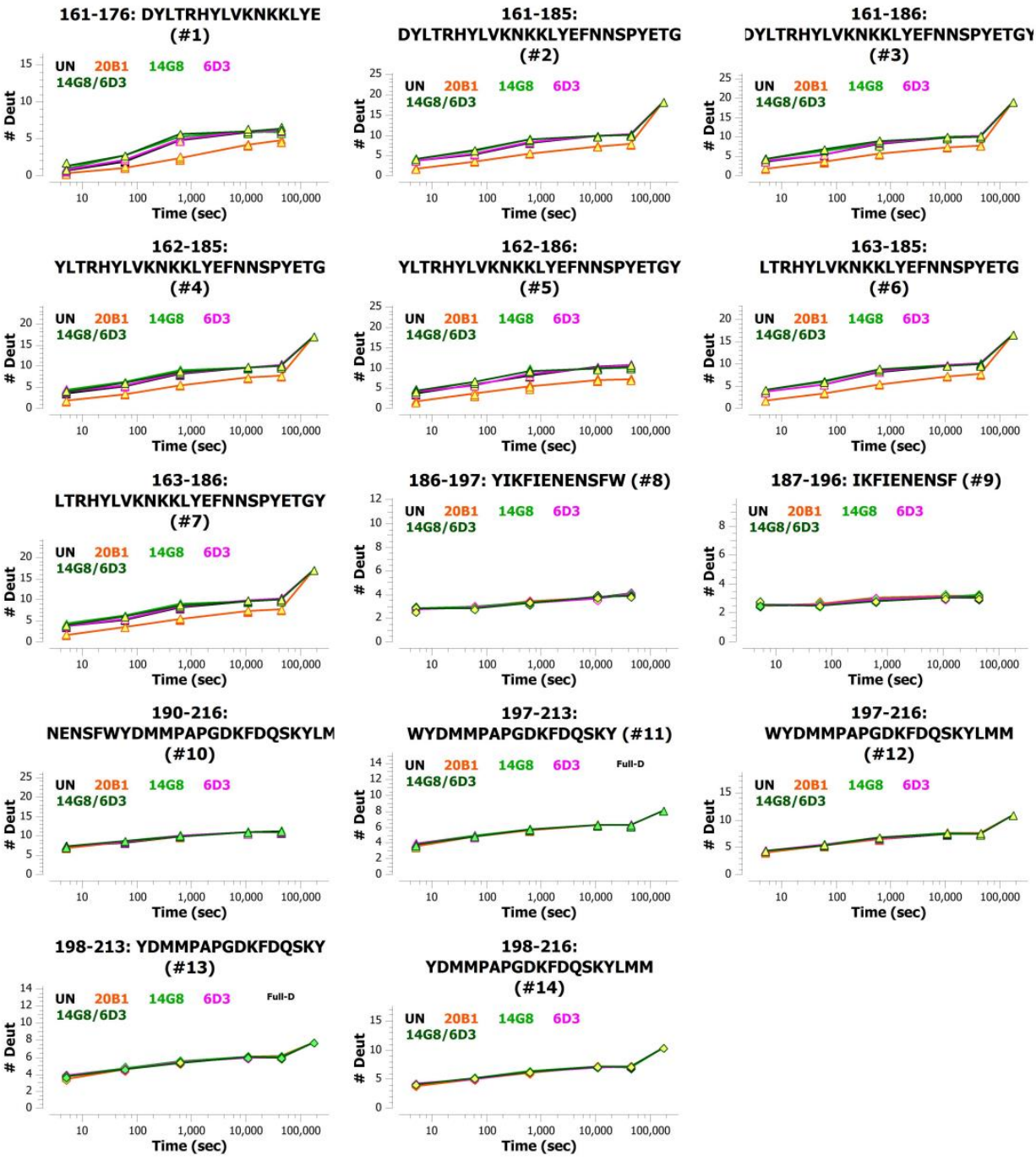
161-176: DYLTRHYLVKNKKLYE (#1)
161-185: DYLTRHYLVKNKKLYEFNNSPYETG (#2)
161-186: DYLTRHYLVKNKKLYEFNNSPYETGY (#3)
162-185: YLTRHYLVKNKKLYEFNNSPYETG (#4)
162-186: YLTRHYLVKNKKLYEFNNSPYETGY (#5)
163-185: LTRHYLVKNKKLYEFNNSPYETG (#6)
163-186: LTRHYLVKNKKLYEFNNSPYETGY (#7)
186-197: YIKFIENENSFW (#8)
187-196: IKFIENENSF (#9)
190-216: NENSFWYDMMPAPGDKFDQSKYLM (#10)
197-213: WYDMMPAPGDKFDQSKY (#11)
197-216: WYDMMPAPGDKFDQSKYLMM (#12)
198-213: YDMMPAPGDKFDQSKY (#13)
198-216: YDMMPAPGDKFDQSKYLMM (#14)
UN 20B1 14G8 6D3
14G8/6D3
Full-D
Deut
Time (sec)

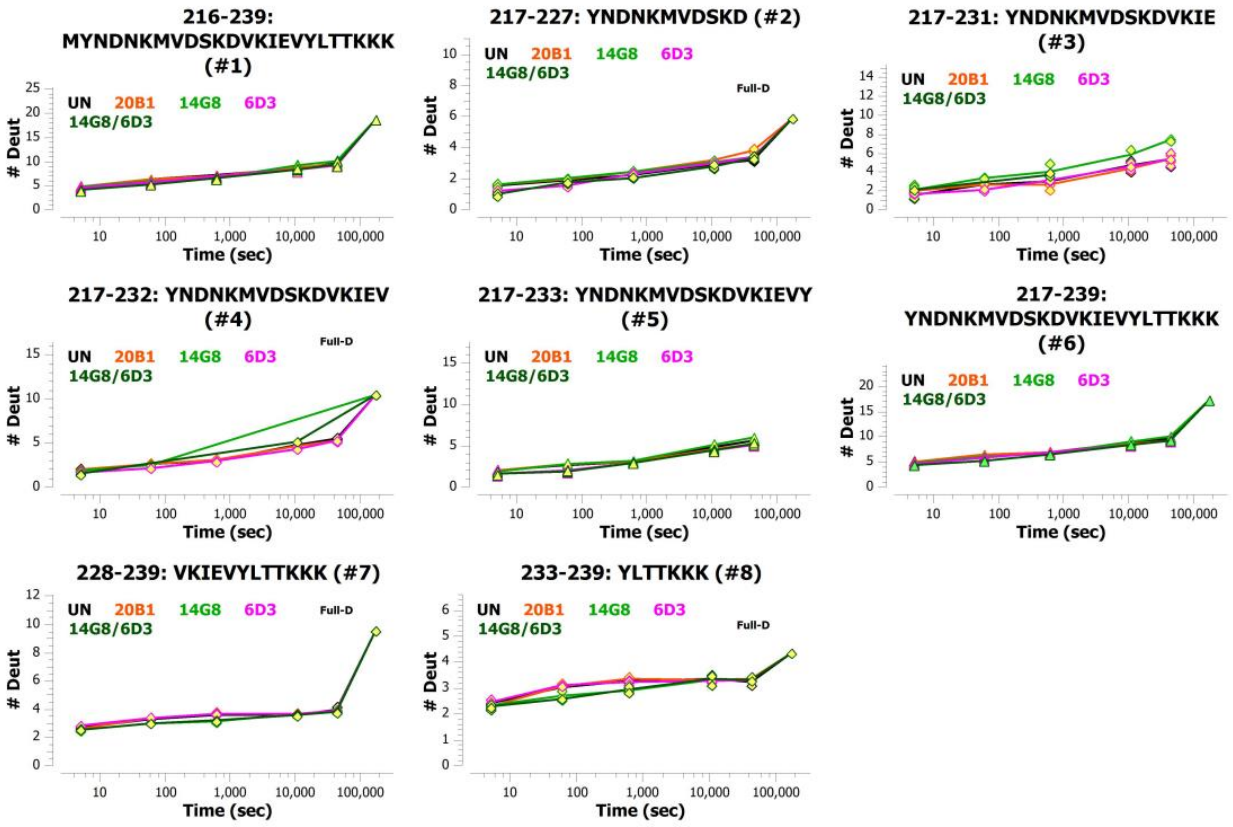

Supplemental Figure 3. All peptides identified from HDX experiments characterizing SEB-mAb interactions.

3.8 References

1 Faulkner, L., Cooper, A., Fantino, C., Altmann, D. M. & Sriskandan, S. The mechanism of superantigen-mediated toxic shock: Not a simple Th1 cytokine storm. *J Immunol* **175**, 6870-6877 (2005). https://doi.org:DOI 10.4049/jimmunol.175.10.6870

2 Krakauer, T. & Stiles, B. G. The staphylococcal enterotoxin (SE) family: SEB and siblings. *Virulence* **4**, 759-773 (2013). https://doi.org:10.4161/viru.23905

3 Schlievert, P. M. Role of superantigens in human disease. *J Infect Dis* **167**, 997-1002 (1993). https://doi.org:10.1093/infdis/167.5.997

4 al-Daccak, R., Mehindate, K., Poubelle, P. E. & Mourad, W. Signalling via MHC class II molecules selectively induces IL-1 beta over IL-1 receptor antagonist gene expression. *Biochem Biophys Res Commun* **201**, 855-860 (1994). https://doi.org:10.1006/bbrc.1994.1779

5 Assenmacher, M. *et al.* Sequential production of IL-2, IFN-gamma and IL-10 by individual staphylococcal enterotoxin B-activated T helper lymphocytes. *Eur J Immunol* **28**, 1534-1543 (1998). https://doi.org:10.1002/(SICI)1521-4141(199805)28:05<1534::AID-IMMU1534>3.0.CO;2-R

6 Bell, S. J., Vroegop, S. M. & Buxser, S. E. Early activation and cell trafficking induced by staphylococcal enterotoxin B: effects of high- versus low-dose challenge on induction of anergy. *Cell Immunol* **154**, 440-452 (1994). https://doi.org:10.1006/cimm.1994.1090

7 Johnson, S. & Gerding, D. N. Bezlotoxumab. *Clin Infect Dis* **68**, 699-704 (2019). https://doi.org:10.1093/cid/ciy577

8 Lowy, I. *et al.* Treatment with monoclonal antibodies against Clostridium difficile toxins. *N Engl J Med* **362**, 197-205 (2010). https://doi.org:10.1056/NEJMoa0907635

9 Leav, B. A. *et al.* Serum anti-toxin B antibody correlates with protection from recurrent Clostridium difficile infection (CDI). *Vaccine* **28**, 965-969 (2010). https://doi.org:10.1016/j.vaccine.2009.10.144

10 Sully, E. K. *et al.* A tripartite cocktail of chimeric monoclonal antibodies passively protects mice against ricin, staphylococcal enterotoxin B and Clostridium perfringens epsilon toxin. *Toxicon* **92**, 36-41 (2014). https://doi.org:10.1016/j.toxicon.2014.09.006

11 Chow, S. K. & Casadevall, A. Monoclonal antibodies and toxins--a perspective on function and isotype. *Toxins (Basel)* **4**, 430-454 (2012). https://doi.org:10.3390/toxins4060430

12 Varshney, A. K. *et al.* Generation, characterization, and epitope mapping of neutralizing and protective monoclonal antibodies against staphylococcal enterotoxin B-induced lethal shock. *J Biol Chem* **286**, 9737-9747 (2011). https://doi.org:10.1074/jbc.M110.212407

13 Xia, T. *et al.* Structural basis for the neutralization and specificity of Staphylococcal enterotoxin B against its MHC Class II binding site. *MAbs* **6**, 119-129 (2014). https://doi.org:10.4161/mabs.27106

14 Chen, G. *et al.* Potent Neutralization of Staphylococcal Enterotoxin B In Vivo by Antibodies that Block Binding to the T-Cell Receptor. *J Mol Biol* **431**, 4354-4367 (2019). https://doi.org:10.1016/j.jmb.2019.03.017

15 Verreault, D. *et al.* Effective Treatment of Staphylococcal Enterotoxin B Aerosol Intoxication in Rhesus Macaques by Using Two Parenterally Administered High-Affinity Monoclonal Antibodies. *Antimicrob Agents Chemother* **63** (2019). https://doi.org:10.1128/AAC.02049-18

16 Hnasko, R., Lin, A. V. & McGarvey, J. A. Rapid Detection of Staphylococcal Enterotoxin-B by Lateral Flow Assay. *Monoclon Antib Immunodiagn Immunother* **38**, 209-212 (2019). https://doi.org:10.1089/mab.2019.0028

17 Turner, K. B., Zabetakis, D., Legler, P., Goldman, E. R. & Anderson, G. P. Isolation and epitope mapping of staphylococcal enterotoxin B single-domain antibodies. *Sensors (Basel)* **14**, 10846-10863 (2014). https://doi.org:10.3390/s140610846

18 Zanganeh, S. *et al.* Rapid and Sensitive Detection of Staphylococcal Enterotoxin B by Recombinant Nanobody Using Phage Display Technology. *Appl Biochem Biotechnol* **187**, 493-505 (2019). https://doi.org:10.1007/s12010-018-2762-y

19 Rodstrom, K. E., Elbing, K. & Lindkvist-Petersson, K. Structure of the superantigen staphylococcal enterotoxin B in complex with TCR and peptide-MHC demonstrates absence of TCR-peptide contacts. *J Immunol* **193**, 1998-2004 (2014). https://doi.org:10.4049/jimmunol.1401268

20 Dutta, K. *et al.* Mechanisms mediating enhanced neutralization efficacy of staphylococcal enterotoxin B by combinations of monoclonal antibodies. *J Biol Chem* **290**, 6715-6730 (2015). https://doi.org:10.1074/jbc.M114.630715

21 Murphree, T. A., Vorauer, C., Brzoska, M. & Guttman, M. Imidazolium Compounds as Internal Exchange Reporters for Hydrogen/Deuterium Exchange by Mass Spectrometry. *Analytical Chemistry* **92**, 9830-9837 (2020). https://doi.org:10.1021/acs.analchem.0c01328

22 Masson, G. R. *et al.* Recommendations for performing, interpreting and reporting hydrogen deuterium exchange mass spectrometry (HDX-MS) experiments. *Nat Methods* **16**, 595-602 (2019). https://doi.org:10.1038/s41592-019-0459-y

23 Wang, L., Pan, H. & Smith, D. L. Hydrogen exchange-mass spectrometry: optimization of digestion conditions. *Mol Cell Proteomics* **1**, 132-138 (2002). https://doi.org:10.1074/mcp.m100009-mcp200

24 Watson, M. J. *et al.* Simple Platform for Automating Decoupled LC-MS Analysis of Hydrogen/Deuterium Exchange Samples. *J Am Soc Mass Spectrom* **32**, 597-600 (2021). https://doi.org:10.1021/jasms.0c00341

25 Vorauer, C. *et al.* Rapid Assessment of Pepsin Column Activity for Reliable HDX-MS Studies. *Journal of the American Society for Mass Spectrometry* (2021). https://doi.org:10.1021/jasms.1c00080

26 Xu, G. & Chance, M. R. Hydroxyl radical-mediated modification of proteins as probes for structural proteomics. *Chem Rev* **107**, 3514-3543 (2007). https://doi.org:10.1021/cr0682047

27 Tong, X., Wren, J. C. & Konermann, L. gamma-Ray-mediated oxidative labeling for detecting protein conformational changes by electrospray mass spectrometry. *Anal Chem* **80**, 2222-2231 (2008). https://doi.org:10.1021/ac702321r

28 Xu, G., Kiselar, J., He, Q. & Chance, M. R. Secondary reactions and strategies to improve quantitative protein footprinting. *Anal Chem* **77**, 3029-3037 (2005). https://doi.org:10.1021/ac048282z

29 MacLean, B. *et al.* Skyline: an open source document editor for creating and analyzing targeted proteomics experiments. *Bioinformatics* **26**, 966-968 (2010). https://doi.org:10.1093/bioinformatics/btq054

Chapter 4: Direct mapping of polyclonal epitopes in serum by HDX-MS

4.1 Introduction

Understanding how serum antibodies bind antigens is central to understanding the adaptive immune response. Serum reactivity has been dominated by ELISA, fluorescent assays, and other methods that can accurately quantify the reactivity to a specific protein but do not interrogate the full complexity of the antibody response. Emerging technologies are being developed to sequence and characterize immune response from serum [1,2]. B-cell sorting and sequencing is often used to glean genomic and transcriptomic information about the B-cell repertoire [3,4], but results do not capture information on actual protein content. Proteogenomic pipelines have been implemented that utilize B-cell receptor genomic findings to identify IgG contents in serum samples [5,6], and *de novo* sequencing of Fab fragments has also been deployed to identify the diversity of the antibodies in serum [7]. These methodologies have revealed the uniqueness of IgG populations between individuals as well as the divergence between the B-cell receptors and IgG repertoires [8]. Notably, most B-cell receptors sequences are not observed as IgG proteins, and key determinants of antibody repertoire remain uncharted. An understanding of binding epitopes across a polyclonal antibody mixture in serum could provide biophysical meaning and link specific antibody diversity with functional insight.

Fragment-based approaches and yeast display platforms are capable of mapping some of the interactions within sera. Bead-based separation, phage display, and DNA barcoding have all been used to identify linear epitopes [9-11]. While these platforms provide useful insights into select interactions, fragment-based approaches fail to characterize non-linear epitopes of target proteins. Interactions of proteins displayed in yeast in the AlphaSeq platform have been shown to track interactions of multiple proteins via fused DNA barcoding [12], but it is not possible to express or mimic the complete swath of proteins in serum in an artificial system of this kind.

Site-directed mutagenesis possesses the potential to interrogate the binding interactions of proteins in complex solutions, and deep mutational scanning has been deployed to map changes that arise in sera antibody binding as a result of widespread mutation. Alanine scanning or shaving, the replacement of specific residues with alanine to test the effect on binding to localize interactions, has been established as a common method of site-directed mutagenesis with known protein pairs [13]. Theoretically, this approach could be used to interrogate the interactions of complex solutions. However, this assumes expression of many mutant versions of the recombinant protein in question is

straightforward. Deep mutational scanning has been deployed to map the effects of widespread amino acid alteration of a target protein with the ability to bind neutralizing antibodies in order to track stabilizing and escape mutants [14-16]. Though previous attempts at using deep mutational scanning to track the effects of mutation have been focused on mapping sites of alteration to antibody binding as opposed to neutralization, a recent study by Dadonaite et al. has integrated genotype-phenotype-linked lentivirus pseudotyping in order to correlate structure-altering mutation with function [17].

Electron Microscopy (EM) is also capable of mapping multiple interactions of purified species on an antigen of interest. Negative stain-EM has primarily been deployed to map complex interactions [18], and recently cryo-EM has been used to map multiple interactions at greater resolution [19]. Epitope findings from EM have been enriched with mutational antigenic profiling to correlate functional effect of single amino-acid mutation [20]. EM-based approaches to mapping polyclonal response effectively map the general location of epitopes and provide useful information on the angle of approach of the antibody, but have, to date, only interrogated purified Fab fragments.

Hydrogen Deuterium Exchange (HDX) MS- HDX-MS is an established and adept method for the study of specific protein interactions that have shown promise in mapping binding sites of polyclonal antibodies. HDX probes the exchange of backbone amide hydrogens to capture residue-level detail of linear and conformational epitopes as well as allosteric changes that arise after binding [21]. Success in the study of multi-protein complexes has inspired interest in interrogating more complex heterogeneous samples by HDX [22]. Additionally, multiple known purified mAb epitopes have been successfully mapped onto the structure of an antigen, at the same time verifying the possibility of epitope mapping of the entire arsenal of antibodies in serum [23]. Recent attempts to probe interactions of serum by HDX-MS have been limited to serum that has been purified [24-27]. Here we introduce an HDX-MS workflow capable of probing and mapping epitopes within fully native interactions in serum. Our approach includes the full complexity of serum: the non-binding immune species, binding antibodies, and non-IgG species innate to serum that can all potentially influence binding activity.

4.2 Methods

4.2.1 Reagents

Staph Enterotoxin B (SEB), anti-SEB sheep serum, and anti-SEB rabbit serum were purchased from Toxin Technologies Inc. (Sarasota, FL). Dynabeads™ M-280 Streptavidin (11206D) and EZ-Link™ NHS-SS-

PEG4-Biotin (21442) were acquired from ThermoFisher. 20B1, 14G8, and 6D3 anti-SEB mAbs were generated as described previously [28].

4.2.2 Sample Preparation

4.2.2.1 *SEB biotinylation*

SEB and EZ-Link™ NHS-SS-PEG4-Biotin were incubated in PBS (pH 6.0) for 1h at 0˚C. Excess biotin reagent was removed by washing the protein using 3k cutoff spin filters in 0.1 M sodium phosphate, 0.15 M NaCl buffer pH 7.4 (PBS). The extent of biotinylation was tracked by the shift in mass of 533 Da by MALDI-TOF using a Bruker Autoflex II operating in linear mode using a matrix of saturated sinapinic acid in 30% acetonitrile and 0.1% trifluoroacetic acid.

4.2.2.2 Serum quantification by biolayer interferometry (BLI)

The magnitude of SEB reactivity with anti-SEB sheep, anti-SEB rabbit, and normal rabbit serum was determined using biolayer interferometry on an Octet Red96 (FortèBio). Streptavidin-coated tips were presoaked in binding buffer (PBS pH 7.4 supplemented with 0.1% BSA, 0.005% Tween 20) for 10 min. The hydrated tips were then loaded with biotinylated SEB prepared at 12 µg/mL in binding buffer for 120 s. After reaching a stable baseline, biotinylated-SEB immobilized biosensors were then moved into wells containing 1 µg/mL biocytin for 120 s to block free streptavidin. After reaching a stable baseline, the biosensor tips were moved into wells containing a 4-fold dilution series of serum (normal, anti-SEB sheep, or anti-SEB rabbit) for 200 s. Responses were calculated and double-referenced against the buffer signal and non-specific binding of analyte to biosensor in the absence of biotinylated-SEB. Kinetic data were analyzed by using FortéBio Data Analysis 11.0 software. Approximate serum concentration of SEB-reactive antibody was determined using normalized signal generated from a 4-fold dilution series of 20B1 using the same format and experimental parameters (Supplemental Figure 4).

4.2.2.3 HDX Sample Preparation

400 µg of M-280 dynabeads were washed in PBS and incubated with 2.5 µg (83 pmol) of biotinylated SEB in 1 mL PBS while gently being rocked for 1 hour at room temperature. Dynabeads were separated from the supernatant using a magnet and custom 1.5mL tube holder. Beads were washed two more times, incubated with a molar ratio of 5:1 serum antibodies:SEB, and incubated with gentle rocking for 1h. Samples were then washed twice, the supernatant removed (to remove unbound serum proteins), and then diluted in deuterated buffer (500µL, PBS, 95% D2O, pH*7.52) for either 60 s or 600 s at room temperature while gently rocking. The reaction was stopped by removing 400 µL of D_2O and subsequently

diluting 1:1 in ice-cold quench buffer (100 µL, 4 M urea, 0.2% formic acid) to a final pH of 2.5 and a total volume of 200 µL. This supernatant (containing serum species that bound SEB) was then removed and saved for later analysis. The remaining beads were then diluted in a second quench buffer (200 µL volume, 200 mM tris(2-chloroethyl) phosphate (TCEP), 4 M urea, 0.2% formic acid pH 2.5). The quenched samples were then briefly vortexed every 5 s for 1 min at 0˚C. At 1 minute, the supernatant was removed and flash-frozen in dry-ice ethanol, followed by storage at −80°C prior to LC-MS analysis.

4.2.2.4 In-line digestion and LC-MS

Online pepsin digestion was performed and analyzed by LC-IMS-MS utilizing a Waters Synapt G2-Si Q-TOF mass spectrometer as described previously utilizing a 15 min gradient and a home-made HDX cold box that maintains the pepsin digestion at 5°C and the LC plumbing at 0°C [29]. MS^E fragmentation was performed on the Synapt G2-Si Q-TOF to identify peptide fragments. Peptides, including those peptides with fragments of the reduced disulfide biotin reagent, were identified using Byonic (Version 3.8, Protein Metrics Inc.) with deamidation at N and Q, oxidation at C, M, W, and Y, and N-terminal cyclization at E and Q variable modifications selected. A cutoff score of 100 was allowed. Deuterium uptake analysis was performed with HD-Examiner (Version 2.5, Sierra Analytics) followed by HX-Express v2 for binomial fitting and bimodal deconvolution [30,31].

4.2.2.5 Identification of SEB-bound serum proteins by LC-MS

The supernatant from the first quench that contained the species that bound SEB and eluted in 2M Urea was brought to a pH of 8.0 with the addition of 50mM Tris and treated with 5 mM DTT at 50˚C for 30 minutes. 4 uL of 500 mM iodoacetamide was then added followed by a 30-minute incubation in the dark. The iodoacetamide was then quenched with an additional 5 mM addition of DTT. The sample was then diluted 2-fold in water to achieve a Urea concentration of 1M and digested with 2 ug trypsin at 37˚C overnight. The digestion was quenched by adding 20 uL of 10% formic acid. Samples were analyzed by LC-MS on a Thermo Orbitrap Elite mass spectrometer. A Waters UPLC CSH C18 column, 130Å, 1.7 µm, 2.1x100 mm with water and acetonitrile, both with 0.1% FA, for 15 min gradient with the LC heated to 70 ˚C was used. Peptides were identified from the Swiss-Prot database using Byonic (Version 3.8, Protein Metrics Inc.) (Table 1.).

4.2.2.6 Pre-bound antibody, serum competition by biolayer interferometry

The magnitude of SEB reactivity after pre-binding with known, characterized antibodies with anti-SEB sheep, anti-SEB rabbit, and normal rabbit serum was determined using biolayer interferometry Octet

Red96 (FortèBio). The same protocol described above to quantify serum concentration was used. Antibodies 20B1, 14G8, and 6D3 were separately pre-bound at analogous binding signals to immobilized SEB prior to dipping in serum-containing wells. The effect of pre-binding different mAbs on the ability to bind different serum species was analyzed and visualized using Microsoft Excel (Figure 5).

4.3 Results

A methodology for studying and mapping interactions of a target protein, *Staph* enterotoxin B (SEB), in this instance, with neutralizing serum was developed. The general concept was to immobilize SEB before exposing it to a complex mixture of binding partners (Figure 1). Non-binding species were removed before assaying the immobilized and bound protein. In the process of quenching, the exchanged, bound antibody species were removed before LC separation and mass spectrometric analyses were performed.

Prior to immobilization and the HDX assay, SEB was selectively biotinylated. Biotinylation was vital in order to extract protein from raw serum after incubation. Established succinamate chemistry was performed to join a biotin-containing linker to free amines on the structure of the protein. The biotin-containing reagent additionally contained four PEG (polyethylene glycol) linkers (to space the biotin away from the protein structure) and a thiol linker (for removal after assaying the protein). Biotinylation of the protein was confirmed via observation of an increase in the mass of SEB by 533 Da (Supplemental Figure 1). Peptide mapping of biotinylated SEB was used to reveal the peptic thiol-SEB peptide fragment post-reduction of the disulfide bond predominantly at two lysine sites— K57 and K109 (Supplemental Figure 3).

Next, we determined the efficiency of SEB capture and release for use with HDX-MS. Confirmation of immobilization was achieved via gel electrophoresis (Supplemental Figure 2). Of the 2.5 ug biotinylated SEB added to the beads, we estimated 1 ug of product was immobilized and released. Washing the beads with HDX quench buffer (pH 2.5) containing 4M Urea, did remove bound anti-SEB species but did not disrupt the streptavidin-biotin interaction, thus leaving SEB on the beads. A subsequent quench containing 4M Urea and 500mM TCEP was able to break the disulfide linker within the biotin tag to release SEB from the beads (Supplemental Figure 2). Importantly, the second quench step could release the SEB within the span of 1 minute to enable the workflow to be used for HDX without severe deuterium loss.

To confirm the feasibility of the immobilized HDX method, we sought to compare differential uptake of a solution HDX experiment of a known anti-SEB monoclonal antibody, 20B1, with the differential

uptake of the immobilized HDX format of the same binding pair. Given the protracted, one-minute-long quench step, back-exchange was a major concern, and inclusion of back-exchange controls was not possible given the removal of the deuterium buffer in the wash step. It was determined that uptake trends across the structure of SEB in the immobilized experiment mimicked those of the solution HDX experiment, albeit with dampened lower overall levels of deuteration (Figure 2). Uptake was similarly muted in both unbound species and 20B1 bound species, indicating back exchange was consistent across the whole assay. Importantly, both solution and immobilized data sets showed the same specific changes of increased protection at peptides 1-22 and 161-185.

Having validated the immobilized HDX-MS approach, we next sought to assay epitopes targeted by anti-SEB serum. To quantify the levels of anti-SEB antibodies in polyclonal serum, we performed BLI side by side with a known mAb (Supplemental Figure 4). 20B1, an antibody known to bind SEB, produced a signal between 0 nm and 1.5 nm after 200 s of association in a 4-fold dilution series with concentrations of 0.5 nM to 500 nM. Anti-SEB sera were diluted 200-fold and assayed by BLI using the same descending 4-fold dilution series. Importantly, normal rabbit serum showed no binding to SEB, confirming the specificity of the antibodies in the anti-SEB sera.

When assayed using the newly established immobilized HDX format, the concentration estimates from BLI were used to ensure at least three-fold excess of SEB reactive antibodies were incubated with the immobilized SEB. Signal from the exchanged 1 µg injected protein signal was sufficiently intense and not suppressed by the background protein in serum. The two different sera produced unique uptake patterns, suggesting distinct epitope targeting between the different species. Notable decreases in the uptake in deuterium for peptides 115-133, 198-208, and 137-146 for the anti-SEB sheep serum and peptides 36-43, 198-208, and 137-146 for the anti-SEB rabbit serum were observed (Figure 3). A significant increase in the uptake of deuterium was also observed on peptide 52-64 after exposure to rabbit serum. The most profound changes were decreases in deuterium uptake on the structure of SEB after exposure to anti-SEB sheep serum at residues 115-133, while the rabbit serum saw largest differences in uptake at residues 134-146 of SEB. Notably, both sera had quiet regions with little or no change in uptake, suggesting antibodies focused on distinct, select regions. Additionally, multimodal behavior was suspected in regions of significant decrease in uptake of deuterium (Figure 4). Multimodal behavior can describe an epitope region either bound partially or bound to different species with distinct exchange kinetics. Normal serum was seen to have no effect on deuterium uptake of SEB relative to the non-

immobilized experiment. Similar to the uptake of 20B1, the uptake profile of the unbound condition was dampened but still qualitatively similar (Figure 2).

The format of this assay allows for removal of bound species in the first, non-TCEP-containing quench step, a step intended to simplify mass spec analysis of the protein of interest. The supernatant of the first quench was pooled and analyzed by bottom-up proteomics to identify what proteins were present. It was observed that the species bound to SEB from both the sheep and rabbit sera were predominantly albumin and IgG of varying isoforms, as confirmed by both light and heavy chains of species-specific immunoglobulin (Table 1.). The non-antibody contents from the first quench confirm the complexity innate to raw serum.

In an effort to confirm the predominant epitopes identified from HDX-MS, we performed a BLI competition assay using mAbs of known specificity (Figure 5). 14G8 and 6D3 are neutralizing antibodies that are known to bind critical sites on the structure of SEB distinct from 20B1, another neutralizing anti-SEB antibody [32]. It was observed that when 14G8 or 6D3 were pre-bound to SEB, they had a larger inhibition of serum binding consistent with the predominant epitopes found by HDX-MS for the rabbit and sheep serum, respectively. As confirmed by a competition BLI assay, the rabbit and sheep sera focus on distinct regions on the surface of SEB to support the novel HDX method for analyzing complex solutions.

4.4 Discussion

An immobilized HDX-MS assay is presented here for studying where antibodies from raw serum bind on the structure of an antigen of interest. Current HDX protocols that interrogate multiple immune species present only a partial view of the full polyclonal repertoire as they are dependent on prior affinity enrichment. Zhang et al. and Abbott et al. outlined the first attempts to screen for epitopes from a heterogenous IgG sample by HDX by using isolated Fab fragments from a purified polyclonal antibody mixture [24,25]. Full-length serum recovered mAbs from target affinity purification were assayed by HDX to determine epitope diversity to aid in the selection of species with favorable therapeutic lead candidate antibodies [26]. Methodology for heterogenous IgG HDX analysis advanced again in 2021 when Ständer et al. proposed a series of clean-up and purification steps to remove non-IgG and non-binding IgG species prior to HDX analysis [27]. In the method presented here, complexes form under biologically relevant conditions, including the non-binding species that can potentially influence the nature of interactions but

are often omitted in structural studies as they complicate analysis. We revealed protection from deuterium exchange at select peptides on the structure of SEB after incubation in anti-SEB serum that corresponds to regions of concentrated interaction, which is consistent with competitive binding assays against antibodies that bind the similar epitopes of interest.

The mass envelope broadening that was observed at the most protected peptides we postulate corresponds to multiple antibody species binding proximal epitopes. Peptides 115-133 and 134-146 for sheep and rabbit, respectively saw the greatest decrease in the number of deuterium exchanged. The peptides in the sheep and rabbit conditions in those areas of interest were seen to have significant peak broadening relative to the same peptides in the other serum condition and unbound (non-anti-SEB serum) condition. Peak broadening is indicative of multimodal behavior, or the presence of multiple unique species present in solution contributing to a variety of deuterium exchange kinetics. The data suggest that antibodies that bind to the same or similar epitopes on the structure of SEB create sub-populations of the SEB peptides analyzed with unique kinetic profiles, which broadens the deuterated mass envelope analyzed. It is likely that HDX is sampling multiple antigen populations that could arise from binding different species or binding multiple species.

Interestingly, peak broadening at peptides 115-133 and 134-146 for rabbit and sheep, respectively (not the most substantial areas of decrease in deuterium uptake for those respective species) also revealed peak broadening relative to the unbound condition, which we speculate is caused by SEB-mAb populations that result from less prominent binding epitopes that include those particular peptides. This suggests that multiple antibody populations bind regions of even mild reduction of deuterium uptake. These findings suggest that multiple, relatively high-affinity species are likely competing for the same predominant epitope region as well as for other, less dominate epitopes.

The kinetic competition assays using antibodies with known binding epitopes on SEB helped to confirm the predominant regions of observed serum binding as identified by HDX-MS. We hypothesized that by pre-binding the region of observed deuterium uptake with a known antibody, we could observe a greater decrease in serum binding signal as compared to pre-binding a mAb for an epitope where no decrease in deuterium was observed in the serum experiments. To standardize the experiments, a similar antibody pre-binding BLI signal was achieved prior to baseline and association with serum. The authors acknowledge that the different monoclonal antibodies have differing kinetic behavior, which might impact dissociation of mAbs as serum is binding. Though this might affect the binding kinetics of anti-SEB serum for SEB, we believe that impact to be negligible. Peptide 115-133 for sheep and 137-146 for rabbit were

peptides observed to see a significant reduction in deuterium, but also known to be part of the binding interface of known neutralizing mAbs 6D3 and 14G8, respectively. Reduction in BLI signal as a result of pre-binding an epitope-specific antibody relative serum association alone is likely the result of the population of serum antibodies specific to that epitope are no longer able to bind. These experiments help confirm that different anti-SEB sera have differences in relative epitope specificity.

A major requirement of our HDX approach is the biotinylation of the antigen with a disulfide-containing reagent. While it is possible to express protein with a biotin tag recombinantly [33], the resulting conjugated biotin will not have the disulfide linker that is necessary for antigen release. Therefore, antigen labeling can currently only be accomplished through *in vitro* protein labeling. In this study, biotinylation of the SEB structure was accomplished using succinamate chemistry that reacts with lysine sidechains. Selective targeting of the protein N-terminal amine is often possible at lower pH (around pH 6.0) [34,35], but unfortunately for SEB, the N-terminal glutamic acid was predominantly cyclized into pyroglutamic acid and thus unreactive. Since several lysines are likely involved in epitopes, it is critical to optimize labeling times and conditions to achieve minimal biotinylation of only a few residues, and not indiscriminate biotinylation of all surface lysines. Each lysine is present in an unmodified form. Despite the likely heterogeneity of biotin labeling, the HDX approach was still able to detect unmodified forms of all peptides and ultimately determine the 20B1 epitope, which contains lysines that are also partially biotinylated. In all likelihood, SEB actually likely reflects a more challenging antigen for biotin labeling, and this approach might be easier with most other antigens.

Perturbation of protein structure and altered affinity to other proteins was a concern upon biotinylation that was ultimately addressed via the control experiment with the known anti-SEB antibody, 20B1 (Figure 1). Peptide mapping allowed for localization of the biotins on the surface of SEB via the detection of the thiol fragment after the breaking of the cleavable disulfide linker. The location of biotins on SEB is in close three-dimensional proximity to the epitope of 20B1. Solution HDX compared with immobilized HDX showed little difference in the relative magnitude shift of the unbound versus bound comparative HDX. This suggests that the biotins had little effect on the ability of a known antibody to bind in close proximity. HDX monitored the unmodified peptide species and given that peptide coverage on SEB was 100%, subpopulations of different biotinylated versions of SEB were present, a notable caveat of this assay.

Bead type was specific for this system and will likely need to be adjusted for different proteins assayed. It was previously reported that protein immobilization does not affect allostery and binding [36],

but the sought to confirm this nonetheless with dynabeads. M-280 dynabead selection was found to be effective for this specific immobilized HDX assay with raw serum, but other application-dependent options exist that may yield more favorable results for proteins with different properties.

Serum concentration also must be determined for protein type, ideally quantitatively. The authors employed BLI to determine a general concentration of anti-SEB species in the serum, but more established ELISA-based titers will likely also suffice. To confirm that serum species had bound to the dynabeads, a BLI experiment comparing serum that had been exposed to bead-immobilized SEB with the original serum at like concentration was performed (Supplemental Figure 5). Depleted rabbit serum signal was observed to drop 30%, while sheep serum signal was observed to drop 10%, both relative to the original serum at the same concentration. These results confirm that some, but not all, anti-SEB species from serum-bound SEB prior to the HDX assay.

The complexity of raw serum cannot be understated. Even after multiple washes to remove non-binding species, the majority of species that were present with the immobilized SEB and the beads were albumin, followed by other abundant serum proteins, including lipoproteins and transferrins. It is possible that additional or more stringent washing might make it possible to remove these species, but we find that their removal was not critical for the assay. Wash and quench optimization is an element of the immobilized assay that may need to be adjusted for different applications and protein systems. The number of post-serum-binding washes is speculated to be a tunable feature of this assay that could influence and select the type of species bound to the immobilized protein. Duration of serum incubation certainly influences the species bound, with shorter duration incubations favoring species with fast “on” rates and tighter K_Ds and longer incubations favoring slower “off” rates. The number of post-incubation washes likely influences the bound species selected, with more washes favoring species with more robust affinity. Additionally, it is well understood that different proteins are denatured with different chaotropic agents [37]. 4M Urea performed notably well for this application. Others could be substituted in this assay. The duration of the first clean-up wash could be extended to remove additional bound species or removed entirely if complexity in MS analysis is not a concern. There are practical considerations for post-quench washes, most notably the increased back exchange that occurs with an increased number or duration of washes, despite the washes being cold and at pH 2.5. It is estimated that the one-minute cold post-quench wash was found to back exchange deuterium approximately 20-25% more than the analogous solution HDX experiment. The format as presented here was most effective when the entire quench series lasted no longer than one minute.

Results from the immobilized HDX experiment of SEB revealed distinct patterns of epitopes mostly, but not entirely, distal to biotinylation sites. It was established, with the control condition using 20B1, that biotinylation does not impact the ability of antibodies to bind epitopes nearby. A notable confirmation of this point is peptide "D" (36-43) in the rabbit anti-SEB condition, which reveals a statistically significant reduction in deuterium uptake. There is at least a subpopulation with no biotin on every peptide analyzed, so the assay still probes all possible epitopes. This could be the result of assay development, which, due to the way the species were washed, could have favored anti-SEB antibodies with slower off rates that may have favored distal epitopes. A robust HDX study of antibodies with different kinetic profiles sampled from sera would inform perspective on these data.

While the immobilized HDX format here is validated for serum antibodies, it can also be applied to study antigens in other complex environments, such as in the presence of highly concentrated molecular crowders [38]. The immobilized HDX format also allows easy removal of excipients, detergents, lipids, and other impurities that might otherwise complicate analysis by LC-MS. Additionally, it is possible to do experiments with low-affinity small molecules where a huge excess is necessary that will add an excessively high background to the LC-MS step. Finally, so long as biotinylation is possible, this method can be applied across all types of proteins, including glycoproteins and membrane proteins.

4.5 Acknowledgments

The authors wish to thank Dale Whittington and J. Scott Edgar for their assistance with data collection and David Weis for insightful discussions. Anti-SEB monoclonal antibodies were kindly provided by Bettina Fries. Dynabeads were provided by Rosa Viner, Kay Opperman, She Yuqi, and Ryan Bomgard at Thermo Fisher.

4.6 Figures

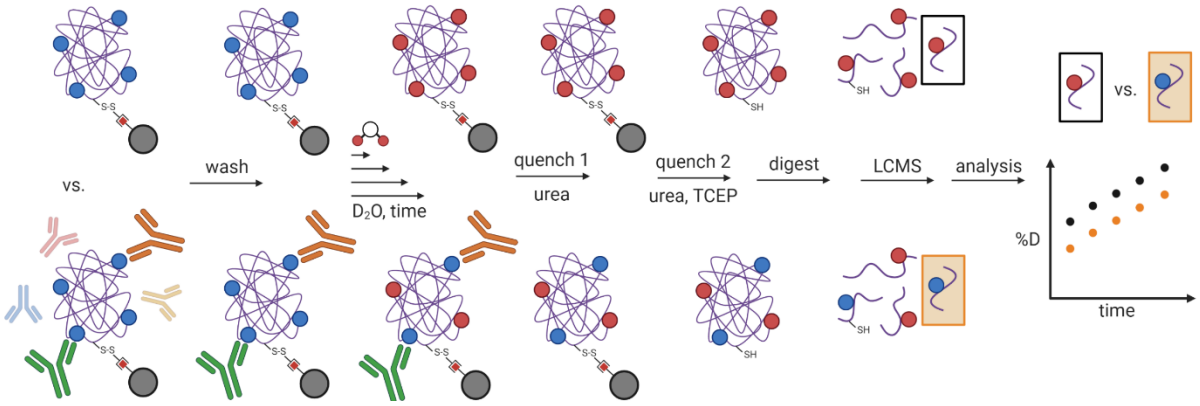

Figure 1. A workflow for mapping serum epitopes using differential HDX-MS. Uptake of immobilized, unbound protein (above) is compared to a serum bound condition. Deuteration is quenched in a two-step process before the final supernatant is digested and analyzed by LC-MS.

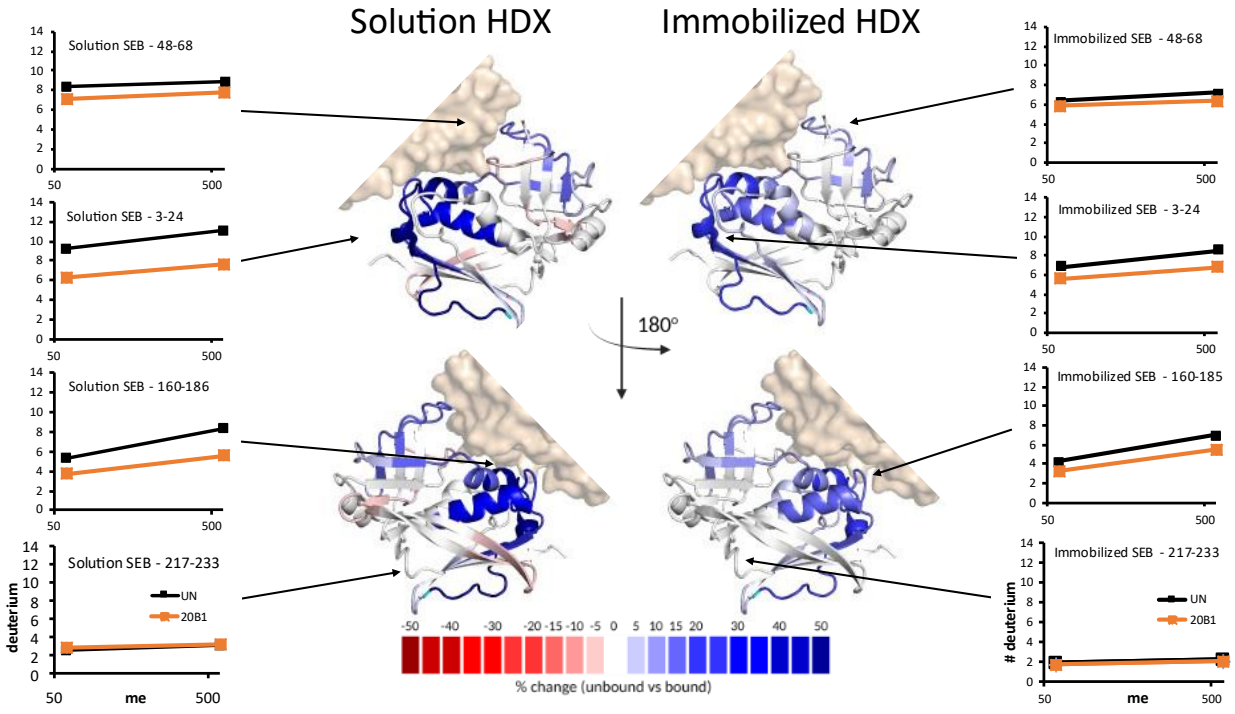

Figure 2. Solution HDX is compared to immobilized HDX using the proposed workflow. Uptake trends are similar between methods. Deuterium uptake is dampened across all peptides and conditions.

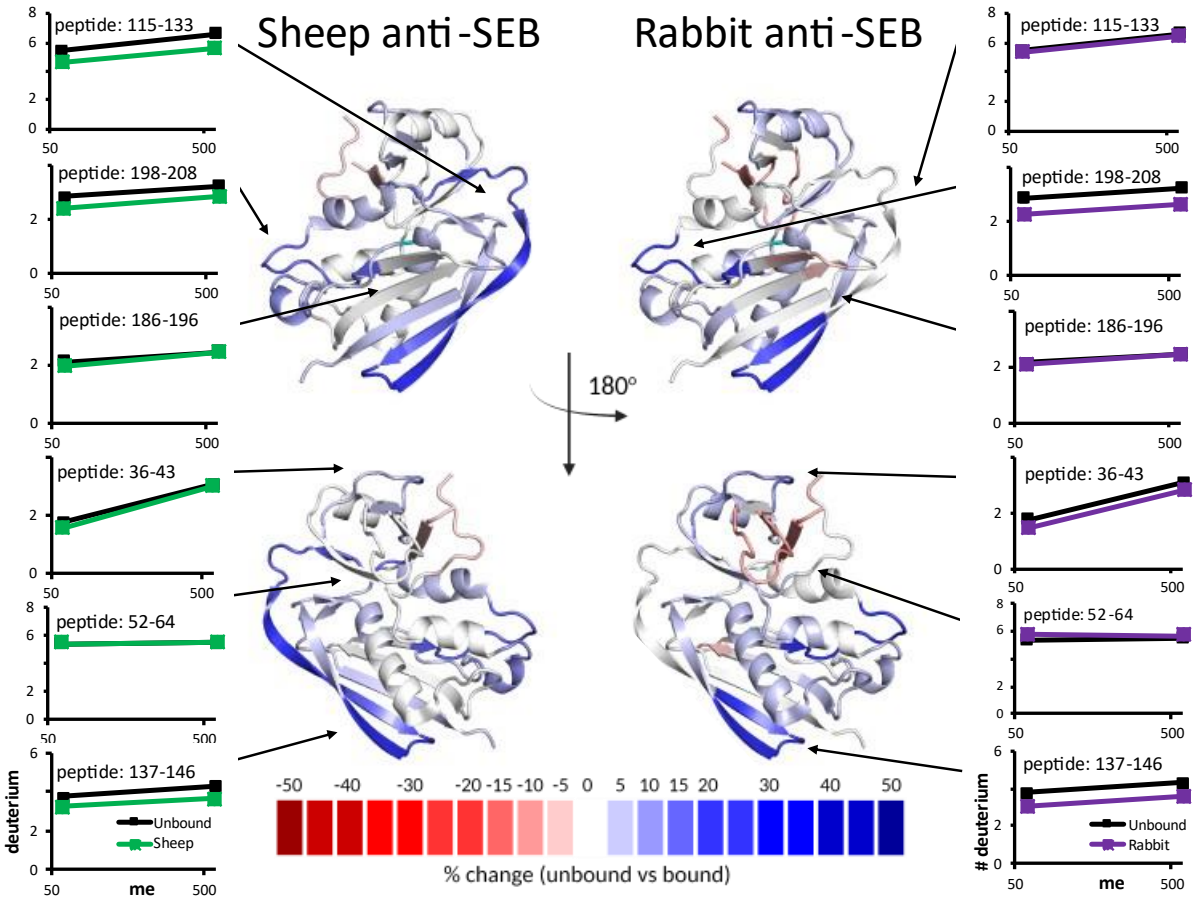

Figure 3. The uptake of deuterium for anti-SEB sheep and anti-SEB rabbit serum bound to SEB are compared relative to an unbound (normal rabbit serum) condition. Uptake is distinct between the two species conditions and significant reduction of deuterium is observed at select peptides.

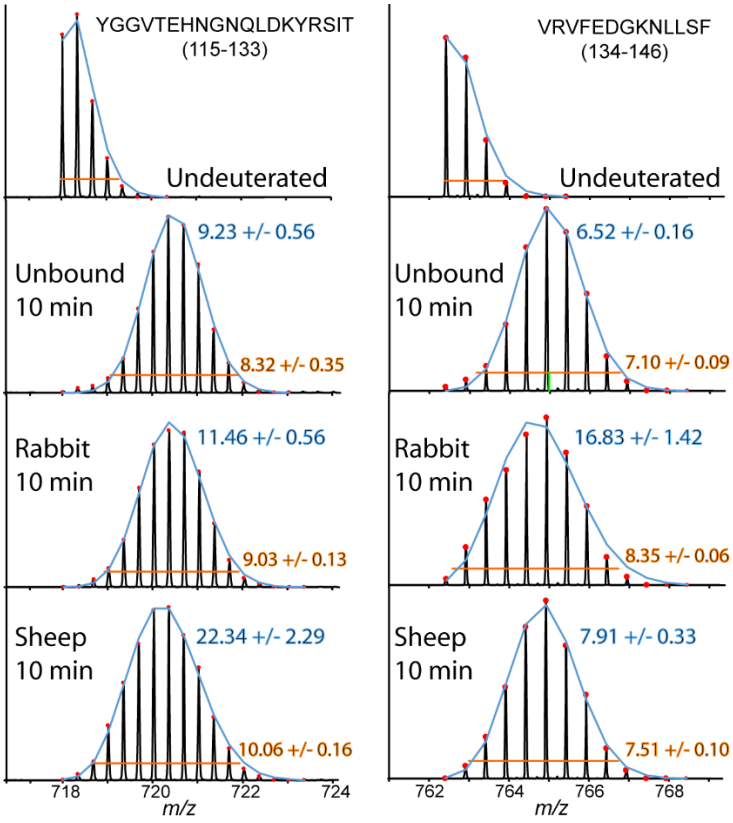

Figure 4. Peak broadening and amide fitting of peptides 115-133 and 134-146 is displayed. For peptide 115-133, the predominant epitope of the sheep serum, the peak width (displayed in orange) is seen to increase substantially more in the sheep serum bound condition. The optimal number of amides fit to the sheep serum bound curve (displayed in blue) is also observed to increase in the sheep serum bound condition. An increase of both peak width and number of amides fit to the mass envelope is observed on peptide 134-146 (the predominant rabbit serum epitope observed) in the rabbit serum bound condition.

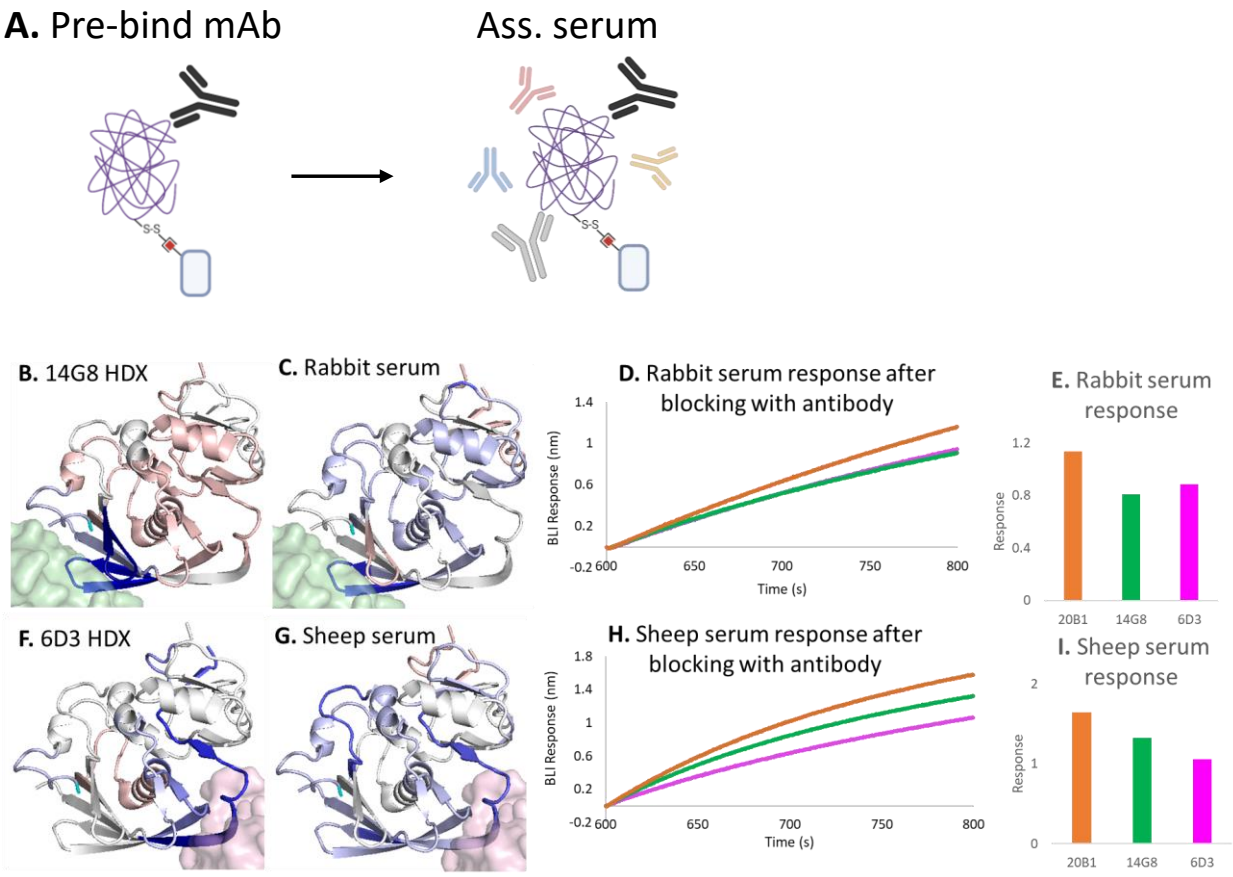

Figure 5. Pre-binding antibody prior to association of serum. **A.** General illustration. **B.** Differential solution HDX of neutralizing antibody 14G8. **C.** Differential immobilized HDX of rabbit serum. **D.** Association of rabbit serum after pre-binding of 6D3, 14G8, and 20B1 at analogous binding signals. **E.** BLI response after 200s association of rabbit serum after pre-binding mAbs. **F.** Differential solution HDX of neutralizing antibody 6D3. **G.** Differential immobilized HDX of sheep serum. **H.** Association of sheep serum after pre-binding of 6D3, 14G8, and 20B1 at analogous binding signals. **I.** BLI response after 200s association of sheep serum after pre-binding mAbs.

	Species Identified: Sheep					
Sample	# Uni	% Cov	Best Disc Score	Best Exp Val	Protein MW	Protein Name
Sheep anti-SEB	17	30.5	3.9	1.30E-06	69188.9	serum albumin precursor
	10	83	3.92	1.20E-06	11328.7	immunoglobulin lambda light chain
	7	38.6	3.75	2.50E-06	33778.4	Ig heavy chain C region
	7	12.9	2.36	2.10E-04	77341.2	serotransferrin
	2	15.2	2.73	1.60E-04	25362.5	Ig kappa chain
	1	29.4	3.37	1.70E-06	12676.5	immunoglobulin heavy chain
	1	25.4	0.38	0.0043	12377.7	immunoglobulin V lambda chain
	Species Identified: Rabbit					
Rabbitt Anti-SEB	22	42.3	3.92	1.20E-06	68910.5	serum albumin precursor
	10	41	3.99	8.90E-07	35292.4	Ig gamma H-chain C-region
	3	7.1	2.41	4.60E-05	66141.3	albumin
	2	11.7	3.06	2.20E-05	30591.7	apolipoprotein
	2	8.1	1.98	0.0047	49897.8	Ig mu chain C region secreted form
	1	7.1	2.86	1.10E-04	25082.2	immunoglobulin kappa chain
	1	5.3	2.62	2.20E-04	25491.9	complement component 1
	1	20.5	1.71	1.30E-04	8654.9	Ig heavy chain precursor V-A1 region
	2	4	1.03	0.0018	76614.1	serotransferrin precursor
	Species Identified: Rabbit					
Normal rabbit	14	29.8	4.39	1.60E-07	76614.1	serotransferrin precursor
	3	16.2	3.38	1.20E-05	30591.7	apolipoprotein
	1	7.1	3.37	1.20E-05	25082.2	immunoglobulin kappa chain
	2	37	1.7	0.0037	13657.4	prealbumin
	2	8.1	1.3	0.0011	38869.6	haptoglobin precursor
	2	10.9	1.2	7.00E-04	60950.4	histidine-rich glycoprotein
	1	4	1.56	5.10E-04	39320.2	alpha-1-microglobulin/bikunin-like
	1	2.9	1.11	0.0061	45684.7	alpha-1-antiproteinase E precursor
	Species Identified: Mouse					
20B1, anti-SEB (mouse)	8	41.8	3.12	1.00E-05	36389.8	immunoglobulin heavy chain gamma
	2	10.3	3.47	8.10E-06	23754.5	immunoglobulin kappa light chain
	4	28.8	1.31	0.0038	26878.2	immunoglobulin kappa light chain
	4	32.1	1.31	0.0038	23998.7	immunoglobulin light chain
	4	32.1	1.31	0.0038	23873.8	monoclonal antibody 13-1 light chain
	3	27.8	1.31	0.0038	13837.5	gene Pvt-1a/Ig-Ck protein
	3	28.9	1.29	0.0041	23845.8	Ig kappa chain V region (Mab13-1)
	3	28.9	1.29	0.0041	23774.5	immunoglobulin light chain
	1	8.6	2.56	1.60E-04	13093.8	immunoglobulin heavy chain
	1	11.8	2.13	0.0024	13969	Immnogloblin light chain
	1	17.2	0.31	0.008	10301.8	immunoglobulin heavy chain

Table 1. Species identified in the first quench step.

4.7 Supplemental Figures

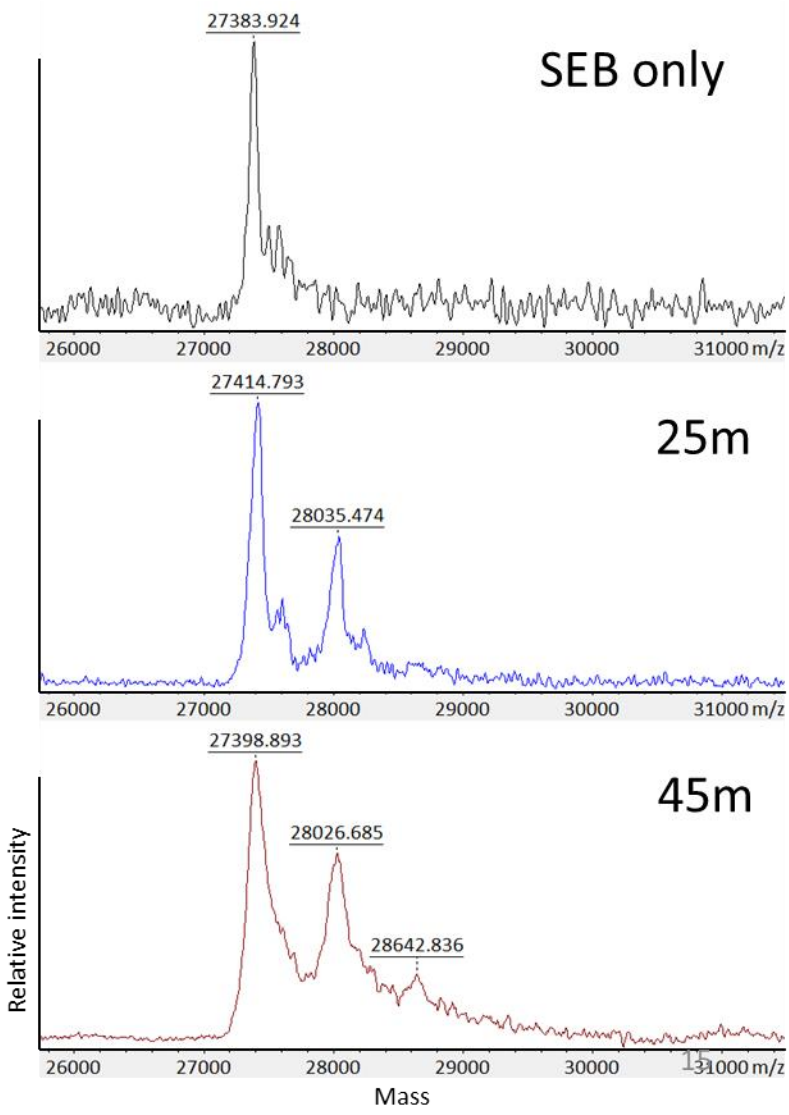

Supplemental Figure 1. Biotinylation of SEB monitored by MALDI-TOF.

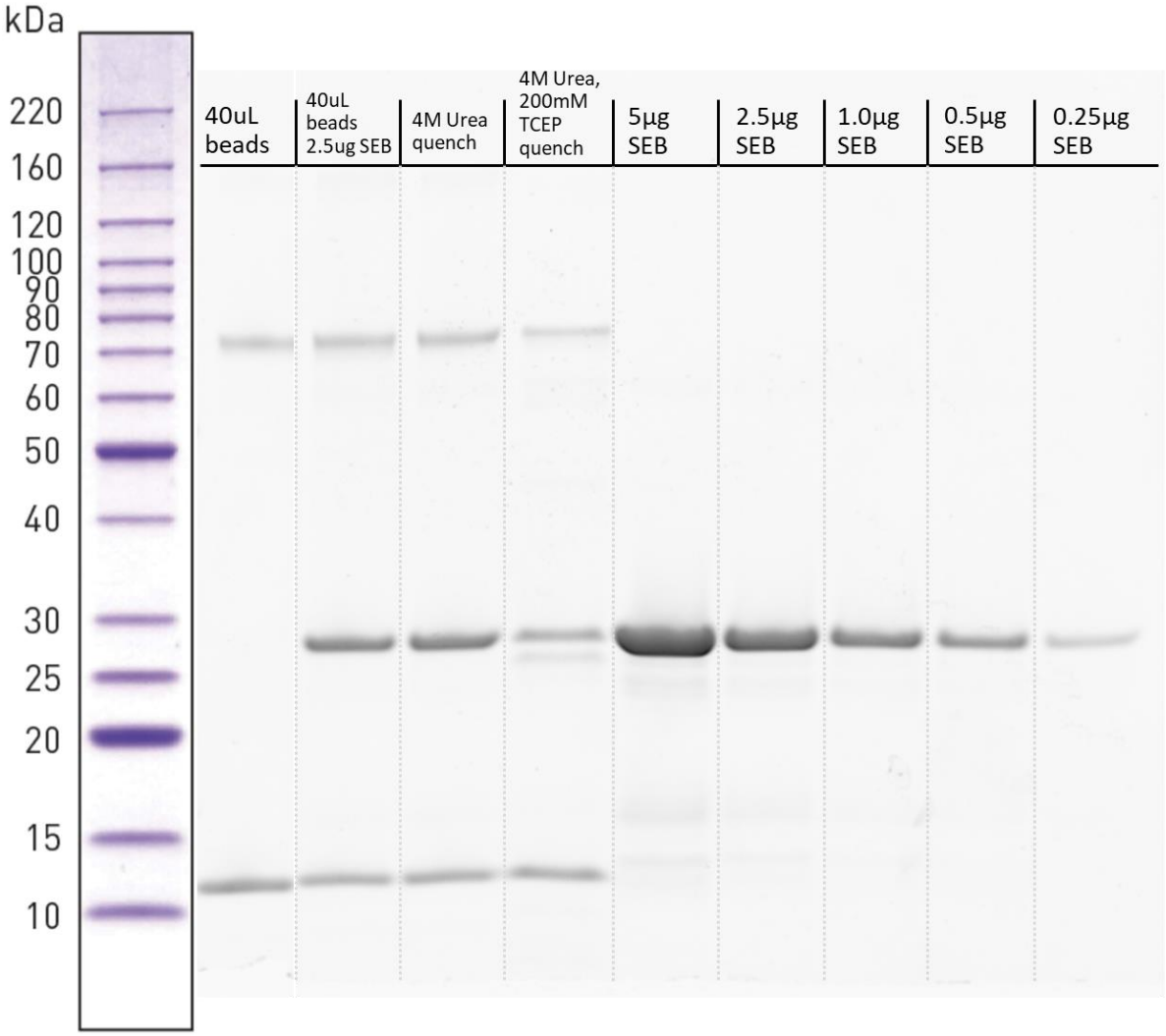

Supplemental Figure 2. Quantification of immobilized SEB including after different quench steps.

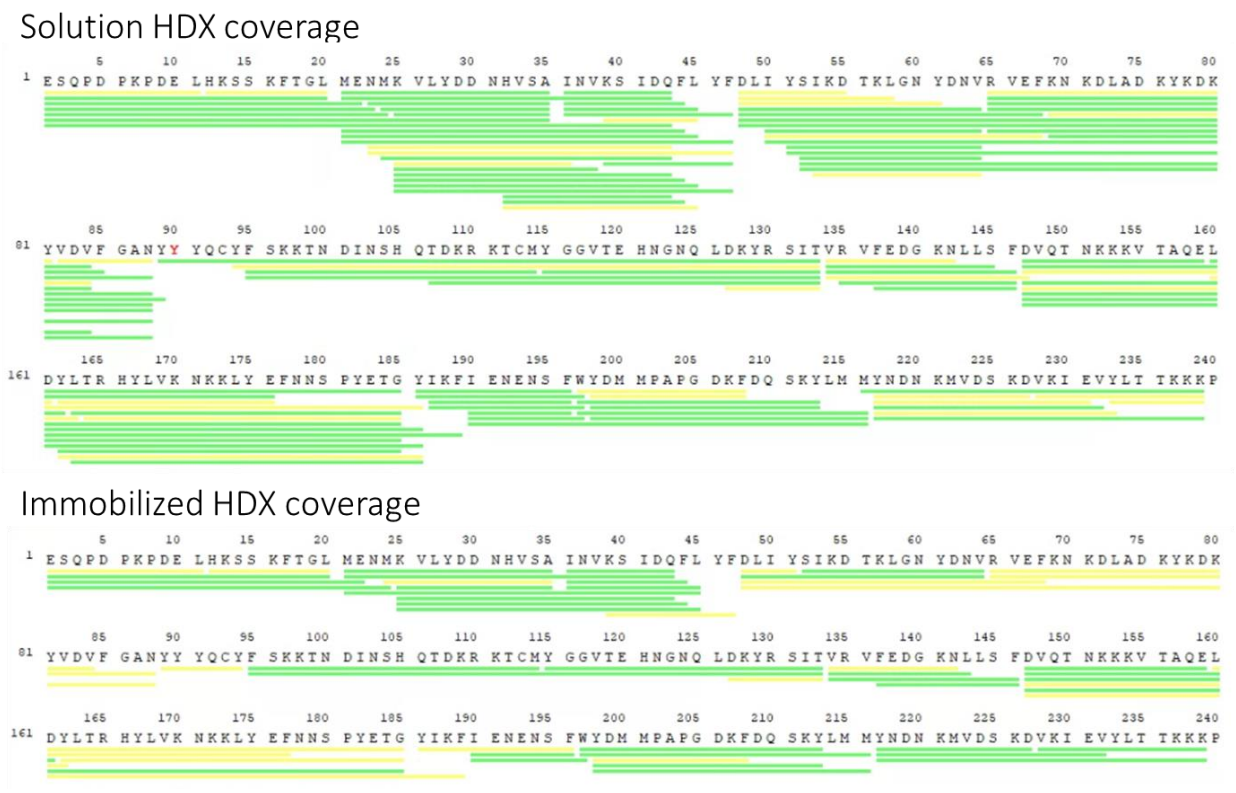

Supplemental Figure 3. Peptide coverage for solution vs immobilized HDX for SEB.

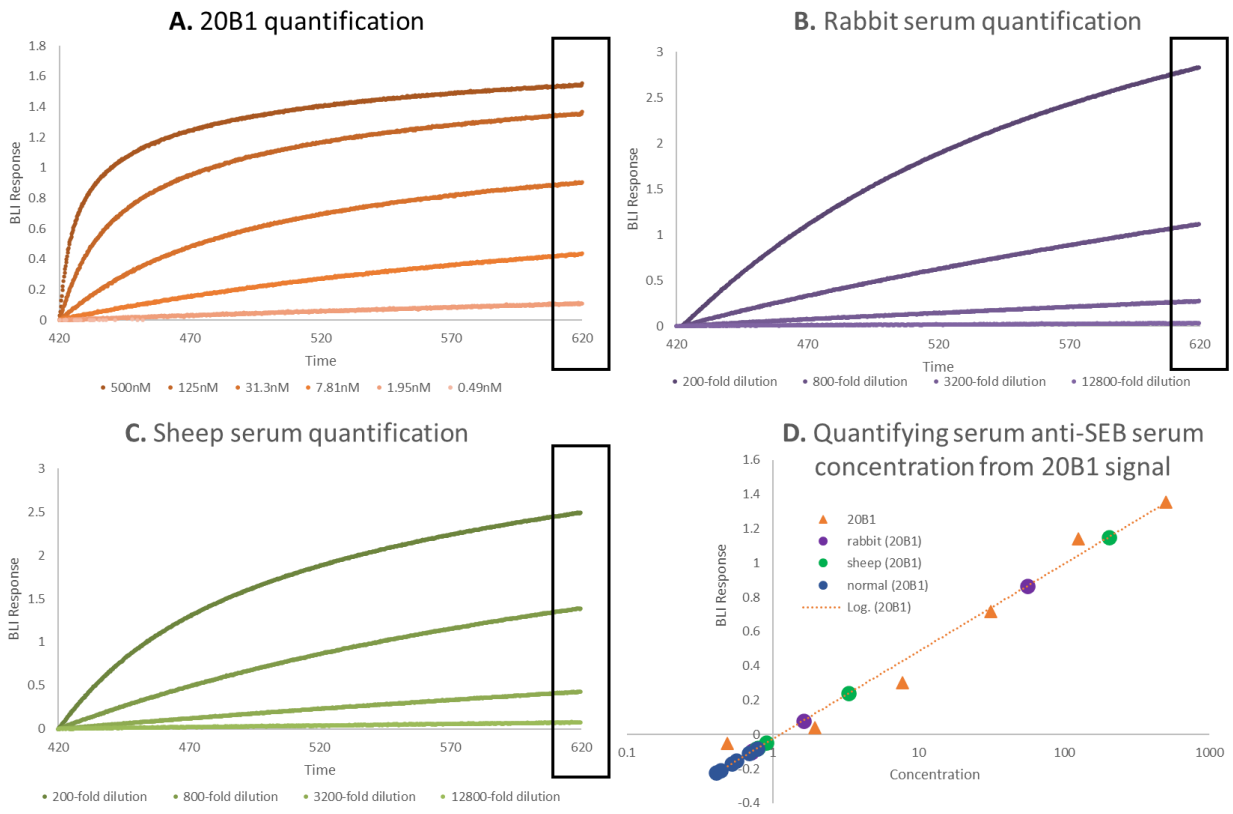

Supplemental Figure 4. Quantification of anti-SEB contents in rabbit and sheep serum using 20B1. **A.** BLI signal of 20B1 after 200s association **B.** BLI signal of rabbit serum after 200s association. **C.** BLI signal of anti-SEB sheep serum after 200s association. **D.** Determination of anti-SEB content in serum using 20B1 concentration plotted against BLI response. Corresponding BLI response from different sera is plotted on concentration. No SEB reactivity was observed.

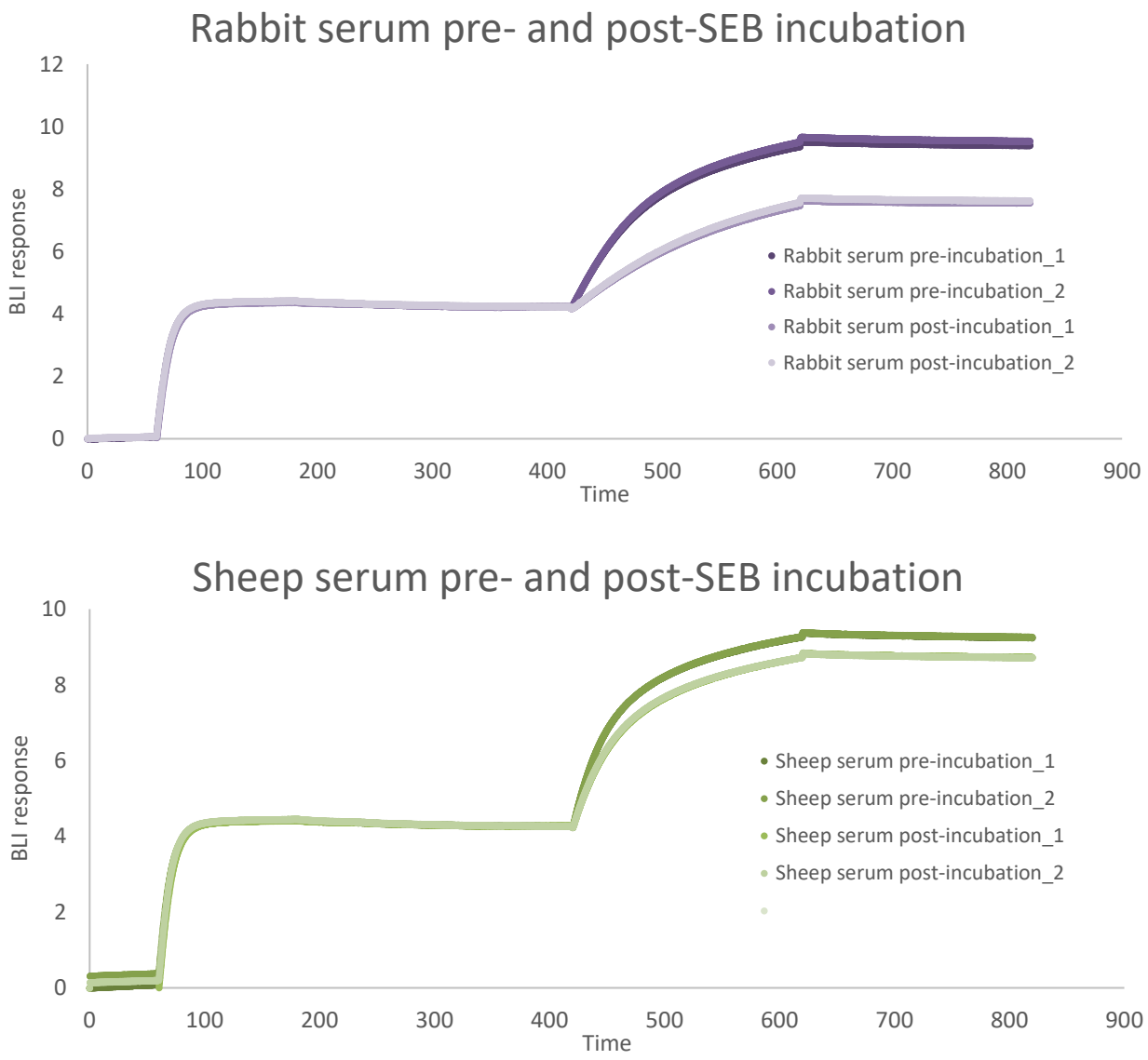

Supplemental Figure 5. Serum binding before and after incubation with immobilized SEB, serum concentrations are comparable. A drop in signal is observed after exposure to SEB, revealing reactivity.

4.8 References

1 Lopez-Santibanez-Jacome, L., Avendano-Vazquez, S. E. & Flores-Jasso, C. F. The Pipeline Repertoire for Ig-Seq Analysis. *Front Immunol* **10**, 899 (2019). https://doi.org:10.3389/fimmu.2019.00899

2 Snapkov, I. *et al.* Progress and challenges in mass spectrometry-based analysis of antibody repertoires. *Trends Biotechnol* **40**, 463-481 (2022). https://doi.org:10.1016/j.tibtech.2021.08.006

3 Jiang, N. *et al.* Lineage structure of the human antibody repertoire in response to influenza vaccination. *Sci Transl Med* **5**, 171ra119 (2013). https://doi.org:10.1126/scitranslmed.3004794
4 Georgiou, G. *et al.* The promise and challenge of high-throughput sequencing of the antibody repertoire. *Nat Biotechnol* **32**, 158-168 (2014). https://doi.org:10.1038/nbt.2782
5 Nesvizhskii, A. I. Proteogenomics: concepts, applications and computational strategies. *Nat Methods* **11**, 1114-1125 (2014). https://doi.org:10.1038/nmeth.3144
6 Lavinder, J. J., Horton, A. P., Georgiou, G. & Ippolito, G. C. Next-generation sequencing and protein mass spectrometry for the comprehensive analysis of human cellular and serum antibody repertoires. *Curr Opin Chem Biol* **24**, 112-120 (2015). https://doi.org:10.1016/j.cbpa.2014.11.007
7 Bondt, A. *et al.* Human plasma IgG1 repertoires are simple, unique, and dynamic. *Cell Syst* **12**, 1131-1143 e1135 (2021). https://doi.org:10.1016/j.cels.2021.08.008
8 Lavinder, J. J. *et al.* Identification and characterization of the constituent human serum antibodies elicited by vaccination. *Proc Natl Acad Sci U S A* **111**, 2259-2264 (2014). https://doi.org:10.1073/pnas.1317793111
9 Suprun, M. *et al.* Novel Bead-Based Epitope Assay is a sensitive and reliable tool for profiling epitope-specific antibody repertoire in food allergy. *Sci Rep* **9**, 18425 (2019). https://doi.org:10.1038/s41598-019-54868-7
10 Monaco, D. R. *et al.* Profiling serum antibodies with a pan allergen phage library identifies key wheat allergy epitopes. *Nat Commun* **12**, 379 (2021). https://doi.org:10.1038/s41467-020-20622-1
11 Henson, S. N. *et al.* PepSeq: a fully in vitro platform for highly multiplexed serology using customizable DNA-barcoded peptide libraries. *Nat Protoc* **18**, 396-423 (2023). https://doi.org:10.1038/s41596-022-00766-8
12 Younger, D., Berger, S., Baker, D. & Klavins, E. High-throughput characterization of protein-protein interactions by reprogramming yeast mating. *Proc Natl Acad Sci U S A* **114**, 12166-12171 (2017). https://doi.org:10.1073/pnas.1705867114
13 Jin, L. & Wells, J. A. Dissecting the energetics of an antibody-antigen interface by alanine shaving and molecular grafting. *Protein Sci* **3**, 2351-2357 (1994). https://doi.org:10.1002/pro.5560031219
14 Javanmardi, K. *et al.* Rapid characterization of spike variants via mammalian cell surface display. *Mol Cell* **81**, 5099-5111 e5098 (2021). https://doi.org:10.1016/j.molcel.2021.11.024
15 Tan, T. J. C. *et al.* High-throughput identification of prefusion-stabilizing mutations in SARS-CoV-2 spike. *Nat Commun* **14**, 2003 (2023). https://doi.org:10.1038/s41467-023-37786-1
16 Starr, T. N. *et al.* Deep Mutational Scanning of SARS-CoV-2 Receptor Binding Domain Reveals Constraints on Folding and ACE2 Binding. *Cell* **182**, 1295-1310 e1220 (2020). https://doi.org:10.1016/j.cell.2020.08.012
17 Dadonaite, B. *et al.* A pseudovirus system enables deep mutational scanning of the full SARS-CoV-2 spike. *Cell* **186**, 1263-1278 e1220 (2023). https://doi.org:10.1016/j.cell.2023.02.001
18 Barnes, C. O. *et al.* Structures of Human Antibodies Bound to SARS-CoV-2 Spike Reveal Common Epitopes and Recurrent Features of Antibodies. *Cell* **182**, 828-842 e816 (2020). https://doi.org:10.1016/j.cell.2020.06.025
19 Antanasijevic, A. *et al.* Polyclonal antibody responses to HIV Env immunogens resolved using cryoEM. *Nat Commun* **12**, 4817 (2021). https://doi.org:10.1038/s41467-021-25087-4
20 Dingens, A. S. *et al.* High-resolution mapping of the neutralizing and binding specificities of polyclonal sera post-HIV Env trimer vaccination. *Elife* **10** (2021). https://doi.org:10.7554/eLife.64281
21 James, E. I., Murphree, T. A., Vorauer, C., Engen, J. R. & Guttman, M. Advances in Hydrogen/Deuterium Exchange Mass Spectrometry and the Pursuit of Challenging Biological Systems. *Chem Rev* **122**, 7562-7623 (2022). https://doi.org:10.1021/acs.chemrev.1c00279

22 McPhail, J. A. *et al.* Characterization of the c10orf76-PI4KB complex and its necessity for Golgi PI4P levels and enterovirus replication. *EMBO Rep* **21**, e48441 (2020). https://doi.org:10.15252/embr.201948441
23 Sun, H. *et al.* Epitope mapping of antibodies in C-reactive protein assay kits by hydrogen-deuterium exchange mass spectrometry explains differential results across kits. *Anal Bioanal Chem* **414**, 3875-3884 (2022). https://doi.org:10.1007/s00216-022-04029-z
24 Zhang, Q. *et al.* Rapid screening for potential epitopes reactive with a polycolonal antibody by solution-phase H/D exchange monitored by FT-ICR mass spectrometry. *J Am Soc Mass Spectrom* **24**, 1016-1025 (2013). https://doi.org:10.1007/s13361-013-0644-7
25 Abbott, W. M. *et al.* Characterization of the complex formed between a potent neutralizing ovine-derived polyclonal anti-TNFalpha Fab fragment and human TNFalpha. *Biosci Rep* **33** (2013). https://doi.org:10.1042/BSR20130044
26 Yang, D. *et al.* Efficient Qualitative and Quantitative Determination of Antigen-induced Immune Responses. *J Biol Chem* **291**, 16361-16374 (2016). https://doi.org:10.1074/jbc.M116.736660
27 Stander, S., L, R. G., Scarselli, M., Norais, N. & Rand, K. Epitope Mapping of Polyclonal Antibodies by Hydrogen-Deuterium Exchange Mass Spectrometry (HDX-MS). *Anal Chem* **93**, 11669-11678 (2021). https://doi.org:10.1021/acs.analchem.1c00696
28 Varshney, A. K. *et al.* Generation, characterization, and epitope mapping of neutralizing and protective monoclonal antibodies against staphylococcal enterotoxin B-induced lethal shock. *J Biol Chem* **286**, 9737-9747 (2011). https://doi.org:10.1074/jbc.M110.212407
29 Watson, M. J. *et al.* Simple Platform for Automating Decoupled LC-MS Analysis of Hydrogen/Deuterium Exchange Samples. *J Am Soc Mass Spectrom* **32**, 597-600 (2021). https://doi.org:10.1021/jasms.0c00341
30 Guttman, M., Weis, D. D., Engen, J. R. & Lee, K. K. Analysis of overlapped and noisy hydrogen/deuterium exchange mass spectra. *J Am Soc Mass Spectrom* **24**, 1906-1912 (2013). https://doi.org:10.1007/s13361-013-0727-5
31 Weis, D. D., Wales, T. E., Engen, J. R., Hotchko, M. & Ten Eyck, L. F. Identification and characterization of EX1 kinetics in H/D exchange mass spectrometry by peak width analysis. *J Am Soc Mass Spectrom* **17**, 1498-1509 (2006). https://doi.org:10.1016/j.jasms.2006.05.014
32 Dutta, K. *et al.* Mechanisms mediating enhanced neutralization efficacy of staphylococcal enterotoxin B by combinations of monoclonal antibodies. *J Biol Chem* **290**, 6715-6730 (2015). https://doi.org:10.1074/jbc.M114.630715
33 Kay, B. K., Thai, S. & Volgina, V. V. High-throughput biotinylation of proteins. *Methods Mol Biol* **498**, 185-196 (2009). https://doi.org:10.1007/978-1-59745-196-3_13
34 Selo, I., Negroni, L., Creminon, C., Grassi, J. & Wal, J. M. Preferential labeling of alpha-amino N-terminal groups in peptides by biotin: application to the detection of specific anti-peptide antibodies by enzyme immunoassays. *J Immunol Methods* **199**, 127-138 (1996). https://doi.org:10.1016/s0022-1759(96)00173-1
35 Grimsley, G. R., Scholtz, J. M. & Pace, C. N. A summary of the measured pK values of the ionizable groups in folded proteins. *Protein Sci* **18**, 247-251 (2009). https://doi.org:10.1002/pro.19
36 Rincon Pabon, J. P., Kochert, B. A., Liu, Y. H., Richardson, D. D. & Weis, D. D. Protein A does not induce allosteric structural changes in an IgG1 antibody during binding. *J Pharm Sci* **110**, 2355-2361 (2021). https://doi.org:10.1016/j.xphs.2021.02.027
37 Masson, G. R. *et al.* Recommendations for performing, interpreting and reporting hydrogen deuterium exchange mass spectrometry (HDX-MS) experiments. *Nat Methods* **16**, 595-602 (2019). https://doi.org:10.1038/s41592-019-0459-y

38 Rusinga, F. I. & Weis, D. D. Soft interactions and volume exclusion by polymeric crowders can stabilize or destabilize transient structure in disordered proteins depending on polymer concentration. *Proteins* **85**, 1468-1479 (2017). https://doi.org:10.1002/prot.25307

Chapter 5: Future Directions

5.1 Pepsin Reproducibility

Further incorporation of peptides to test for protease activity could be achieved for different emerging protease types, including nep-2 or ANPEP (Citation for Woods paper). Another potential direction of improving protease reproducibility could be by including protein standards within HDX samples. Peptides for monitoring protease activity, like the mix proposed in the author's study, could be incorporated into individual HDX samples at similar concentrations. The peptides could be monitored in tandem with peptides of interest to achieve an on-the-fly assessment of protease activity.

5.2 SEB Epitope mapping, allostery, and synergy

The mapping of staph enterotoxin epitopes, allosteric interactions, and synergistic effects could progress in several directions. Different SE strains could be mapped in a similar way to the author's studies of SEB. With knowledge of the epitope regions of interest for different SEs, a focus on broadly neutralizing species could be undertaken. Antibodies that neutralize multiple SE species are of therapeutic interest. If it is understood that similar regions of enterotoxins elicit similar neutralizing effects, various therapeutics could be designed to target multiple toxins. Additionally, the HDX-MS mapping of other antibodies (beyond 14G8 and 6D3) in tandem for both SEB or other SEs could be done to measure and quantify the synergistic effects.

Additional synergistic characterization of 14G8 and 6D3 for SEB could be undertaken. Interrogation of the synergistic effects of 14G8 and 6D3 via kinetic experiments that incorporate labeling a particular antibody with a fluorescent agent might be capable of coaxing out differences in individual mAb kinetics due to another mAb binding.

5.3 Polyclonal/Immobilized HDX

The mapping of polyclonal epitopes in the immobilized HDX-MS experiment could be expanded in various ways. Of interest could be the fractionating of different antibody subpopulations based on kinetic profiles by sorting by incubation time. Selective antibody kinetic fractionation could be achieved by incubating serum with a target protein of interest for different amounts of time and studying those different time populations by HDX to measure how the epitopes change.

Another way to study different subpopulations of epitopes that arise from binding raw serum could be fractionation with chaotropic agents. Including chaotropic agents at low concentrations could remove

species that bind weakly to a target protein and keep proteins that bind at a high affinity. Additionally, it may be of interest to remove antibodies of different affinities sequentially to classify different binding partners based on binding strength.

Another potential direction for expanding the immobilized HDX assay could be integrating this method with other methods for mapping polyclonal response, including EM or deep mutational scanning. By incorporating these other complementary methods for mapping polyclonal response, it might be possible to link immune response more robustly with a specific biophysical response.

Finally, this method could be further expanded by integrating different high-resolution methods for further classification of bound antibody species. It's recently been reported that different high-resolution proteomic approaches can sequence different antibody fab regions. Integration of protein sequencing could help distinguish beyond subclasses of antibodies to identify the relevant antibody repertoire binding to an antigen of interest.